PACIFIC EARTHQUAKE ENGINEERING
RESEARCH CENTER

Self Compacting Hybrid Fiber Reinforced Concrete Composites for Bridge Columns

Pardeep Kumar

Gabriel Jen

William Trono

Marios Panagiotou

Claudia P. Ostertag

Department of Civil and Environmental Engineering
University of California, Berkeley

PEER 2011/106
SEPTEMBER 2011

Self Compacting Hybrid Fiber Reinforced Concrete Composites For Bridge Columns

Pardeep Kumar

Gabriel Jen

William Trono

Marios Panagiotou

Claudia P. Ostertag

Department of Civil and Environmental Engineering
University of California, Berkeley

PEER Report 2011/106
Pacific Earthquake Engineering Research Center
College of Engineering
University of California, Berkeley

September 2011

ABSTRACT

Although fiber-reinforced composites have the potential to enhance the seismic performance of bridge columns, their use has been hampered by their poor workability and inadequate compaction for cast-in-place applications. To address this issue, this study developed a self-compacting hybrid fiber reinforced concrete (SC-HyFRC) composite. Optimized specifically for bridge columns, this composite flows under its own weight, completely filling the formwork and achieving full compaction without internal or external vibration. In addition, this SC-HyFRC provides enhanced ductility, shear resistance, and damage tolerance compared to conventional fiber-reinforced composites.

To investigate the seismic performance and post-earthquake damage resistance of bridge columns composed of SC-HyFRC, two 1:4.5 scale column specimens were built and tested statically under uni-directional cyclic loading. In both specimens the volumetric transverse reinforcement was 0.37%, which is two to three times less than that of typical Caltrans bridge columns. Both test specimens had the same longitudinal steel ratio of 1.2%.

The design of the two specimens differed in terms of the location where the nonlinear deformations were accommodated. The first specimen was designed to rock at the column's base–foundation interface. Incorporating stainless steel bars as longitudinal reinforcement, the second specimen was designed to form a flexural plastic hinge at its base. Both specimens attained large drift ratios of up to 11% without losing axial load carrying capacity and were successful in resisting damage due to spalling of concrete up to drift ratios of 3.6%. Compared to a conventional reinforced concrete column of same dimensions, longitudinal steel ratio, and axial load ratio, the SC-HyFRC columns exhibited superior damage resistance and better load carrying capacity despite a 50% reduction in transverse reinforcement.

ACKNOWLEDGMENTS

This work was supported by the State of California through the Transportation System Research Program of the Pacific Earthquake Engineering Research Centers (PEER). Any opinions, findings, and conclusions or recommendations expressed in this material are those of the authors and do not necessarily reflect those of the funding agency.

We would like to thank Joel Carr, Lev Stepanov, Philip Wong, Jeff Higginbotham, and Matt Cateleta for their help in preparing and conducting the experiments.

CONTENTS

LIST OF FIGURES

LIST OF TABLES

1 Introduction

1.1 BACKGROUND

Reinforced concrete (RC) bridges located in areas of high seismicity are designed to allow nonlinear deformations to occur in specific parts of the bridge during a design level earthquake. For low- and moderate-intensity earthquakes, the main objective of the seismic design is that a bridge remain functional immediately after the earthquake, sustaining relatively little to no damage.

Typical RC bridge design allows nonlinear deformations to develop, preferably in flexure, in specific regions of the columns referred to as "flexural plastic hinges," while the other parts of the bridge are intended to remain nearly elastic. Current seismic design provisions (Caltrans 2006) include prescriptive requirements consistent with traditional capacity design concepts (Park and Paulay 1975) to ensure that capacity exceeds the expected deformation demands in these plastic hinge regions. Seismic isolation is a seismic design alternative for RC bridges (Buckle et al. 2006; JRA 2002; CHBDC 2000; AASHTO 1998), whereby the nonlinear deformations are accommodated within the isolation devices themselves, while the rest of the bridge remains nearly elastic.

Another strategy is to allow rocking to occur at the column-foundation interface (Hewes 2007; Ou et al. 2007; Mahin et al. 2006; Yoon and Billington 2002; Sritharan et al. 1999; Cormack 1998; Mander and Cheng 1997a, 1997b) and/or at the column-deck interface (NCHRP 12-74 2010). Such systems usually incorporate unbonded post-tensioning to better control the stiffness and strength characteristics of the bridge. Similarly, bridges designed with shallow foundations that rock at the foundation-soil interface (Espinoza and Mahin 2006; Mergos and Kawashima 2005) can reduce residual deformations and post-earthquake damage of a bridge column, and thus of the bridge as a whole.

For the RC bridges designed so that nonlinear deformation occurs in the columns, damage is concentrated in plastic hinges. For small to moderate seismic events, cracking, spalling, and crushing of concrete may occur. Under more severe seismic loading conditions, fracture of the transverse reinforcements, and buckling and fracture of the longitudinal reinforcing bars may occur in the column plastic hinge regions. If the bridge column is unable to maintain its load-bearing capacity, this may interfere with disaster recovery operations. Being more frequent, small to moderate intensity seismic events may have a major economic impact on structures due to their continuous need for repair. Cracking and spalling of concrete due to corrosion [see Figure 1.1(a)], alkali silica reaction (ASR) [see Figure 1.1(b)], or both [see Figure 1.1c)] is frequently observed in bridge columns prior to a seismic event and will undoubtedly reduce their seismic performance.

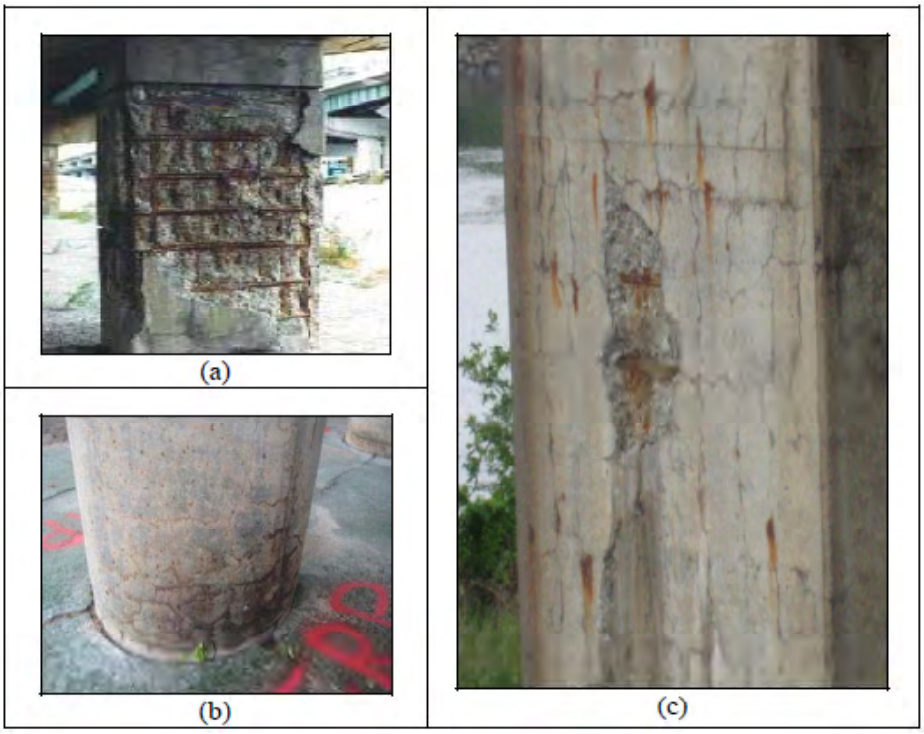

Figure 1.1 **Damage of bridge columns due to environmental loading conditions: (a) spalling of concrete due to corrosion exposing the transverse reinforcements; (b) map cracking in plastic hinge region due to ASR; and (c) deterioration of bridge column due to both corrosion and ASR.**

The use of high performance fiber reinforced composites (HPFRCs) in bridge columns has recently received considerable interest by the engineering community (Aviram et. al. 2010; Saiidi et. al. 2009; Billington and Yoon 2004; Parra-Montesinos and Wight 2000). Designed with superior properties compared to conventional RC, fiber reinforced composites (FRCs) have the potential to enhance the damage resistance of bridge columns in regards to seismic as well as environmental loading conditions if they exhibit deflection or strain-hardening behavior. The current study investigates the performance of bridge columns that utilize a self-compacting hybrid fiber reinforced concrete (SC-HyFRC) composite exhibiting deflection as well as strain hardening behavior. The HyFRC was initially developed to provide better crack resistance to structures exposed to harsh environmental conditions. The performance of a HyFRC compared to a conventional FRC is discussed briefly in Section 1.2.

1.2 HYBRID FIBER REINFORCED COMPOSITES (HYFRC) FOR BRIDGE COLUMNS

In comparison with conventional RC columns, FRCs have great potential to enhance the performance of bridge columns if they exhibit a more ductile behavior both in tension and compression. Figure 1.2 compares the performance characteristics of conventional FRCs [see Figure 1.2(a)] with those that exhibit a deflection hardening behavior where dominant cracking is delayed up to higher strength and strain values [see Figure 1.2(b)]. A FRC that exhibits a behavior where dominant crack formation coincides with the cracking strength and strain capacity of the matrix [see Figure 1.2(a)] will not be as effective despite its extended softening behavior. This type of behavior is commonly observed in conventional FRCs.

Deflection hardening FRCs have the potential to enhance seismic performance of bridge columns due to their superior crack resistance and high ductility in both compression and tension. However, since this type of deflection hardening is commonly accomplished through multiple cracking, the performance of these FRCs with regard to damage resistance associated with environmental loading conditions will depend on their crack widths as well. For corrosions resistance in particular, the crack width has to be small enough to prevent water and chloride ions from entering the concrete thus avoiding ASR and corrosion-related deterioration mechanisms.

This study utilizes an innovative hybrid fiber reinforced concrete (HyFRC) composite that was developed based on extensive research by the PI's research group. It complies with the necessary material performance criteria for bridge columns, such as crack resistance and deflection hardening behavior, high ductility in compression and tension, high shear resistance, and resistance to corrosion and other environmentally induced deterioration processes (Ostertag and Blunt 2010; Blunt and Ostertag 2009A; Blunt and Ostertag 2009B; Ostertag et. al. 2007).

A HyFRC that resists deterioration due to corrosion, frost, and scaling action was also developed for Caltrans for use in bridge approach slabs exposed to both mechanical and harsh environmental loading conditions (Ostertag and Blunt 2008). The rationale behind using a HyFRC-based mix can be referred to as Deterioration Reduction through Micro- and Macrocrack Control, or the DRMC approach, whose PVA microfibers and hooked end steel macrofibers are used simultaneously to control the micro and macrocracks, respectively [see Figure 1.3]. The control of microcracks is essential for enhancing the durability of RC structures (Yi and Ostertag 2005; Grubb et. al. 2007). Because cracking due to expansive deterioration processes initiate as microcracks in close vicinity to the reaction sites, these micocracks need to be influenced at onset before they become macrocracks.

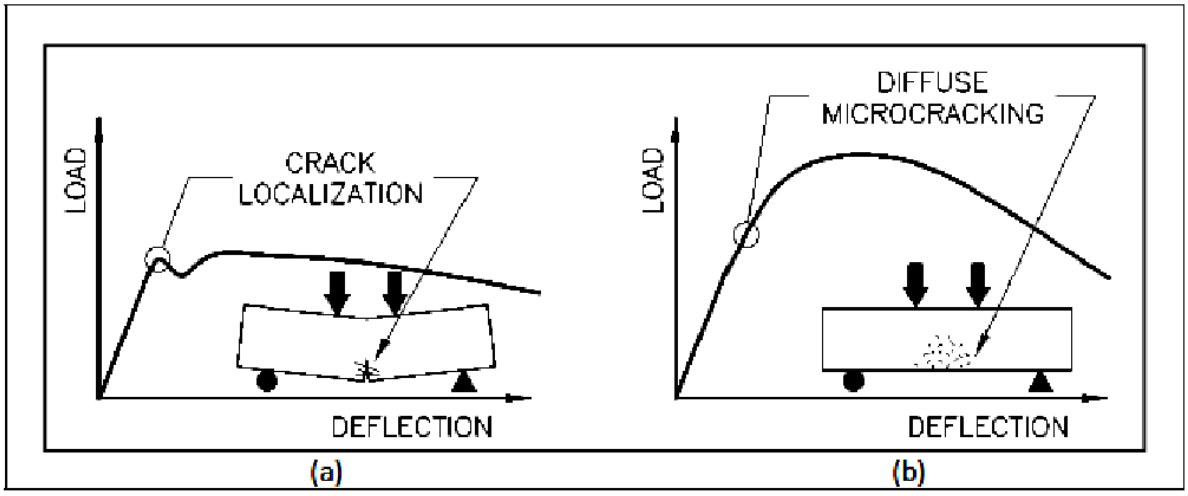

Figure 1.2 **Performance characteristics of fiber reinforced composites: (a) conventional fiber reinforced composite with deflection softening behavior; and (b) deflection hardening behavior where dominant cracking is delayed up to higher strength and strain levels.**

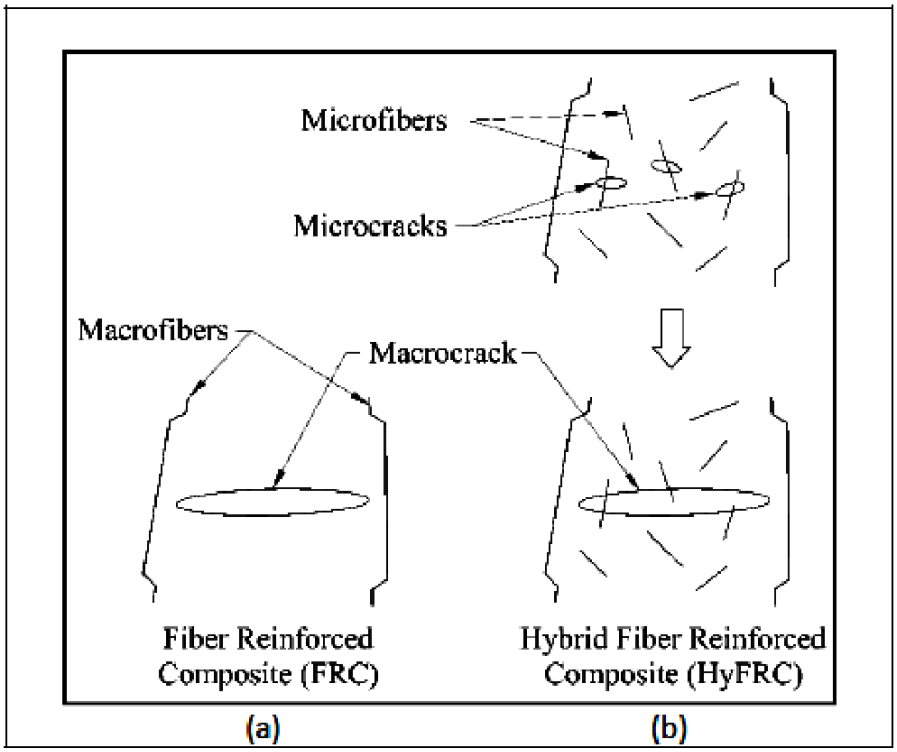

Figure 1.3 **Schematic representation of fiber spacing and characteristic cracking in: (a) a fiber reinforced composite with conventional macrofibers only; and (b) a HyFRC with micro and macrofibers.**

The HyFRC concept was initially introduced by (Rossie 1997) and further developed by other researchers (Qian and Stroeven 2000; Banthia and Nandakumar 2003; Lawler et. al. 2005). The DRMC approach is based on a performance-based materials approach (Blunt and Ostertag 2009A); therefore, the sole combination of micro and macrofibers alone does not necessarily lead to the desired deflection hardening behavior [shown in Figure 1.2(b)] and damage resistance due to environmental loading conditions. Not only does the DRMC approach lead to deflection hardening behavior, but it also delays—and in some cases even mitigates—deterioration processes such as corrosion and ASR commonly observed prior to a seismic event, as shown in Figure 1.1. Hence, the HyFRC based matrix appears to be an effective solution to enhance the overall damage resistance and performance of bridge columns.

In order to implement this HyFRC for cast-in-place field applications, however, the material requires additional properties such as high workability, uniform compaction, and ease of placement. Using FRC for bridge columns has been hampered by the inability of the fibers to pass through the congested areas of reinforcements present in bridge columns built to withstand

seismic excitation. Bridge columns cast with FRCs require excessive vibration (Aviram et. al. 2010), and even if correctly executed results in uneven compaction. This enhances the selective ingress of aggressive substances, leading to poor durability overall. Fortunately, the development self-compacting concrete by Okamura (1997) offers a potential solution to this problem as it is easy to place, thereby reducing the number of construction workers required on-site, resulting in cost savings. Even critical, self compacting concrete does not require vibration during placement; it is able to flow under its own weight, completely filling the formwork and achieving full compaction, even in the presence of congested reinforcements.

Task 1 of this research project is to develop and design a self-compacting HyFRC for the use in bridge columns. While some researchers have attempted to make self-compacting FRCs (Aoude et. al. 2009) and even hybrid FRCs (Nehdi and Ladanchuk 2004), the fiber volumes that could be incorporated to classify the composites as self-compacting were often not sufficiently high enough to produce the desired toughening mechanisms that result in deflection hardening behavior. In addition, in many cases the mixes eliminated coarse aggregates, and testing was done on mortars that only enhanced their propensity for shrinkage and creep. Fundamentally, the basic objectives for the self-compacting HyFRC (denoted as SC-HyFRC in this report) was to achieve adequate distribution of fibers and self-compacting properties with the addition of coarse aggregates at a fiber volume fraction that ensures the desired response. According to the authors' knowledge, this has not yet been achieved. If successful, it will not only enhance the safety but also reduce the environmental burden of concrete on the environment by extending the life-cycle and hence the sustainability of RC structures.

1.3 RESEARCH OBJECTIVES

The main objectives of this research program are as follows: (i) to enhance the damage resistance of bridge columns exposed to both seismic and environmental loading conditions; (ii) to improve the load carrying capacity of bridge columns at large drift ratios; and (iii) to provide full compaction and ease of construction of bridge columns.

Modern highway bridges in California are required to perform adequately during frequent (M4-6) and extreme (M7-9) seismic events. A "grade" of adequate implies a ductile performance, limited and repairable damage, and the ability to maintain at minimum a gravity

load-carrying capacity. Bridge columns cast with HyFRC composites have the potential to outperform conventional RC bridge columns. Due to their high ductility and crack resistance, bridge columns made out of HyFRC are anticipated to sustain higher ductility demands without considerable damage compared to conventional bridge columns (Bayasi and Gebman 2002; Vasconez et al. 1998; Filiatrault et. al. 1995; Henager 1977). In addition, plastic shrinkage cracks, drying shrinkage cracks, and cracking due to corrosion and ASR—which makes bridge columns even more susceptible to damage during an earthquake—can be successfully prevented through the use of these HyFRC composites.

To assure full compaction and ease of construction, self-compacting hybrid fiber reinforced concrete for bridge columns was developed and two 1:4.5 scale SC-HyFRC bridge columns were built and tested statically under uni-directional cyclic loading to investigate the effect of SC-HyFRC on seismic performance.

It was anticipated that the hybrid fiber reinforcement—due to its superior shear resistance and more ductile behavior in tension and compression compared to conventional RC—justified reduction in the transverse reinforcement in bridge columns. Therefore, for both specimens the transverse reinforcement was reduced by factor of two compared to conventional RC Caltrans bridge columns, and what affect this had on the seismic performance investigated. In addition, innovative structural design approaches were incorporated in each specimen. Test Specimen 1 was designed to rock at the column's base- foundation interface by incorporating unbonded longitudinal reinforcing bars. Test Specimen 2 was designed to develop a plastic hinge region and incorporated a corrugated steel duct to prevent crack localization at the cold joint at the column base-foundation interface. In addition, Test Specimen 2 utilized stainless steel longitudinal reinforcement to enhance the spread of plasticity in the plastic hinge region.

1.4 ORGANIZATION OF THE REPORT

The report is organized into six parts. The first part introduces the concept behind a hybrid FRC The second part describes the development and design of the SC-HyFRC for bridge columns, including discussion of the flow property measurements, the optimization processes that were involved in order for the HyFRC to meet the requirements of self-compaction without segregation of fibers and aggregates, and the mechanical properties of trial batches. The third

part focuses on the design and construction of two SC-HyFRC bridge columns. The fourth part focuses on the experimental setup, instrumentation, and loading protocol of the two test specimens. The fifth part provides the results and discussion on the column performance of the two test specimens. This section also includes a brief comparison between the test columns and bridge columns based on Caltrans design of same size and similar loading conditions—but built with conventional concrete and with double the transverse reinforcement. A brief summary and conclusions are provided in part six.

2 Development of Self-Compacting HyFRC for Bridge Columns

2.1 HYFRC MIX DESIGN FOR LIGHTLY REINFORCED CONCRETE STRUCTURES

The development of SC-HyFRC for bridge columns was based on a HyFRC mix design (see Table 2.1) that was developed for lightly reinforced concrete structures (Ostertag and Blunt 2008). The admixture suite consisted of a polycarboxylate superplasticizer (Glenium 3030 NS) and an organic viscosity modifying agent (Rheomac VMA 358); both admixtures are BASF products. The mix contains three types of fibers with different size and materials, and their pertinent characteristics are summary in Table 2.2.

Polyvinyl Alcohol (PVA) fibers were chosen as microfibers, and two steel fibers of different length and diameter were chosen as macrofibers. The PVA fibers have the benefit of high stiffness when compared to a stiffness of 725 ksi (5 GPa), which is typical of polypropylene and polyethylene fibers. Steel fibers were chosen for crack resistance at the macro level because of their high stiffness and hooked end, providing mechanical anchorage through which the fiber stiffness can be fully developed. Figure 2.1 demonstrates the desired deflection hardening behavior of the HyFRC mix to ensure crack resistance and durability enhancement when beam samples were tested in flexure. The beams were wet cured for 7 days followed by 21 days of dry curing prior to testing to simulate field conditions.

The HyFRC mix had a slump of 6.5 in., which allowed the 6 in × 12 in. cylinders and 6 in. × 6 in. × 2 in. beams (with conventional reinforcements up to 0.3% reinforcement ratios) to be properly compacted. Although a slump flow of 6.5 in. is sufficient for lightly reinforced structures such as bridge approach slabs, it does not provide the adequate flow properties and high compaction that are required for highly reinforced structures such as bridge columns. The

testing, development, and design of a self-compacting hybrid fiber reinforced composite for use in bridge columns to assure proper compaction and ease of construction is discussed in the following sections.

Table 2.1 Mix proportions for HyFRC mix with slump flow of 6.5 in. (used as base for the development of the SC-HyFRC for bridge columns).

Cement[a]	Fly Ash[b]	Water	CA[c]	FA[d]	Super[e]	VMA[e]	Fiber Dosage V_f [%]		
							PVA	S1	S2
1.0	0.33	0.6	1.24	2.45	0.0012	0.0003	0.2	0.5	0.8

[a] ASTM C150 Type II, [b] ASTM C618 Type C, [c] pea gravel, 3/8 in. MSA, [d] coarse sand, FM = 3.2, [e] value shown as the weight of solids content.

Table 2.2 Fiber properties.

Designation	Material	Length in. (mm)	Diameter in. (mm)	Strength ksi (MPa)	Stiffness ksi (GPa)
PVA	PVA	0.32 (8)	0.0016 (0.04)	230 (1600)	6090 (42)
S1	Steel, Hooked	1.18 (30)	0.0217 (0.55)	160 (1100)	29000 (200)
S2	Steel, Hooked	2.36 (60)	0.0295 (0.75)	150 (1050)	29000 (200)

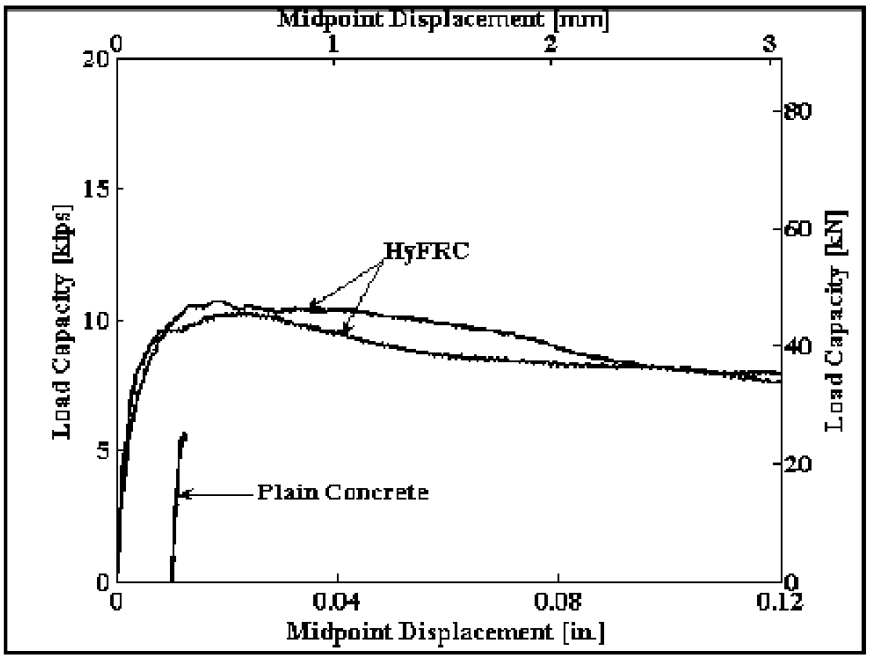

Figure 2.1 Four point bend tests (plain concrete shifted from origin for clarity).

2.2 FLUIDITY TESTING PROCEDURES

The self compacting properties of various trial mixes were tested by two methods: the slump flow test and the J-ring test. The slump flow test followed the guidelines of ASTM C1611 (ASTM Standard C1611 2009), while the J-ring test followed the guidelines outlined in ASTM C1621 (ASTM Standard C1621 2009).

2.2.1 Slump Flow Test

The slump flow test involved filling a standard slump cone standing upright with a representative sample of the mix and measuring the diameter of concrete spread achieved when the cone was vertically lifted, as shown in Figure 2.2(a).

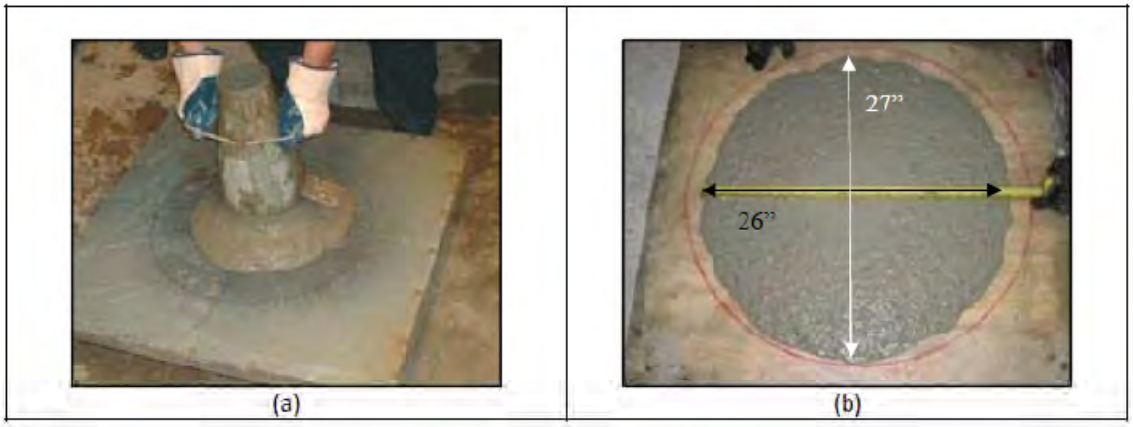

Figure 2.2 **Slump flow test: (a) standard slump cone; and (b) measurement of flow diameters.**

A rigid board made of wood (in some later tests this board was made of plastic) was used to achieve a flat surface. When using the wooden board, a sheet of plastic was placed over the board. The plastic sheet and plastic board were wiped clean with a wet sponge before the beginning of each test. Potential tilt of the board was not measured but an effort was made to perform tests on the flattest portion of the lab floor. The slump test was carried out immediately following the mixing process for all trial batches which had not segregated within the mixing bowl during mixing. Flow diameters were measured along the longest axis of the resulting circle or ellipse and the axis perpendicular to the longest axis, as shown in Figure 2.2(b). In general, mixes that did not achieve diameters of similar scale in each principal direction were not considered viable. Because of its ease of testing, the slump flow test became the principal measurement taken in determining fluidity of each trial batch. Segregation of concrete components was determined by visual inspection. If fine and coarse aggregates did not flow to the outermost edge, the mix was determined to have undergone "concrete segregation." Segregation of fibers was determined by visual inspection and sifting through the outermost 2 in. ring to determine whether fibers were present and in what concentration.

Figure 2.3 Example of "concrete segregation" and "fiber segregation."

Visual inspection was also used to determine whether fiber "clumping" within the original slump cone diameter had occurred, which would lead to a mound of interlocked fibers at the center. Failing either of these subjective measurements led to the trial batch being labeled "fiber segregation." Both "concrete segregation" with cement paste separation along the perimeter and "fiber segregation" with fiber clumping at the center can be observed in one of the failed trial batch mix designs (see Figure 2.3). Later mixes also incorporated a measurement of the highest peak of concrete remaining following the slump flow procedure, with smaller heights indicating a more uniform spreading behavior.

2.2.2 J-ring Test

The J-ring test was used to measure passing ability of concrete and fibers through uniformly spaced bars. The J-ring consists of a ring with vertical rods placed at a preset spacing along the circumference. Flow diameter measurements were made with and without the J-ring to investigate the flow reduction caused by evenly spaced obstructions. Measurements of concrete height both directly inside and outside the vertical rods were taken to determine passing ability of concrete through the given obstruction.

Initial J-ring testing utilized a steel testing setup purchased from Forney, Inc. (Figure 2.4). While plain self-compacting concrete (SCC) had no difficulties passing through the closely spaced vertical rods, fiber mixtures incorporating steel fiber types S1 and S2 were unable to pass.

Closer inspection revealed that the fibers bridged the gap between the rods initiating blockages, which quickly entangled and incorporated many more fibers.

Figure 2.4 Forney, Inc. J-ring test.

Consequently, it was decided to relax the bar spacing of the J-ring to the bar spacing that would be encountered in the columns. The geometry of the Forney J-ring had 0.625 in.-diameter rods placed such that there was 1.75 in. of clear space between adjacent rods. Referencing the reinforcing geometry of the anticipated column specimen, an aluminum J-ring setup was fabricated in the Mechanical Engineering machine shop at UC Berkeley, with vertical rod spacing of 3.125 in. and ring diameter of 16 in., exactly matching the design drawings for the column specimen. The vertical rod diameter was set to be equal to the nominal diameter of #4 rebar shown in the design drawings. In addition to rods placed at the same circumferential spacing as expected in the column sample, the aluminum J-ring has the capability to support additional vertical rods at one-half the spacing should determination of the passing ability of concrete through a more obstructed pathway be desired. Shown in Figure 2.5, the aluminum J-ring test setup was designated the “modified J-ring.”

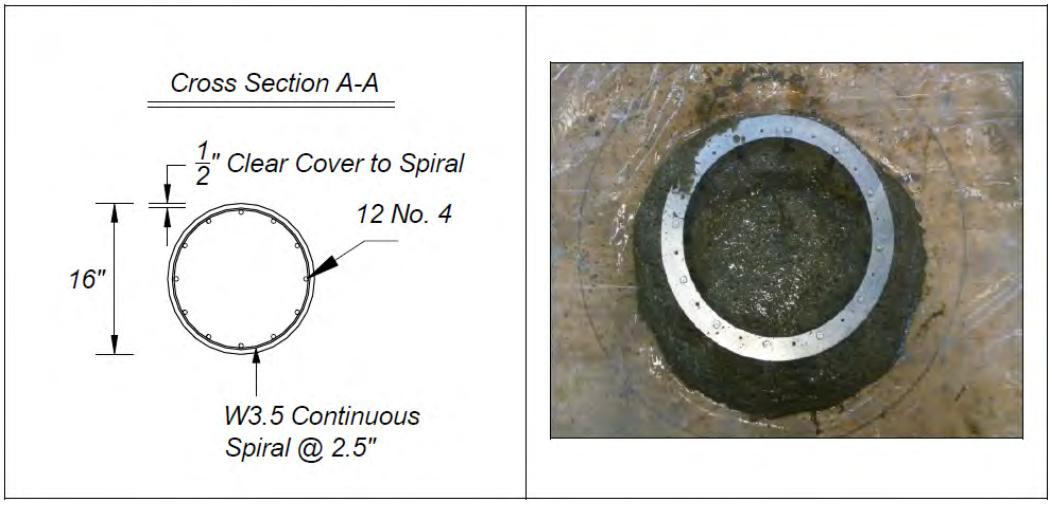

Figure 2.5 Custom designed J-ring test with same rebar spacing as bridge columns.

2.3 PARAMETRIC STUDY

In its most basic form, SCC requires the addition of two chemical admixtures during the mixing process: a high-range water-reducing agent (superplasticizer) and a viscosity modifying agent (VMA). The superplasticizer (SP) provides the increased fluidity necessary to allow the force of gravity to be sufficient to consolidate the concrete (Ouchi et. al. 1996). The VMA increases the viscosity of fresh concrete such that it will not suffer from segregation of aggregates or fibers.

For the HyFRC to be considered self-compacting, a flow diameter of 24 in. in both directions without signs of segregation was targeted. Several key parameters were identified and optimized in order for the HyFRC to achieve the target flow properties without segregation:

- Chemical admixtures proportions and SP/VMA ratio
- Fiber types and volume fraction
- Paste/aggregate volume ratio
- Aggregate content and FA/CA ratio

The mix proportions and flow diameters of the various trial batches were modified according to the parameters listed above and are described in detail in Appendix A. Trial batching took place over several months with greater than fifty-nine variations tested.

All concrete mixing was conducted in the Concrete Laboratory at the UC Berkeley campus by UC Berkeley students with the assistance of the onsite lab technician. The mixing

laboratory has four mechanical concrete mixers in total, each of different capacities. For trial batching, the smallest mixer with a capacity of 0.04 yd^3 was used. For testing that required multiple beams and cylinders, the second largest mixer with a capacity of 0.125 yd^3 was utilized. The third largest mixer with a capacity of 0.20 yd^3 was used to investigate the effect of batch size on mix properties. The SC-HyFRC batches for the columns were produced in the largest capacity mixer (0.33 yd^3 nominal capacity). The two smallest mixers have a single operational speed, while the two largest mixers have variable operational speed.

2.4 MECHANICAL TESTING AND PROPERTIES OF TRIAL BATCHES

Compression tests and flexure tests with and without conventional steel reinforcements were conducted on trial batches to investigate their mechanical properties. In addition, the effect of omitting the S2 fibers from the final mix design on mechanical properties was investigated. As discussed in Appendix A, due to severe clumping of the S2 fibers, their addition had to be restricted to 0.2% by volume. Furthermore, superior flow properties with greater segregation resistance were achieved in trial mixes with 0 volume percent of S2 fibers. Hence, the effect of 0.2 volume percent versus 0 volume percent of S2 fibers on the mechanical properties while maintaining a constant total fiber volume of 1.5% was investigated. Mix #34 and Mix #35 (see Appendix A) were utilized for the compression and flexure tests without conventional steel reinforcements. Mix #58 and Mix #59 (see Appendix A) were utilized for the compression and flexure tests with conventional steel reinforcements. Typical curing behavior for all samples consisted of a 7-day wet curing regime within the fog room (~96% relative humidity) located in the Concrete Laboratory on the UC Berkeley campus. Samples were then moved to an auxiliary laboratory room for a 21-day dry curing regime at ambient temperature and humidity. Samples were tested at 28 days unless noted otherwise.

2.4.1 Compression Tests

Compression tests were performed in order to determine whether the incorporated water/cement ratio achieved the specified strength and to compare the results between mixes with 0.2 volume percent and 0 volume percent of S2 fibers for the trial mixes #34 and #35 (see Table A.5). The compression setup used to capture axial stress-strain response was a compressometer shown in

Figure 2.7 with an 8 in.-gauge length tested by a 300 kips servo hydraulic Universal Testing Machine (UTM) in the Concrete Laboratory at UC Berkeley.

Figure 2.6 View of compressometer.

The compressometer consists of two aluminum rings that have three contact points with the cylinder via screws at 120^{o}. Linear Variable Differential Transformers (LVDTs) on opposing sides measure the axial displacement across the 8 in.-gauge length and are averaged to determine axial strain. Load is monitored by a load cell in the hydraulically controlled loading platform. Plots of axial stress–strain response are shown in Figure 2.7. Note that the end of a stress-strain curve does not indicate sudden failure for these fiber reinforced samples; it signifies that the test was stopped due to reaching the limit of an LVDT or when bearing on one of the aluminum rings occurred. All samples experienced a stable softening regime with no sudden changes in strain level or load capacity. The target value of 5 ksi in compressive strength was reached with the SC-HyFRC, and no considerable difference was observed in regards to compressive strength and softening behavior with and without the S2 fibers.

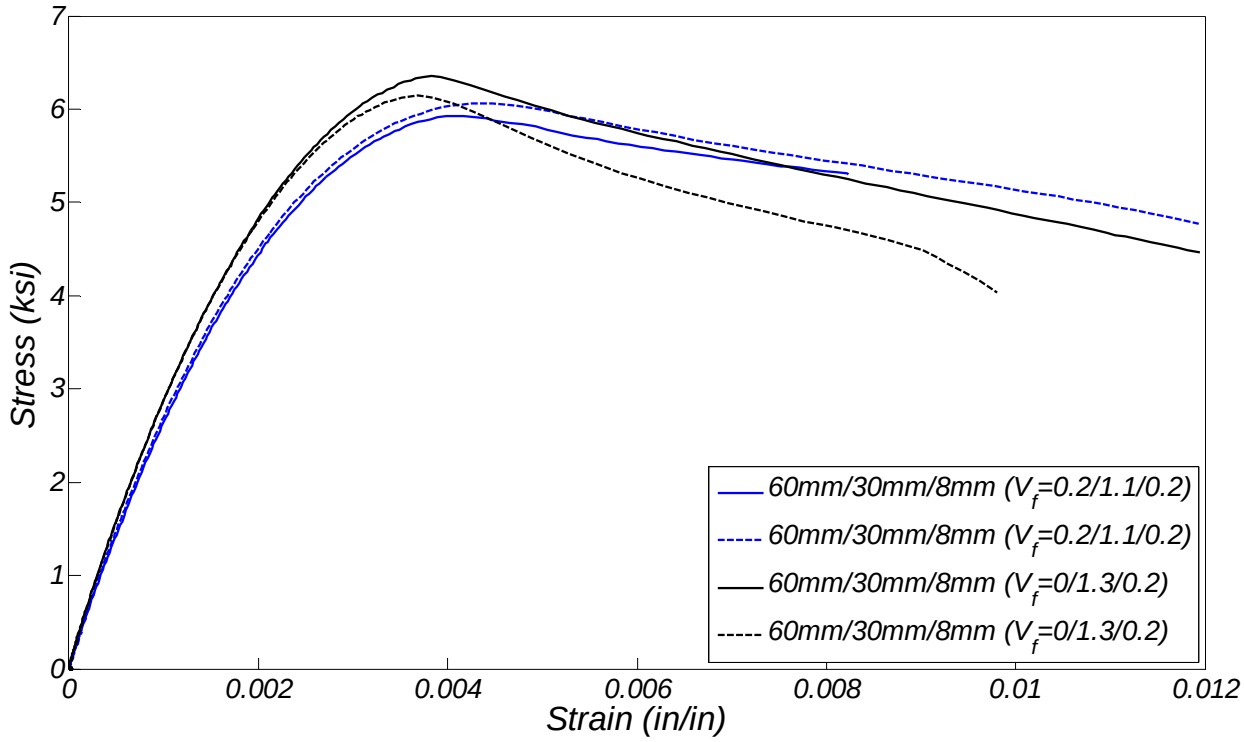

Figure 2.7 Compression test result comparison of mixes with and without S2 type steel fibers.

2.4.2 Flexure Tests without Conventional Reinforcement

Beams were tested with a 300 kips servo hydraulic Universal Testing Machine at the Concrete Laboratory at UC Berkeley. The test apparatus consisted of a four-point bending jig with pin and roller type supports. Both the load jig and support system allowed for out-of-plane rotation in order to eliminate torsional effects due to minor imperfections in specimen orthogonality. Specimen dimensions were 6 in. by 6 in. by 24 in. with a clear span of 18 in. This is illustrated in Figure 2.8. Flexure tests were carried out per ASTM C1609 (ASTM Standard C1609 2006), using displacement control with a servo controlled, closed loop system. A bending yoke—used in order to isolate actual beam displacements from extraneous displacements associated with support settlement and stiffness of the test apparatus—was anchored at the support points along the beam neutral axis. An LVDT was attached to the yoke on both sides of the beam, with the average displacement between the two LVDT's used as the measure of the beam centerline displacement. The average peak load and residual load at different deflections determined according to ASTM C 1609 are given in Table 2.3.

The principal points of interest are the load and displacement at the peak of the load deflection response (P_{peak} and δ_{peak}), residual load capacities at predefined deflection states ($P_{0.03}$ and $P_{0.12}$, which correspond to 0.03 in. and 0.12 in. of midpoint deflection respectively) and a measure of energy absorption capacity by means of toughness ($T_{0.12}$) which is calculated up to a midpoint deflection value of 0.12 in. Load-displacement plots were generated as shown in Figure 2.9. The trial mixes with and without S2 fibers exhibited the desired deflection hardening behavior, although a more consistent behavior was observed with the presence of the S2 fibers. There was no difference in the softening behavior with or without S2 fibers.

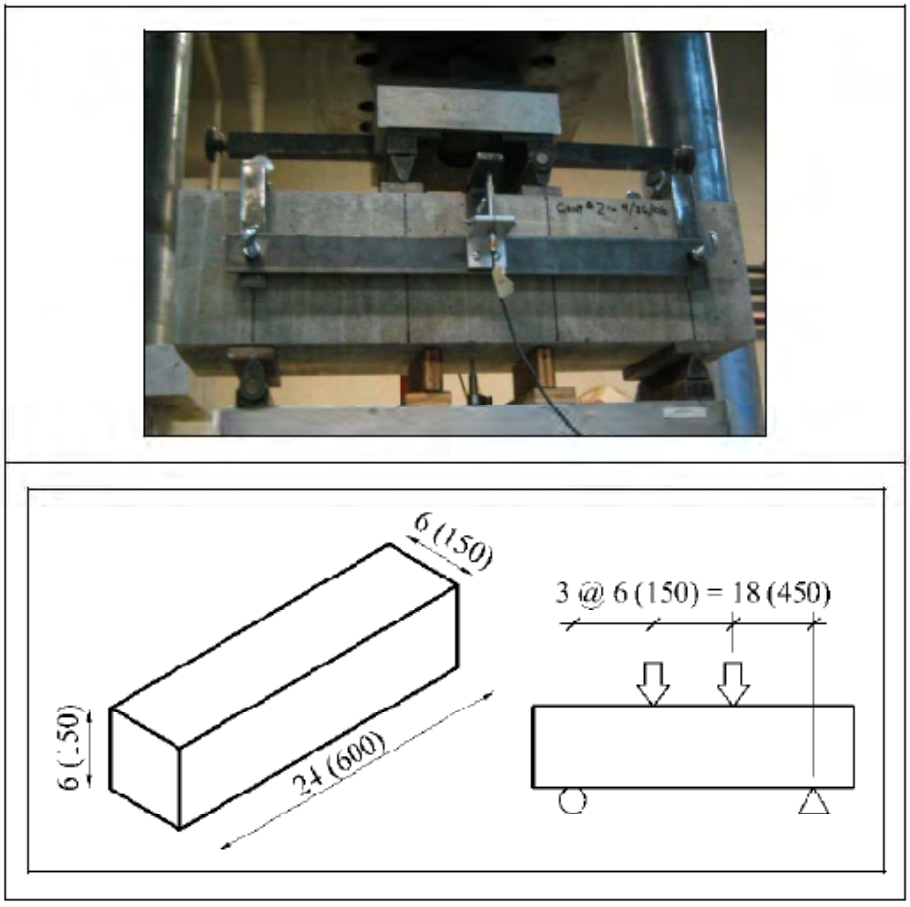

Figure 2.8 View of bending yoke and bending test setup.

Table 2.3 Bending test results of SC-FRC mixes with and without S2 type steel fibers.

V_f (S2/S1/PVA)	0.2/1.1/0.2	0.2/1.1/0.2	0/1.3/0.2	0/1.3/0.2
P_{peak} (kips)	13.71	14.03	14.87	11.19
δ_{peak} (in.)	0.022	0.028	0.026	0.022
$P_{0.03}$ (kips)	12.52	14	14.63	10.69
% Peak	91.32	99.79	98.39	95.53
$P_{0.12}$ (kips)	8.12	7.27	9.17	6.43
% Peak	59.23	51.82	61.67	57.46
$T_{0.12}$ (kips-in.)	1.257	1.262	1.460	1.055

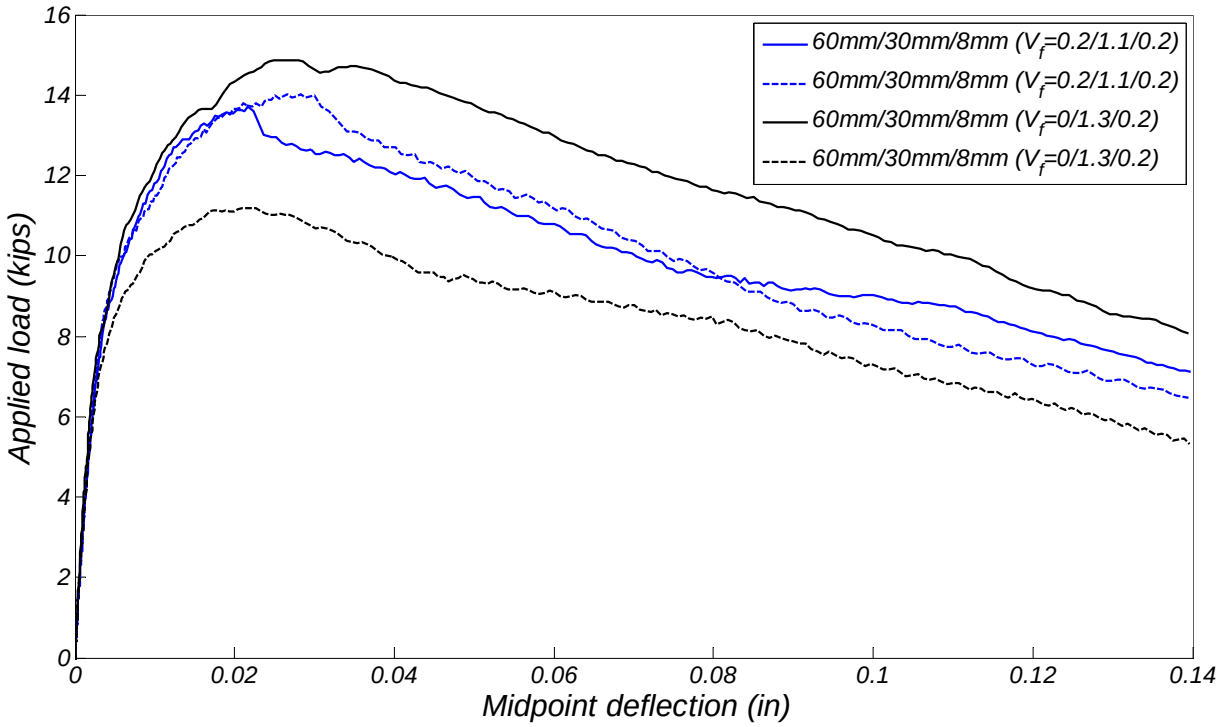

Figure 2.9 Bending test result comparison of mixes with and without S2 type steel fibers.

2.4.3 Flexure and Compression Tests with Conventional Reinforcement

Further testing was performed to establish the flow properties of self-compacting trial mixes in RC elements with samples of SCC and SC-FRC with and without S2 fibers. Reinforcing cages consisting of two #3 rebar at top and bottom with 0.25 in.-diameter steel rod transverse ties at 2 in. on center were constructed, as shown in Figure 2.10.

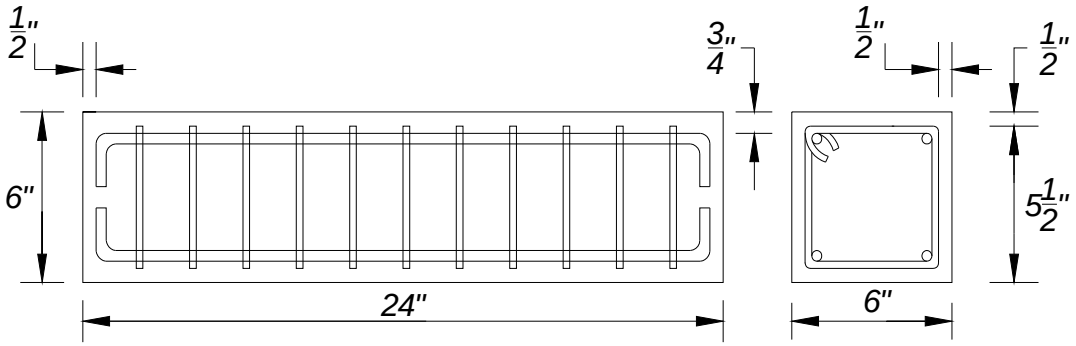

Figure 2.10 Reinforced beam design with #3 rebar and 0.25-in. ties.

The results of three coupon tension tests of the #3 rebar were conducted; the results are shown in Figure 2.11(a). The #3 rebar exhibited average yield strength of 54 ksi and an ultimate strength of 77 ksi. Three coupon tension tests of the 0.25 in. diameter steel rod were also conducted [see Figure 2.11(b)]. The steel rods exhibited average yield strength of 44 ksi and an ultimate strength of 64 ksi.

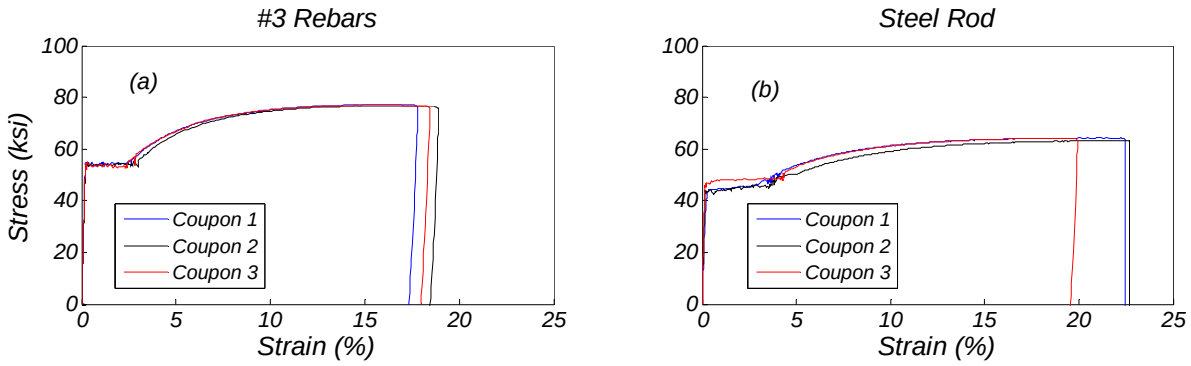

Figure 2.11 Tension test results: (a) #3 rebar; and (b) 0.25 in.-diameter steel rod.

A total of five reinforcing cages were produced, two for each fiber mix and one for a control sample of plain SCC. As observed during the casting procedure, the S2 fibers had

difficulty passing through the 2 in. tie-spacing without getting caught. The S1 fibers also exhibited some blockages but to a much lesser extent than the longer fibers. Consequently, a 1 in.-diameter vibration rod was used assist in the compaction of the concrete mixture.

To measure and generate load displacement curves, three point bending tests [see Figure 2.12(a)] were conducted using the same testing setup as previously described in Section 2.4.2. Nonlinearity of the control sample indicating crack initiation began at approximately 3 kips of loading [see Figure 2.12(b)]. In contrast, all reinforced SC-FRC beams remained linear until 5-7 kips of loading. Furthermore, at all displacements the load capacity of the SC-FRC beams was superior to the plain SCC beam. While shear cracks developed in the reinforced plain SCC beams [see Figure 2.11(c)], no shear cracks were observed in both fiber reinforced mixes as shown in Figure 2.11(d) for the beam reinforced with the S2 fiber. Again, no difference in behavior was observed between the 0 volume percent and 0.2 volume percent of S2 fibers in these specimens.

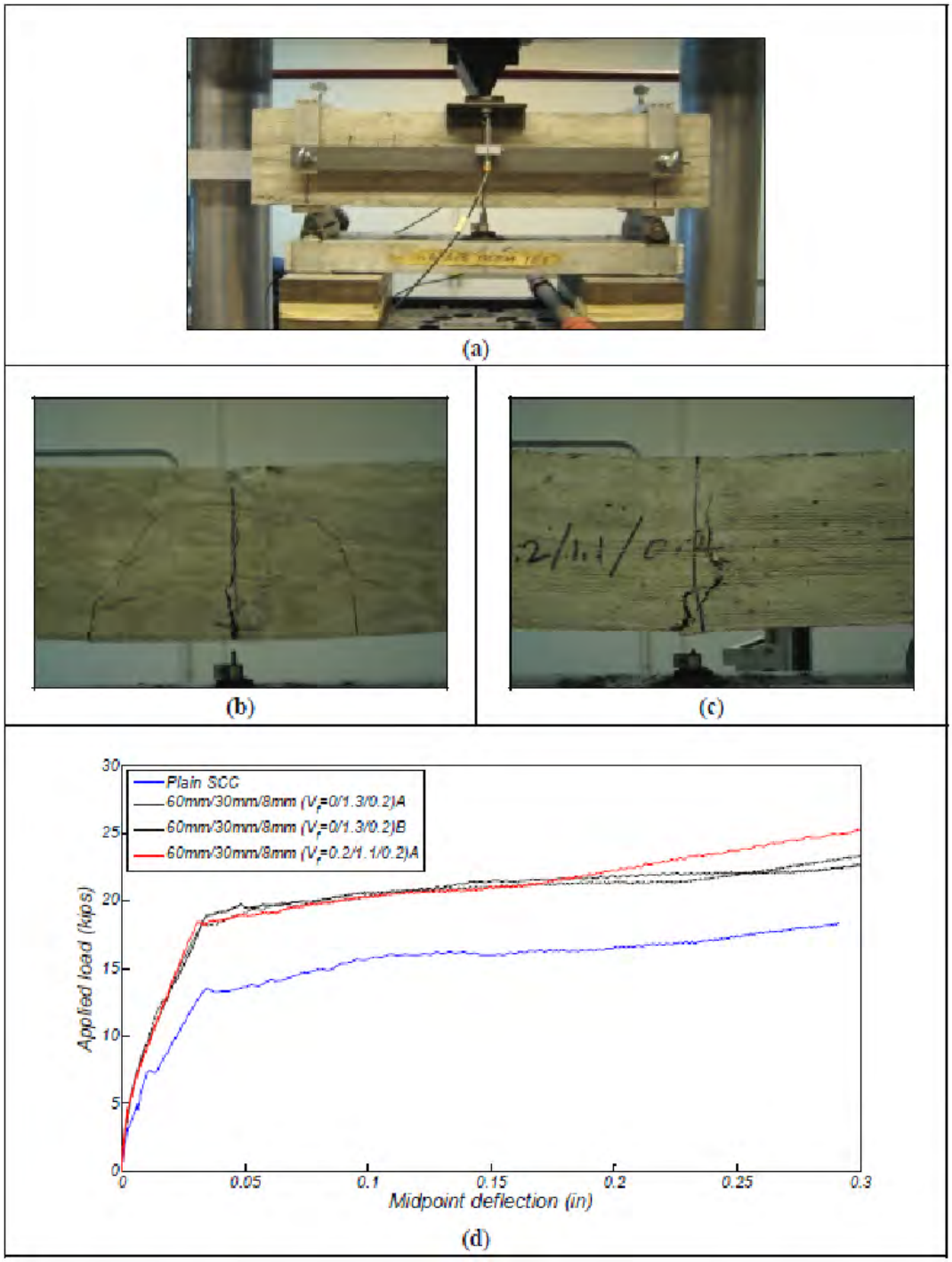

Figure 2.12 **Flexure tests of plain SCC and SC-FRC mixes with conventional reinforcing bars: (a) flexure test set-up; (b) flexure and shear cracks in conventionally reinforced plain SCC; (c) flexure cracks in conventionally reinforced SCC fiber reinforced composite with 0.2 volume percent of S2 fibers; and (d) flexure results for reinforced SC-FRC mixes and reinforced plain SCC.**

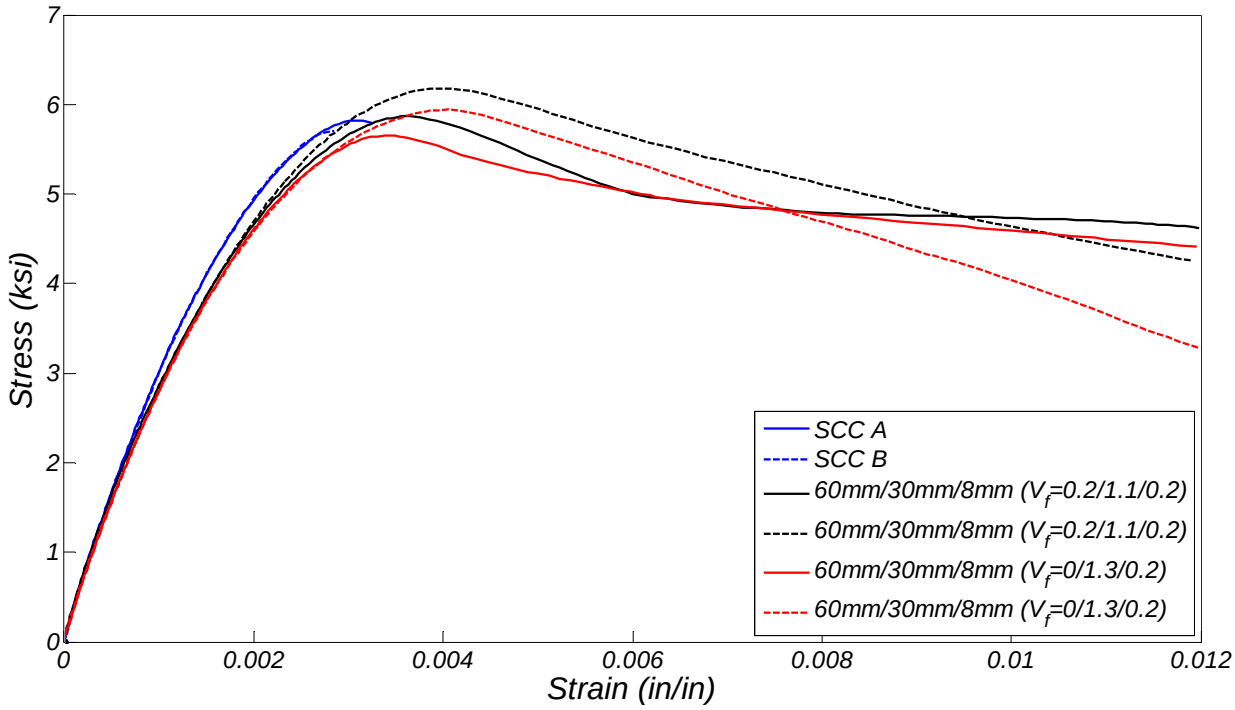

Figure 2.13 Compression test result comparison of SC-FRC mixes with plain SCC.

Table 2.4 Compression results of plain SCC and SC-FRC mixes.

Sample ID	SCC A	SCC B	0-1.3-0.2 A	0-1.3-0.2 B	0.2-1.1-0.2 A	0.2-1.1-0.2 B
Peak Stress (psi)	5822	5703	5869	6180	5651	5940
Axial Strain @ Peak (microstrain)	3154	2849	3645	3970	3375	4055
Lateral Strain @ Peak (microstrain)	1586	1004	1985	2290	2039	2303

Compression tests were also performed on 6 in. × 12 in. cylinder samples with and without S2 fibers and from the plain SCC sample. Two cylinders were tested for each mixture. The compression results are shown in Figure 2.12 and Table 2.4. While plain SCC samples failed in a brittle manner, both fiber reinforced samples with and without S2 fibers sustained a stable softening branch. No major difference in strength and softening behavior was observed between 0 volume percent and 0.2 volume percent of S2 fibers.

2.5 FINAL SC-HYFRC MIX DESIGN FOR BRIDGE COLUMNS

Since both the compression and flexure results with and without conventional reinforcements indicated no appreciable gain in strength or softening behavior with the presence of S2 fibers, they were eliminated in the final mix in favor of a more homogeneous fiber distribution with superior flow properties. The final mix design that exhibits the target flow characteristics and flow diameters of 24 in. in perpendicular directions without segregation while maintaining the deflection hardening properties with a total fiber volume of 1.5% is given in Table 2.5. The final mix design, designated SC-HyFRC, was utilized in both columns to accelerate their construction and to enhance their seismic performance.

Table 2.5 SC-HyFRC mix design in SSD condition.

Materials	lb / yd^3
Cement	670
Fly Ash	220
Water	400
FA	1760
CA	705
S1 Fiber	173
PVA Fiber	4
Superplasticizer	8.24
VMA	19.65

3 Specimen Design and Construction

3.1 GENERAL DESCRIPTION OF TEST PROGRAM

An experimental investigation was conducted to study the behavior of SC-HyFRC bridge columns subjected to static uni-directional cyclic load reversals. Two 1: 4.5 scale models were built and tested. The axial load was kept constant during testing and equal to 10% of the nominal axial load capacity of the column specimens for nominal concrete compressive strength f'_c = 5 ksi. The design of the two specimens differed only in the way nonlinear deformations were accommodated [see Section 3.3].

3.2 DETAILS OF PROTOTYPE COLUMN

A prototype highway overpass bridge was chosen based on the study by Ketchum et. al. (2004), which described a number of typical Caltrans bridges. Figure 3.1 shows the prototype tall overpass bridge, a five-span bridge single column bent with inner and outer spans of 150 ft and 120 ft, respectively, and a 39 ft wide deck. Figure 3.2 shows a section view of the deck and the column as well as the reinforcement details of the column. The column's longitudinal reinforcing steel ratio (ρ_l) is 1.2% while its transverse steel volumetric ratio (ρ_v) is 0.7%. The aspect ratio (H / D) of column height to the column diameter is 8.3.

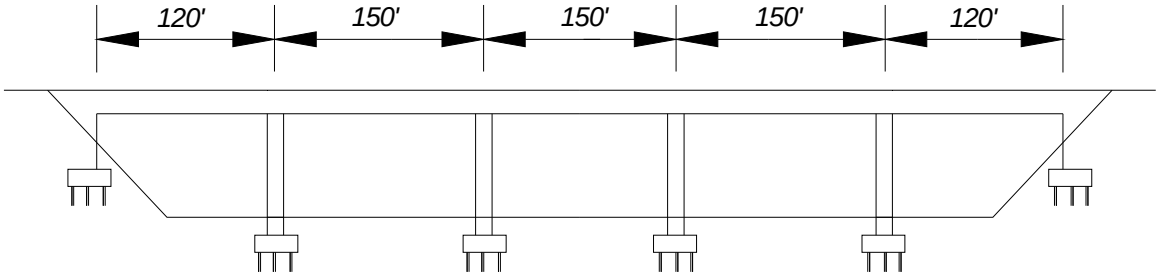

Figure 3.1 Elevation of prototype bridge (Ketchum et al. 2004).

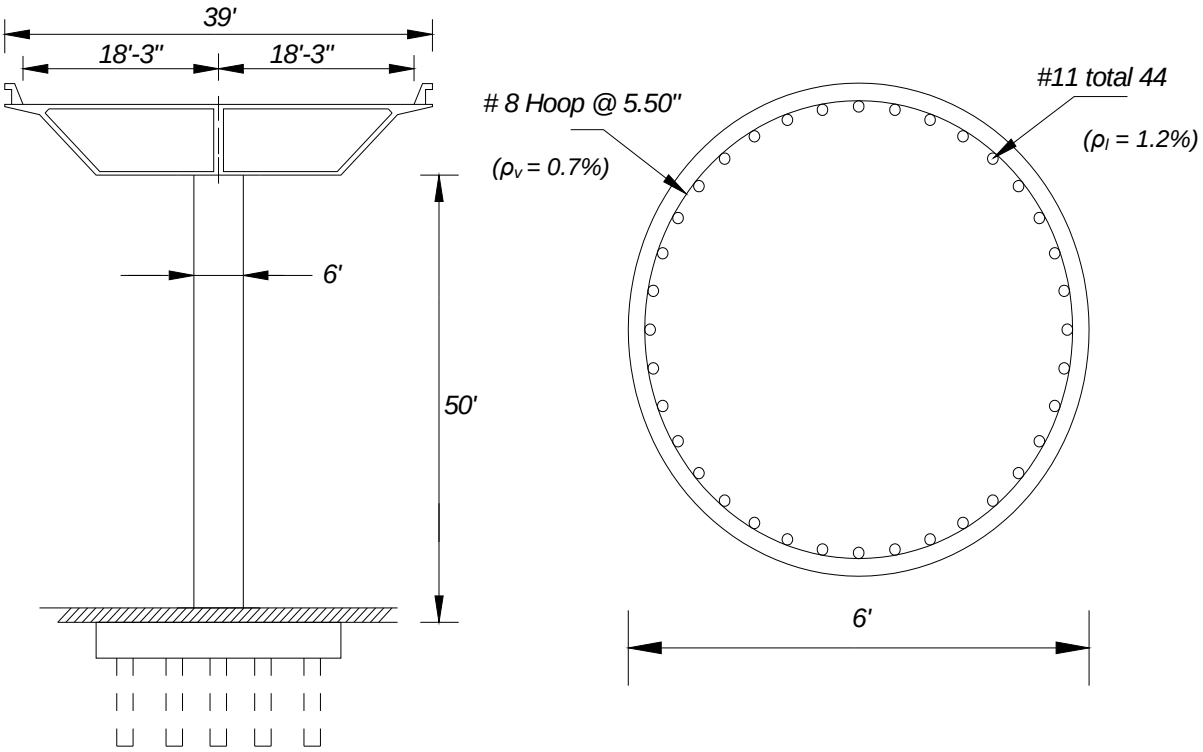

Figure 3.2 Geometry and reinforcement details of the prototype bridge column (Ketchum et al. 2004).

3.3 DESIGN OF TEST SPECIMENS

Assuming an inflection point at the mid-height of the prototype bridge column, M / VH is equal to 4, where M and V are the bending moment and shear force at the column ends, respectively, and H is the column height. To obtain the approximately same ratio of M / VH as the prototype

column, the test specimens had a column diameter of D = 16 in. and H = 67.25 in. where H is from the top of the foundation to the point of load application. These specimens were then subjected to single bending.

The two test specimens were identical in terms of their dimensions and longitudinal and transverse reinforcing ratios, the only difference being the way nonlinear deformations were accommodated. The first specimen, referred to as Test Specimen 1 (TS-1), was designed to rock at the column-foundation interface. The longitudinal reinforcement of this specimen was detailed so that it was unbonded over the bottom part of the column. Here SC-HyFRC was used only in the column part above the foundation. The second test specimen, referred to as Test Specimen 2 (TS-2), was designed to form a flexural plastic hinge at the column base and used stainless steel for the longitudinal reinforcement. Here the column was cast into the foundation that contained a corrugated metal pipe. The SC-HyFRC was used in the column above the foundation and within the corrugated pipe located in the foundation. Table 3.1 summarizes the design parameters of the two test specimens.

Table 3.1 Test specimen design parameters.

Specimen	Scaling factor	D (in.)	H (in.)	H / D	ρ_l (%)	ρ_v (%)
1	4.5	16	67.25	4.20	1.2	0.37
2	4.5	16	67.25	4.20	1.2	0.37

3.3.1 Specimen TS-1

Figure 3.3 shows an elevation and a section view of specimen TS-1, as well as column reinforcement details. The longitudinal reinforcement consisted of twelve #4, A706, bars distributed uniformly around the column perimeter, corresponding to longitudinal steel ratio of ρ_l = 1.2%. A W3.5, ASTM A82 continuous steel spiral was chosen with a 2.5 in. center-to-center spacing corresponding to volumetric confinement steel ratio of ρ_v = 0.37%. The clear concrete cover was 0.5 in. thick.

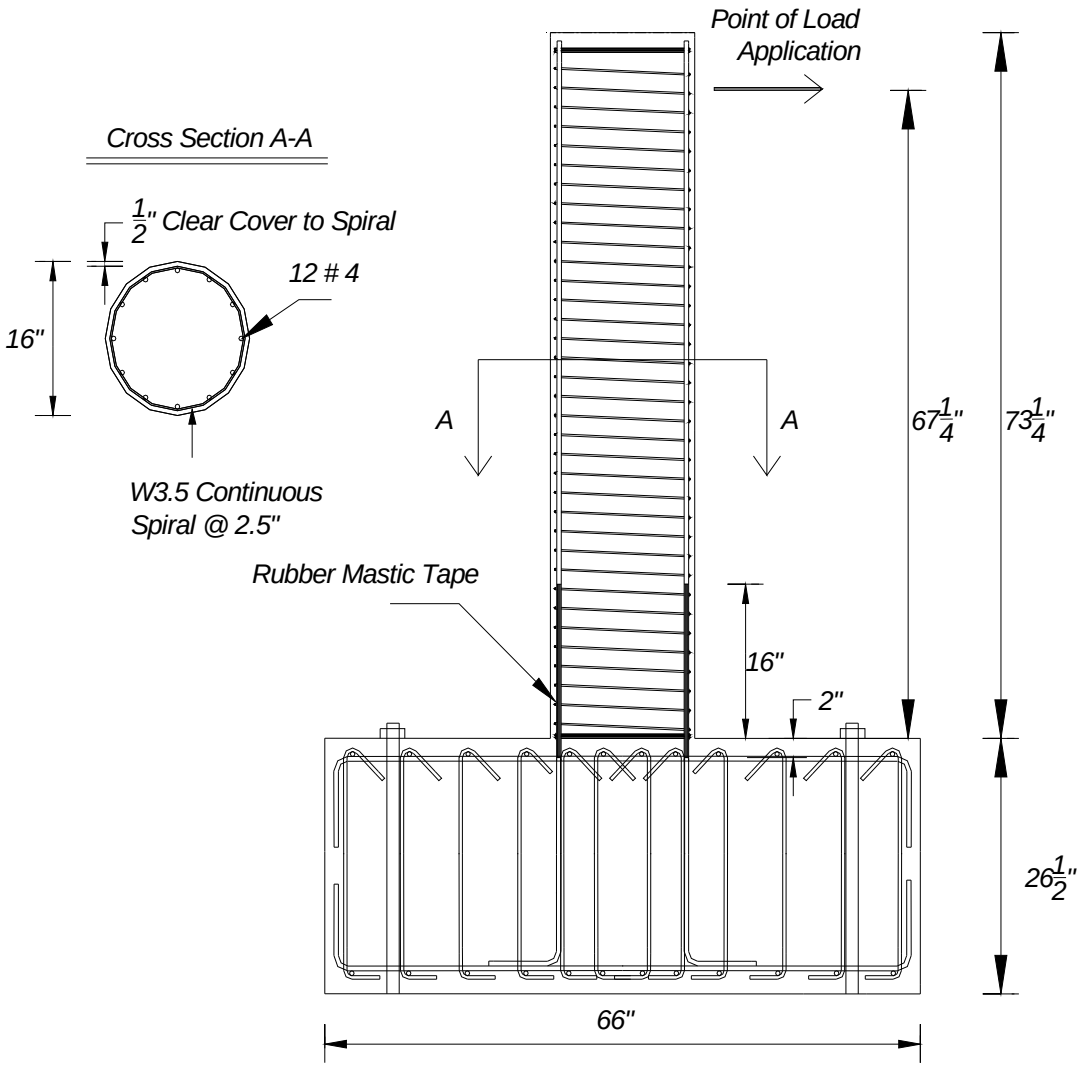

Figure 3.3 Geometry and reinforcement details of TS-1.

In order for the column to rock at the column/foundation interface with acceptable smeared strains in the reinforcing steel along the unbonding length, the longitudinal reinforcement was unbonded, using a rubber mastic tape, over the bottom 16 in. of the column and 2 in. inside the foundation to avoid tension failure of the foundation top concrete cover. An unbonding length of 18 in. was chosen to achieve a smeared strain of 4.4% at a drift ratio of 5%. The calculation for the smeared strain (i) assumes that the column deforms as a rigid body that rocks at the column-foundation interface, (ii) ignores the neutral axis depth, and (iii) ignores the strain penetration at both ends of the unbonding length. The calculated nominal shear strength of the column for a concrete compressive strength of 5 ksi, and a steel yield strength of f_y = 90 ksi

for the spiral reinforcement [see Figure 3.3], based on section 21.5.4.2 of ACI-318 (ACI 318, 2002) was equal to V_n = 38 kips. In order to avoid premature buckling of the longitudinal reinforcement, the ratio of transverse reinforcement spacing to longitudinal bar diameter was set equal to 5.

3.3.2 Specimen TS-2

Figure 3.4 shows the geometry and the reinforcement details of TS-2. The dimensions of the test TS-2 were identical to those of TS-1. This specimen was designed to form a flexural plastic hinge at the column base. To account for the enhanced bond between the steel rebar and the SC-HyFRC, and to enhance the spread of plasticity within the plastic hinge, stainless steel was used for the longitudinal reinforcement. Stainless steel is characterized by strain hardening behavior immediately after yielding without the presence of a yield plateau. This stress-strain behavior was considered optimal to avoid localized cracking of the concrete and to improve the spread of plasticity. In addition, stainless steel has a very high strain capacity that can delay bar fracture. To take advantage of the enhanced properties of the SC-HyFRC in tension, and to avoid a possible single crack localization at the column-foundation interface, the column was cast into the foundation with SC-HyFRC using a corrugated steel pipe located inside the foundation [see Figure 3.6(b)].

The longitudinal reinforcement consisted of eight #5, stainless steel A316L bars distributed uniformly around the column perimeter, corresponding to ρ_l = 1.2%. Similarly to TS-1, a continuous W3.5 (ASTM A82) steel spiral at center-to-center spacing of 2.5 in. was provided, corresponding to ρ_v = 0.37%. For TS-2, the ratio of transverse reinforcement spacing to longitudinal bar diameter was equal to 4.

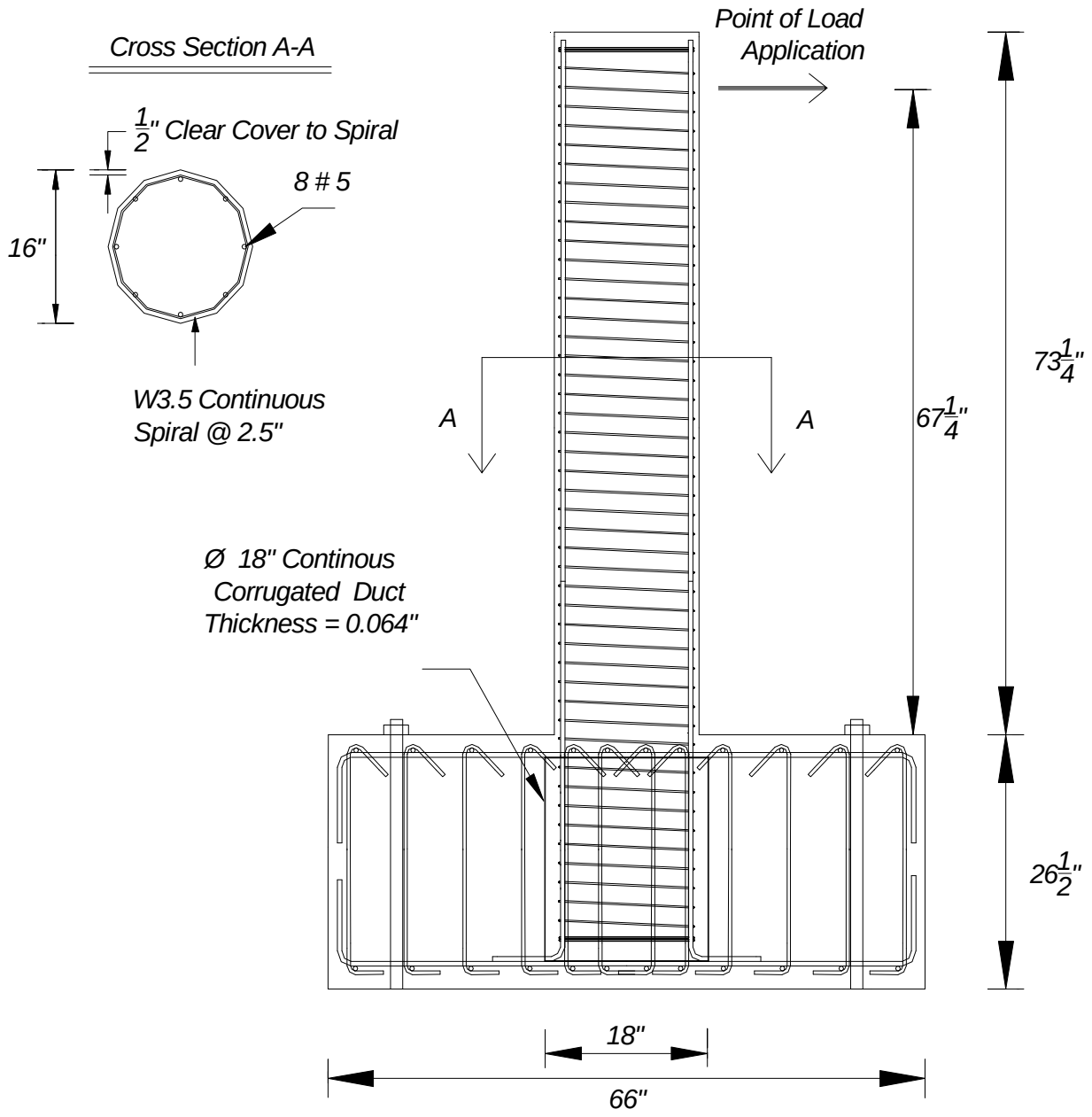

Figure 3.4 Geometry and reinforcement details of TS-2.

3.4 CONSTRUCTION OF TEST SPECIMENS

Construction and testing of the test specimens took place in the Structural Laboratory located in Davis Hall, which houses the Civil and Environmental Engineering Department of the University of California, Berkeley. For both specimens the reinforcing steel cages for the foundation and the column as well as the foundation formwork were constructed by an outside contractor. Next, the

concrete foundations were cast and allowed to set before casting of the columns. A contractor was hired to cast the concrete for the foundation; the SC-HyFRC was developed and cast by the research team with the support of the Davis Hall Laboratory personnel. Figure 3.5 and Figure 3.6 show photos of the construction procedure of the two specimens at different stages.

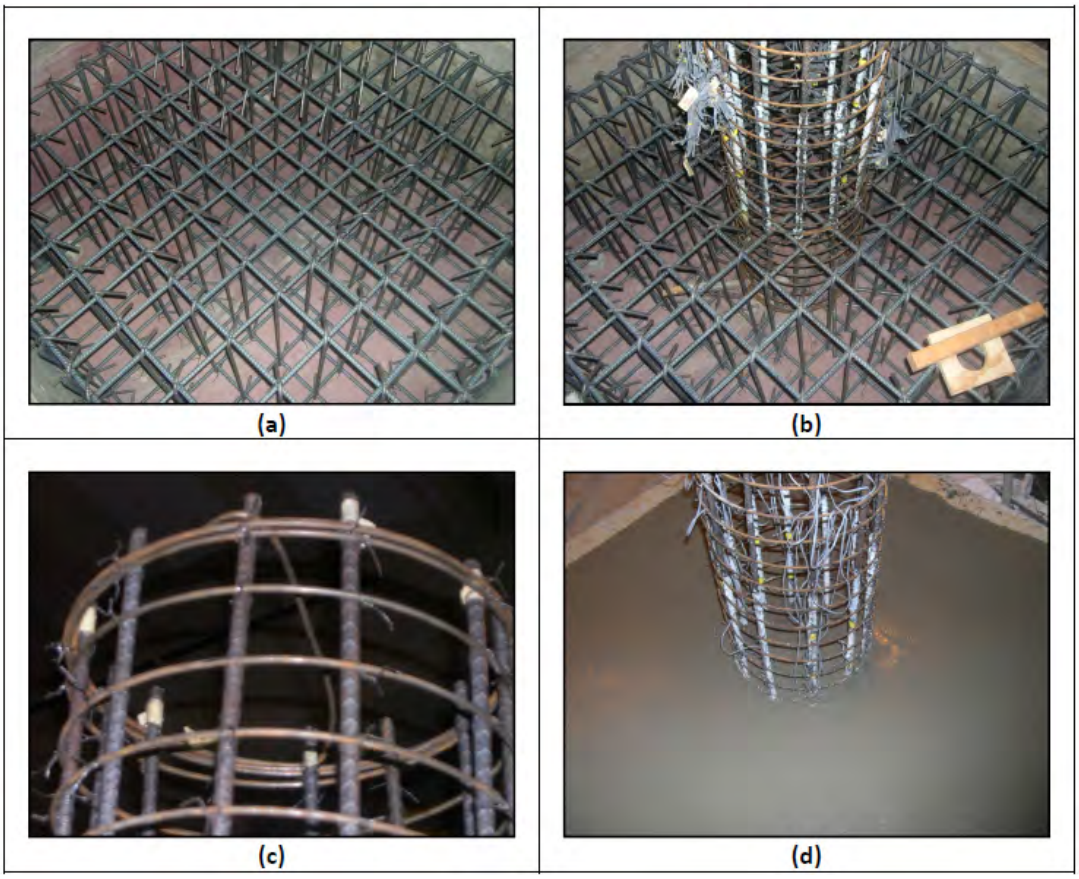

Figure 3.5 **Construction photos of TS-1: (a) foundation reinforcement cage; (b) foundation and column reinforcement cage; (c) close up of top of spiral reinforcement cage; and (d) foundation after casting.**

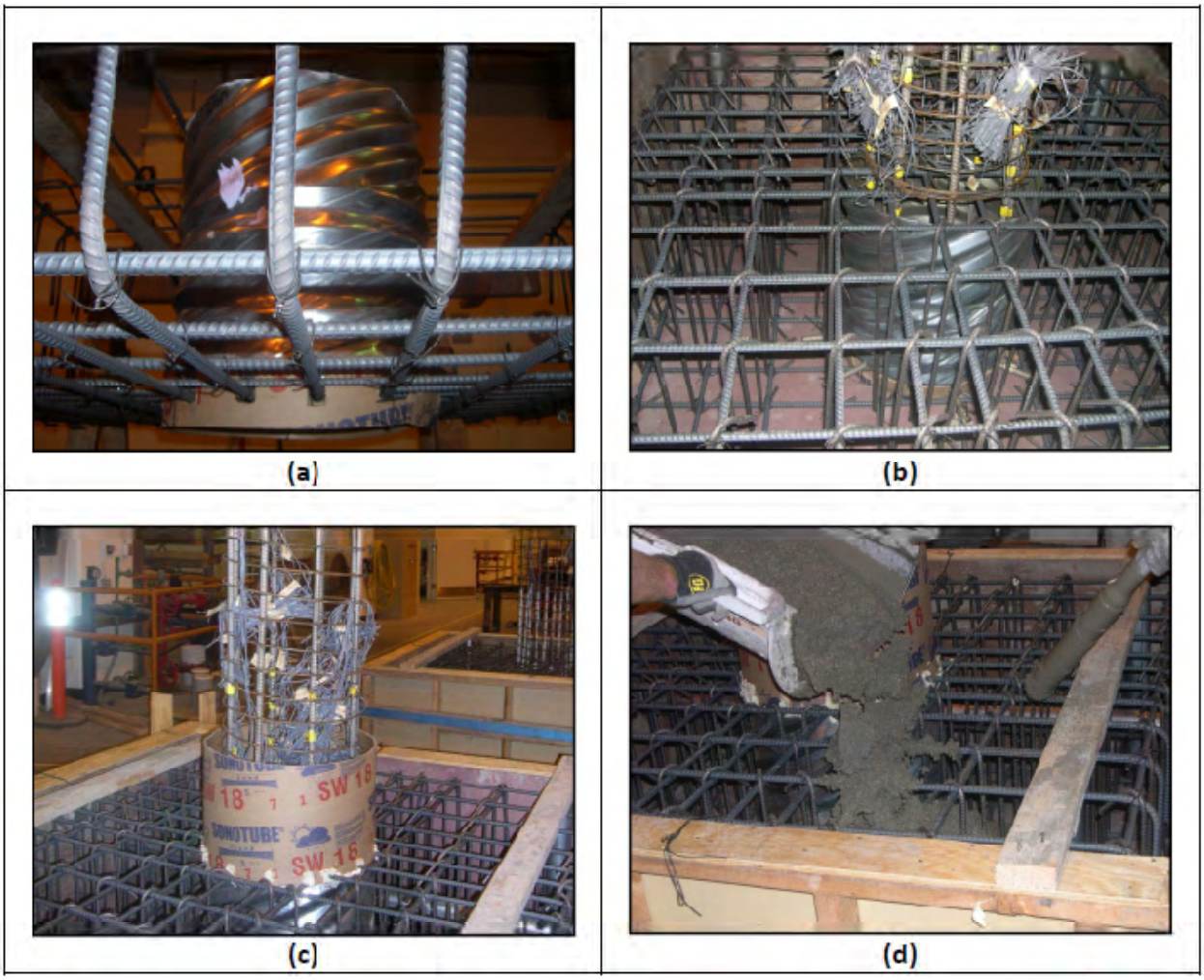

Figure 3.6 **Construction photos of TS-2: (a) side view of corrugated steel pipe; (b) top view of corrugated steel pipe; (c) foundation and column reinforcement cage; and (d) pouring of foundation concrete.**

3.5 DESCRIPTION OF MATERIALS USED IN CONSTRUCTION

3.5.1 Steel

Table 3.2 summarizes the different types of steel used in the construction of the two test specimens: TS-1 and TS-2 were constructed using ASTM A706 Grade 60, and A316 stainless Grade 60 steel, respectively, for the longitudinal reinforcement. Both test specimens had smooth continuous W3.5 ASTM A82 spiral wire as transverse reinforcement.

Table 3.2 Type of steel used in test specimens.

	TS-1	TS-2
Longitudinal Reinforcement	Steel706, Grade 60	Stainless Steel 316, Grade 60, ASTM A955
Transverse Reinforcement	ASTM A82	ASTM A82
Foundation Reinforcement	Steel706, Grade 60	Steel706, Grade 60
Corrugated Pipe	N / A	Galvanized Steel, ASTM A92

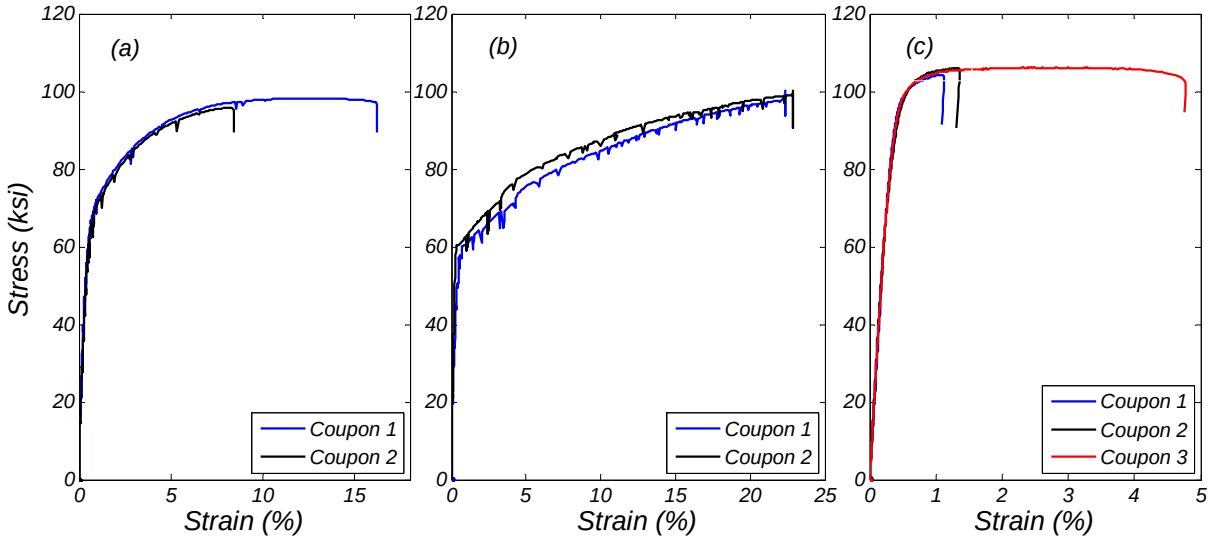

Figure 3.7 Tensile stress-strain coupon test results of the three types of steel used in the test specimens: (a) # 4 A706, Grade 60 rebar; (b) #5 A316 stainless steel rebar; and (c) smooth W3.5 spiral.

Figure 3.7 plots the measured stress-strain behavior of the steel coupons tests: Figure 3.7(a) plots the stress strain of the #4 A706 Grade 60 steel, which did not demonstrate any yield plateau and hardened directly after yielding. In general, typical reinforcing bars experience yield plateau before the strain hardening region; Figure 3.7(b) as expected, A316 #5 bars demonstrated no yield plateau but a hardening behavior directly after yielding and were able to attain large strains up to 25% before failure; and Figure 3.7(c) plots the stress strain behavior of the W3.5 spiral wire reinforcement, which also did not demonstrate any yield plateau. This type of steel was intentionally selected to avoid the reduced stiffness of transverse reinforcement associated with a yield plateau. The coupon tests of the W3.5 spiral wire showed significant variations in

maximum attained strain, which is believed to be due to the procedure used to extract and straighten the test coupons from the spiral. The maximum strain capacity of the spiral was limited to less than 5%.

3.5.2 Casting SC-HyFRC and Mechanical Properties of SC-HyFRC

Because TS-1 required a total volume of 0.32 yd^3, two SC-HyFRC mixes were produced on site in the concrete laboratory at UC Berkeley, termed Mix 1 and Mix 2, respectively. Two 6 in. × 12 in. cylinders and two 6 in. × 6 in. × 24 in. beams were cast for each mix in order to conduct material test. The mix volumes produced on the day of casting were 0.237 yd^3 and 0.227 yd^3. Mixing weights are included in Appendix B with relevant free moisture measurements of the fine and coarse aggregate accounted for. Slump flow property testing of fresh concrete taken during the specimen casting exhibited perpendicular flow diameters of 19 in. × 18 in. for Mix 1 and 20 in. × 19 in. for Mix 2. The casting of TS-1 with Mix 1 which was used for the bottom part of the column is shown in Figure 3.8

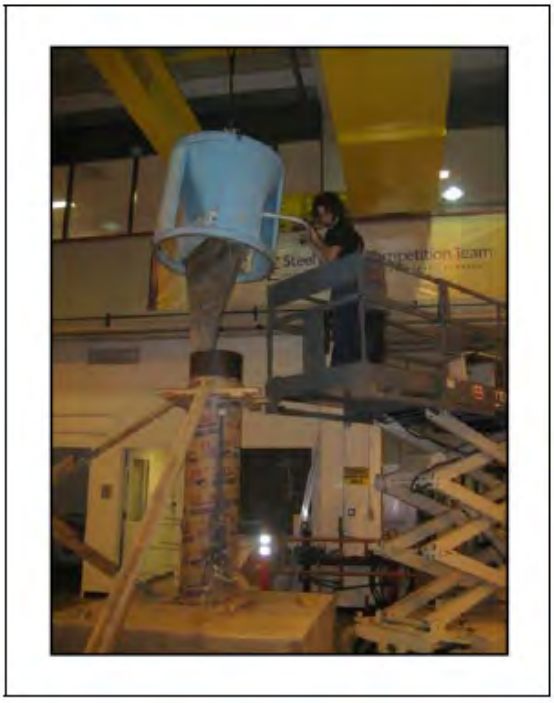

Figure 3.8 Casting of TS-1 with Mix 1.

When casting the test specimen, a 1 in-diameter stick vibrator was used to lightly vibrate the concrete once placed in the formwork. With no previous encounters with mixing and casting at this large a scale, the self-compacting properties and air entrapping properties of the mix were uncertain. The light vibration was done to ensure that no large air voids remained. The level of vibration was much less than would be performed on conventional concrete during placement.

Compression cylinder and beam four point tests of Mixes 1 and 2 were conducted 1t 58 days; results are shown in Table 3.3 and Table 3.4, respectively. The designation of which sample should be “a” and which should be “b” was arbitrary, and simply determined by the order of sample testing. The bending test results for Mixes 1 and 2 after 58 days are plotted in Figure 3.9.

Table 3.3 Compression test results of TS-1 SC-HyFRC mixes after 58 days.

Mix #/Sample ID	1-a	1-b	2-a	2-b
f'_c (psi)	5121	5135	5662	5634

Table 3.4 Bending test results of TS-1 SC-HyFRC mixes after 58 days.

Mix # - Sample ID	1-a	1-b	2-a	2-b
P_{peak} (kips)	11.75	11.34	8.51	11.50
δ_{peak} (in)	0.018	0.012	0.018	0.032
$P_{0.03}$ (kips)	11.41	9.55	8.04	11.37
% Peak	97.13	84.24	94.49	98.85
$P_{0.12}$ (kips)	6.39	4.69	3.87	6.87
% Peak	54.36	41.34	45.44	59.75
$T_{0.12}$ (kip-in)	0.626	0.564	0.449	0.707

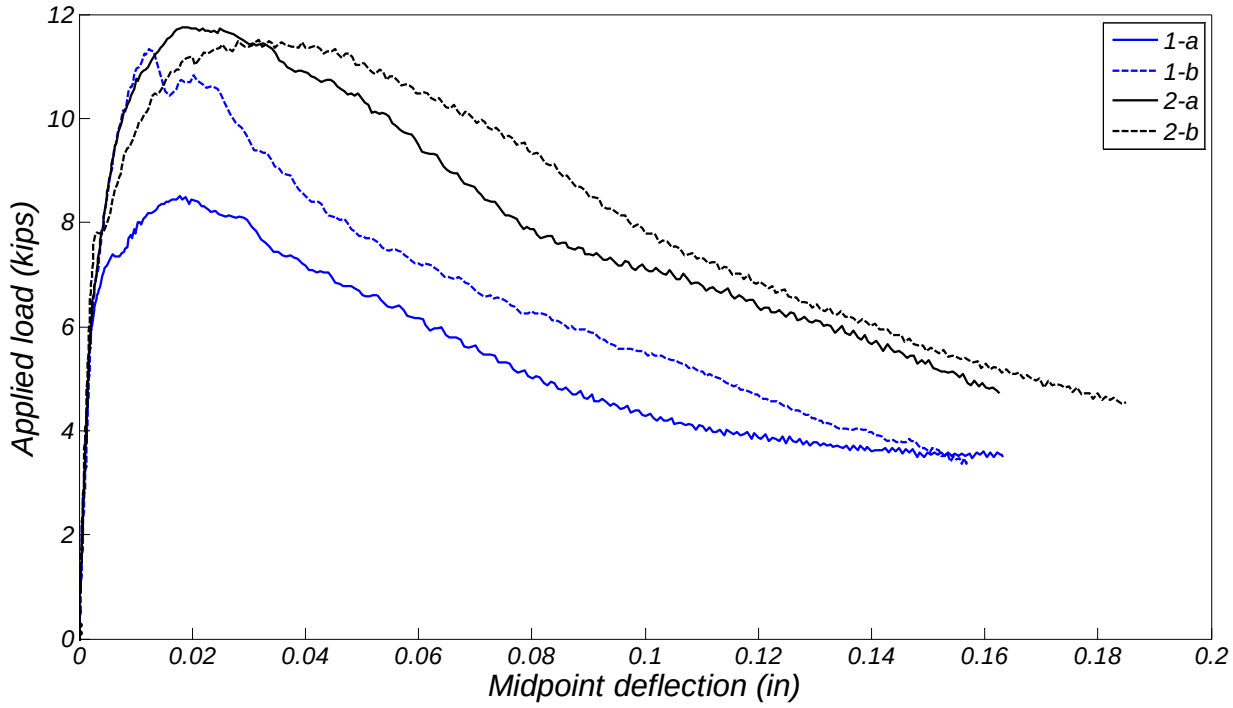

Figure 3.9 Applied load versus midpoint deflection curves of SC-HyFRC for TS-1.

Because Specimen TS-2 had a total volume of 0.46 yd^3 requiring three SC-HyFRC mixes—termed Mixes 3, 4 and 5, respectively, which were produced on site in the concrete laboratory at UC Berkeley—once again an additional two 6 in.× 12 in. cylinders and two 6 in. × 6 in. × 24 in. beams were cast for each mix in order to conduct material test in conjunction with the second specimen test. The mix volumes made on the day of casting were 0.153 yd^3, 0.396 yd^3, and 0.227 yd^3.*. Potential FRC-FRC cold joints were placed away from locations considered critical regions (such as the base of the free standing portion of the test specimen and the lower third which would experience the largest bending stresses). Testing of the flow property of the fresh concrete was performed during the casting of the columns. The perpendicular flow diameters were 16.5 in. × 15.5 in. for Mix 3, 19 in. × 16.5 in. for Mix 4, and 19 in. × 18 in. for Mix 5. Mix 3 was cast into the lower section of the corrugated steel pipe up to 3 in below the top of the foundation. Mix 4 was cast such that it was in all of the critical locations of TS-2 (column-foundation interface and plastic hinge region). Mix 5 was used in the top part of the column.

* Mixing weights are included in Appendix B with relevant free moisture measurements of the fine and coarse aggregate accounted for

During the casting process it was noted that the setting time of Mix 3 appeared to be faster than had been previously encountered, which made the mix more difficult to work with.

A 1 in.-diameter stick vibrator was again used to ensure the expulsion of any large air voids due to the uncertainty associated with large scale mixing and air entrapping properties of SC-HyFRC. Care was taken to limit the effect that vibration might have on segregating the concrete mix.

Cylinder samples made from Mix 5 were tested at early ages to ensure strength development. Compression tests were performed at 10 days and 19 days, respectively; results are listed in Table 3.5. The strength of Mix 5 at the test date was determined to be inconsequential due to the expected low bending stresses developed at that height of the test specimen. Cylinder and beam samples of Mixes 3 and 4 were tested at 62 days for compressive strength and bending properties in accordance with ASTM C1609; results are shown in Figure 3.10 (Table 3.6) and Figure 3.11 (Table 3.7), respectively.

Table 3.5 Compression test results of TS-2 SC-HyFRC Mix 5.

Mix# - Sample ID	5-a	5-b
Age (days)	10	19
P_{max} (lbs)	98500	122900
f'_c (psi)	3480	4347

Table 3.6 Compression test results of TS-2 SC-HyFRC Mixes 3 and 4 at 62 days.

Mix# - Sample ID	3-a	3-b	4-a	4-b
P_{max} (lbs)	186700	186400	164200	165500
f'_c (psi)	6603	6593	5809	5855

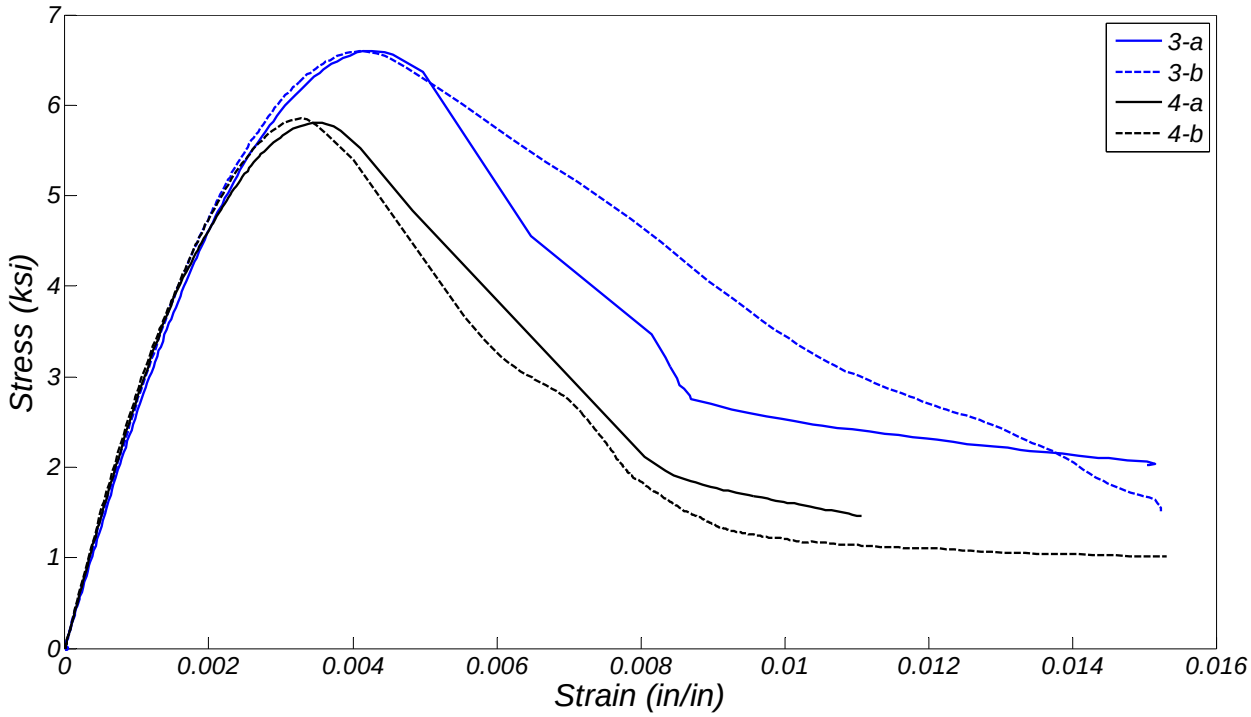

Figure 3.10 Longitudinal compression stress-strain curves of SC-HyFRC for TS-2.

All cylinders tested at 62 days achieved their targeted strength goals [see Table 3.6], with peak strength being reached at 4000 ± 1000 microstrain [see Figure 3.10]. Softening behavior was observed in both samples, though the residual strengths of Mix 3 and 4 cylinders were lower than previously encountered.

Beam testing in accordance with ASTM Standard C1609 was performed* As previously noted, the setting of Mix 3 occurred noticeably faster compared to the other mixes and was correspondingly more difficult to place in the beam forms and ensure adequate and homogeneous compaction. This may explain the poor performance exhibited by beam samples 3a and 3b, neither of which illustrates the characteristic deflection hardening behavior to be expected with this mix design. Since this mix was used only in the corrugated steel pipe located in the foundation, its performance is not as critical. Regardless, all mixes were exceptionally good at maintaining near 90% residual load capacity at a midpoint deflection of 0.03 in. with several samples still undergoing hardening behavior [see Table 3.7]. Residual strength values at the second displacement target (0.12 in.) ranged from approximately 40-70%.

* See plots in Appendix B.

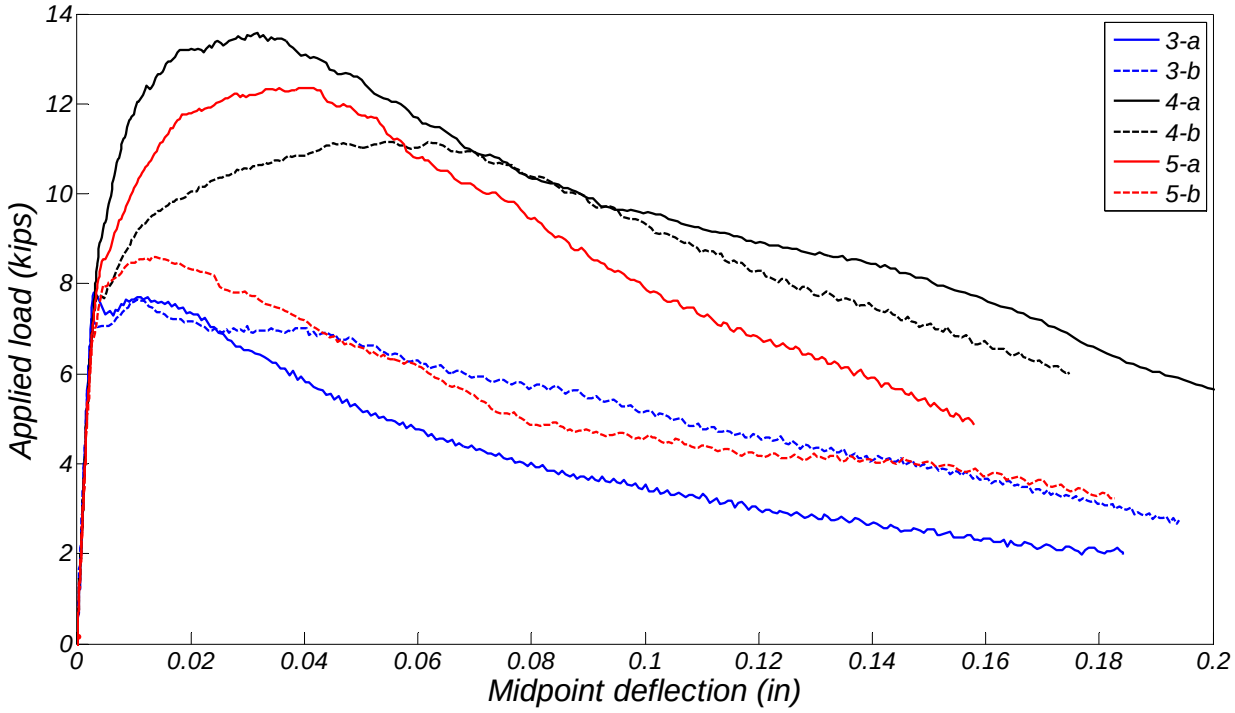

Figure 3.11 **Applied load versus midpoint deflection curves for TS-2 SC-HyFRC mixes after 62 days.**

Table 3.7 **Bending test results of TS-2 SC-HyFRC mixes after 62 days.**

Mix # - Sample ID	3-a	3-b	4-a	4-b	5-a	5-b
P_{peak} (kips)	7.65	7.81	11.16	13.58	8.58	12.36
δ_{peak} (in)	0.011	0.003	0.055	0.032	0.013	0.036
$P_{0.03}$ (kips)	7.06	6.52	10.576	13.52	7.76	12.20
% Peak	92.33	83.51	N/A	N/A	90.40	N/A
$P_{0.12}$ (kips)	4.60	2.97	8.29	8.92	4.17	6.78
% Peak	60.16	38.04	74.27	65.69	47.76	54.84
$T_{0.12}$ (kip-in)	0.736	0.602	1.187	1.326	0.732	1.185

4 Experimental Setup and Test program

4.1 TEST SETUP

Both test specimens were tested statically under uni-directional cyclic load reversals. Figure 4.1 and Figure 4.2 show a plan view and east elevation view, respectively, of the test setup. The lateral load was applied using two horizontal actuators inclined at 45^o. Two vertical actuators applied a constant 100 kips vertical load for the duration of the test. The N = 100 kips of axial load corresponded to an axial load ratio $N / f'_c A_g = 0.1$, where $f'_c = 5$ ksi, the nominal concrete compressive strength and A_g the column gross sectional area. The vertical load was applied through a spreader beam placed at the top of the test specimen. Figure 4.3 shows a photo of the test setup. The foundation of each test specimen was anchored to the strong floor using four post-tensioned DSI rods. The direction of loading was in the east-west direction.

4.2 INSTRUMENTATION

The external and internal instrumentation of the test specimen consisted of displacement transducers and strain gauges, respectively. A total of 8 vertical transducers and 38 strain gauges were used in TS-1 and 14 vertical transducers and 52 strain gauges for TS-2, respectively.

4.2.1 Instrumentation of TS-1

The cross section of TS-1 with reference numbers of the twelve #4 longitudinal rebar is shown in Figure 4.4 As shown in Figure 4.5, TS-1 was instrumented internally with 4 strain gauges on each of the longitudinal bars: C101, C102, C107, C108 and C110. A total of 18 strain gauges were placed on the spiral reinforcement as shown in Figure 4.6. These strain gauges were placed

on both sides of the spiral at each instrumented location. As shown in Figure 4.7, eight vertical displacement transducers were attached to the test specimen.

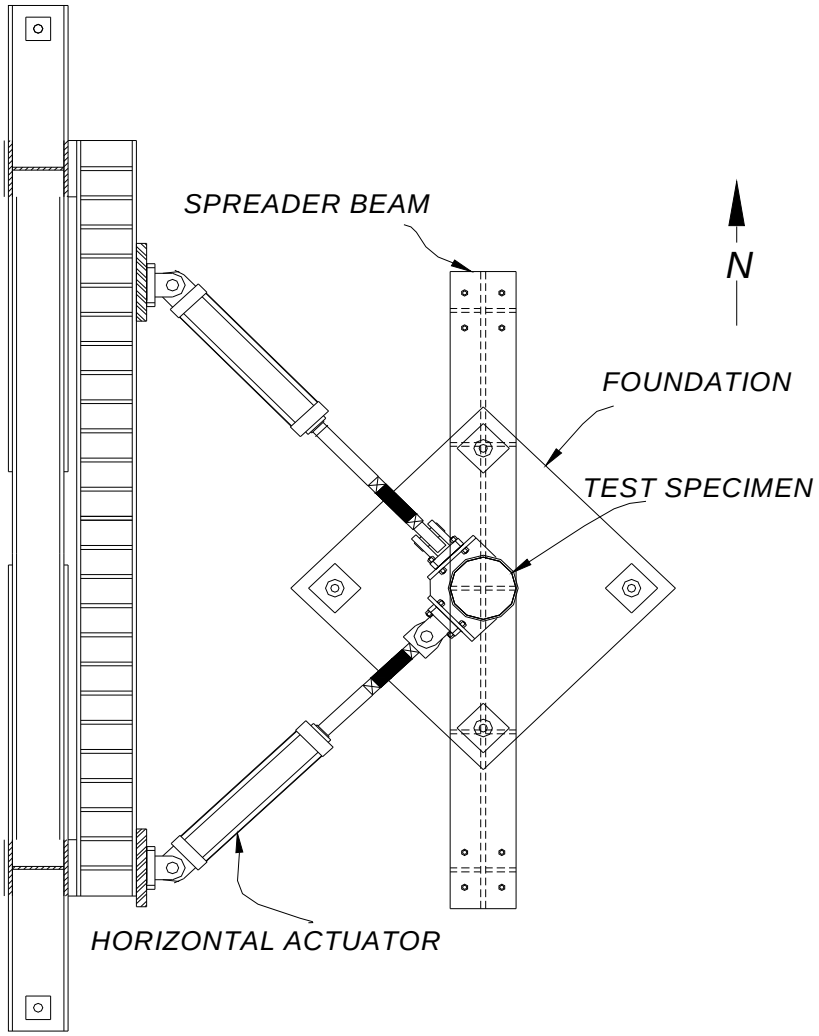

Figure 4.1 Plan view of test setup.

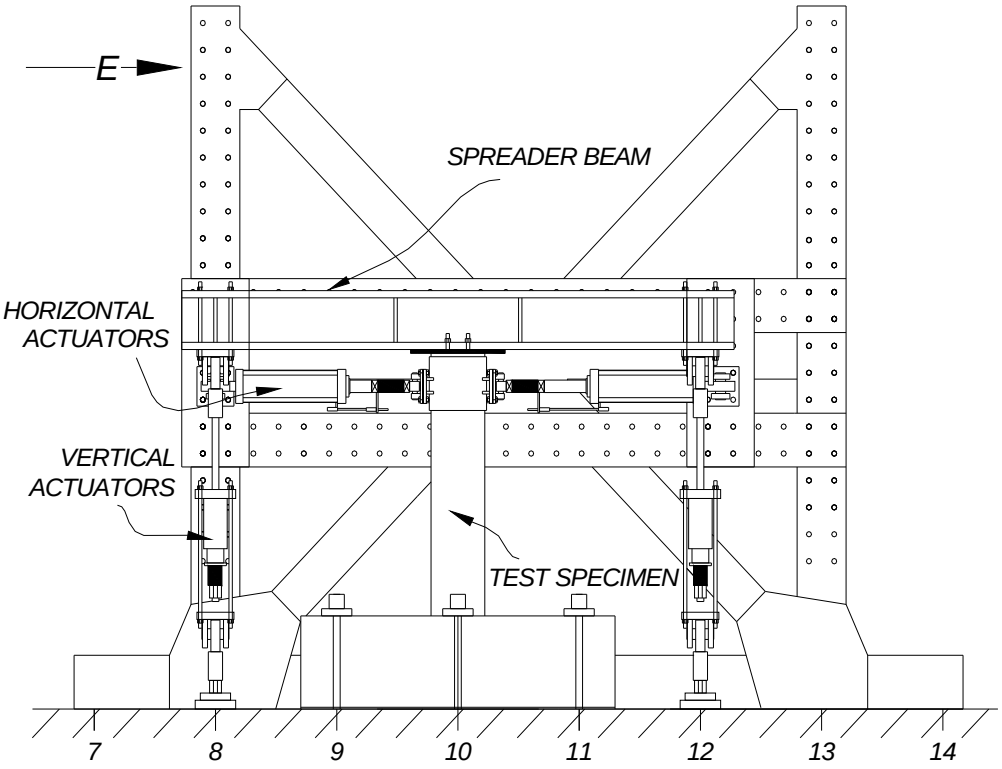

Figure 4.2 Elevation view of the test setup.

Figure 4.3 Global view of the test set up.

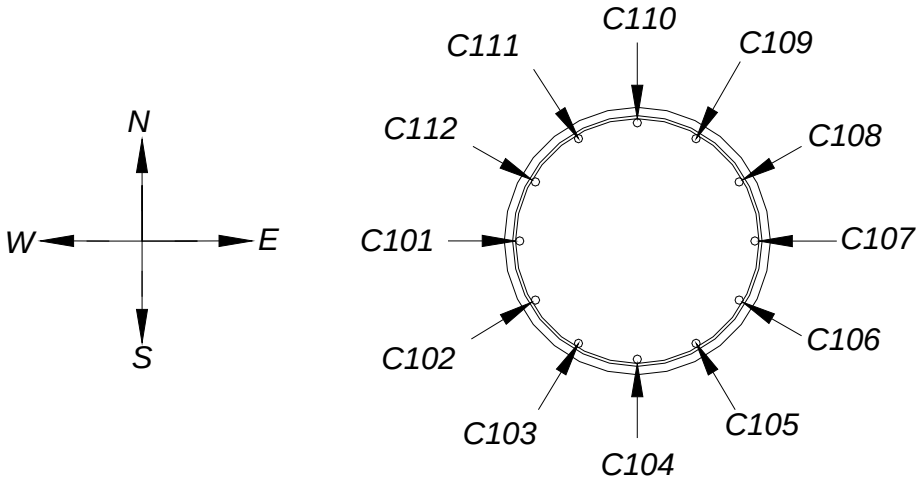

Figure 4.4 **Cross section of TS-1 showing the reference numbers of the twelve #4 longitudinal rebar.**

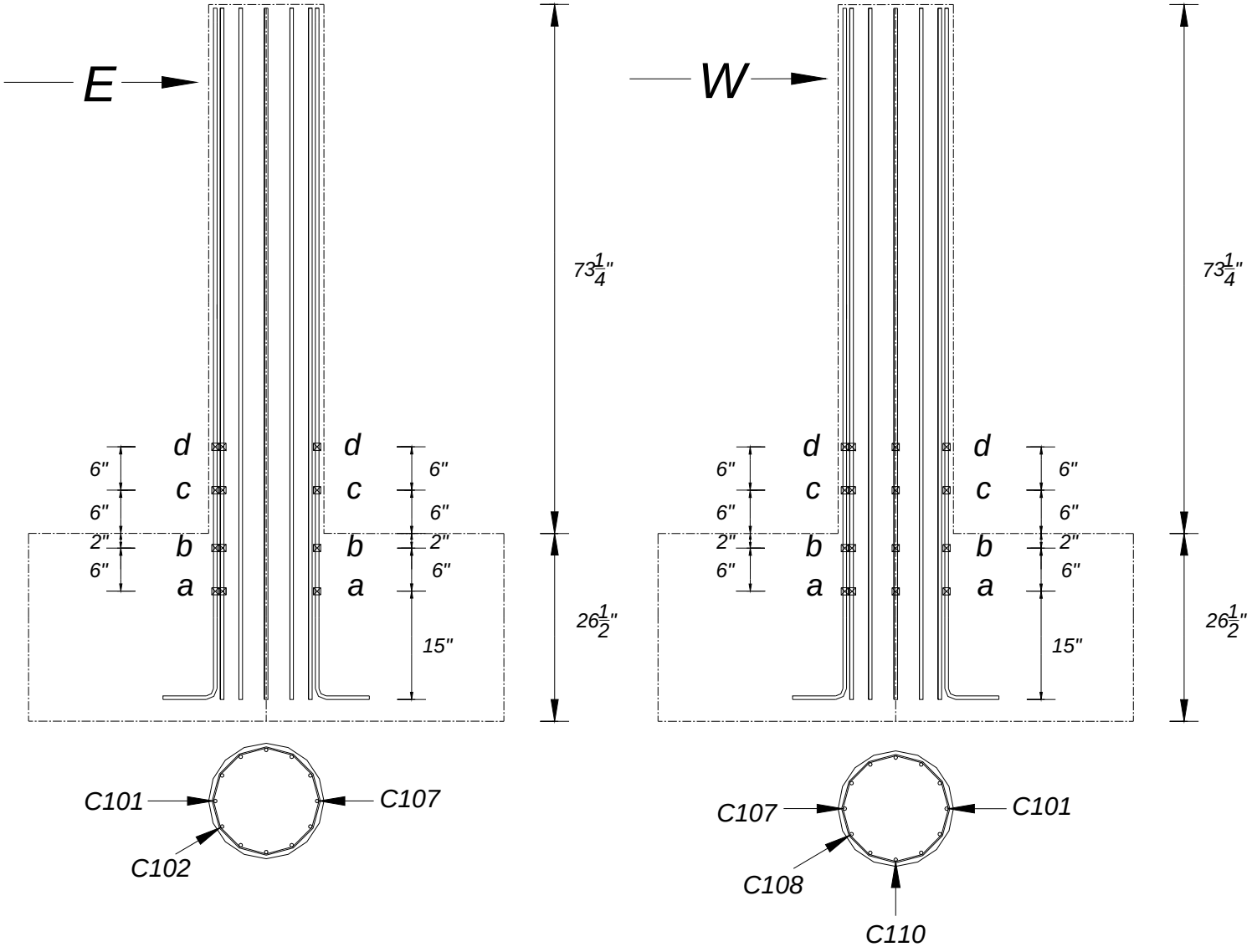

Figure 4.5 Elevation view of strain gauges location on the longitudinal rebar of TS-1.

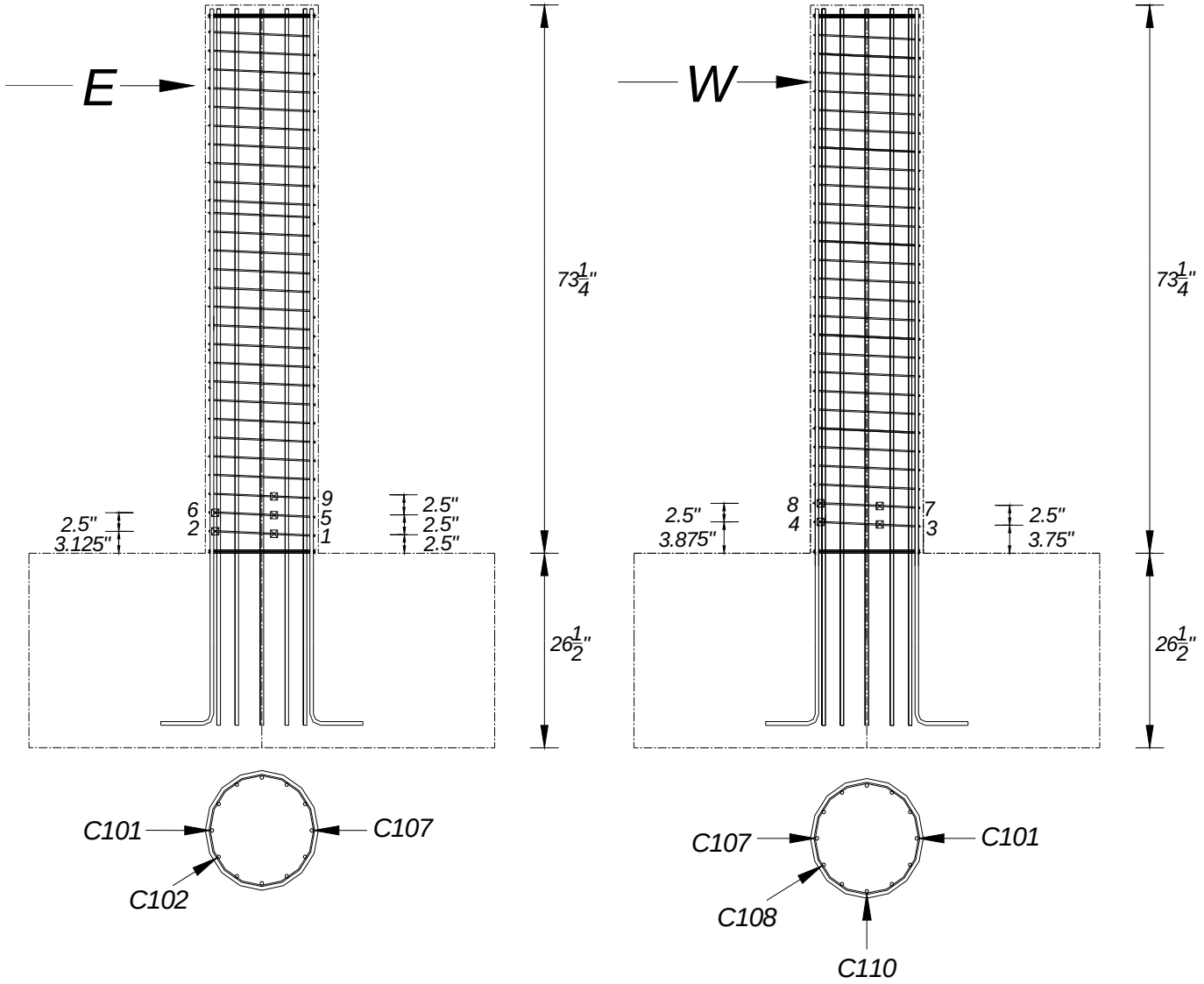

Figure 4.6 Locations of strain gauges on the spiral reinforcement of TS-1.

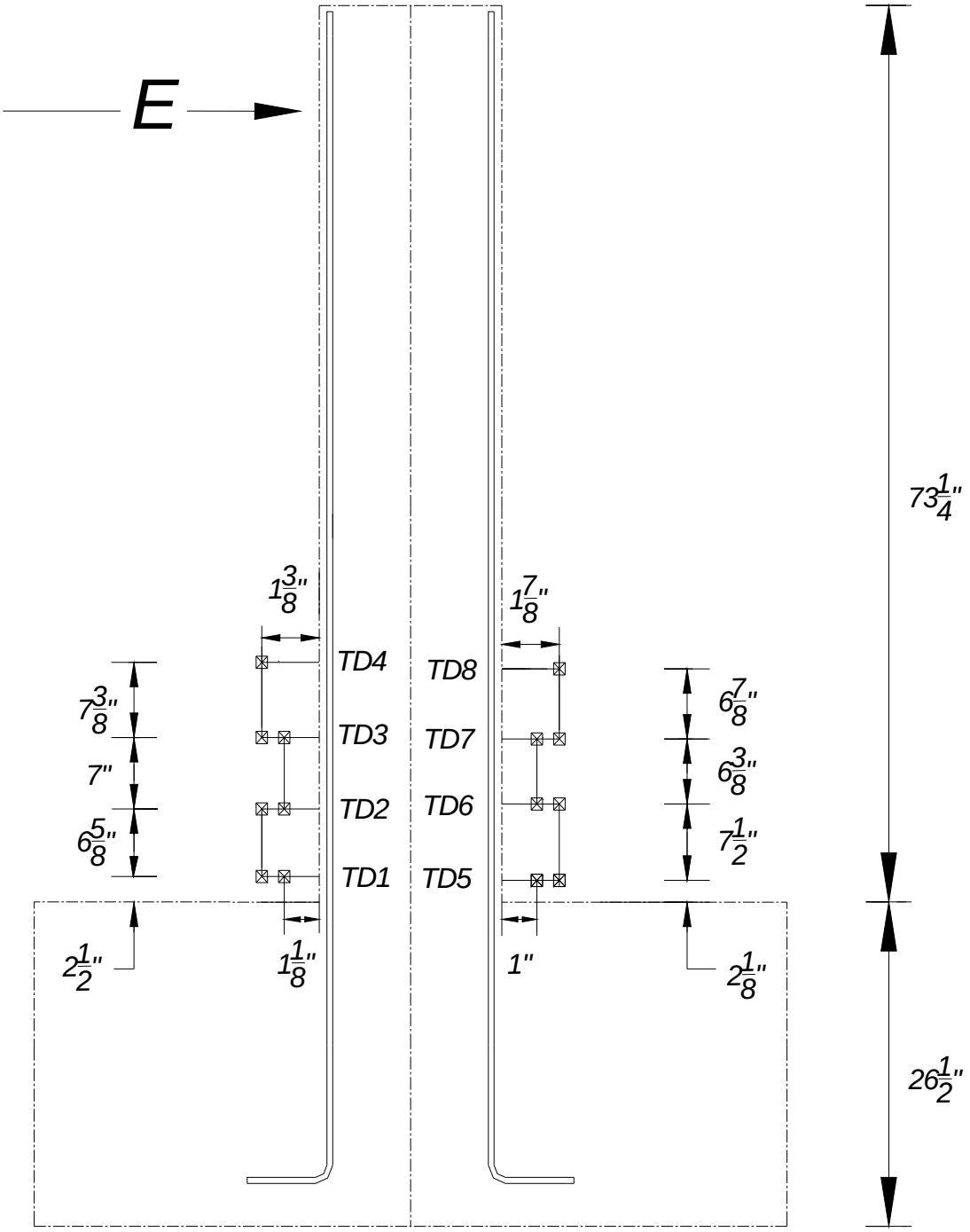

Figure 4.6 Locations of displacement transducers of TS-1.

4.2.2 Instrumentation of TS-2

Internal instrumentation of TS-2 consisted of 52 strain gauges attached on the longitudinal and spiral reinforcement. Figure 4.7 shows the rebar reference numbers of TS-2. Figure 4.8 shows the locations of the strain gauges on the longitudinal rebar, while Figure 4.9 shows the location of the strain gauges on the spiral reinforcement. Figure 4.10 and Figure 4.11 depict elevation views of the displacement transducers used in TS-2 in the east-west and north-south faces of the column, respectively.

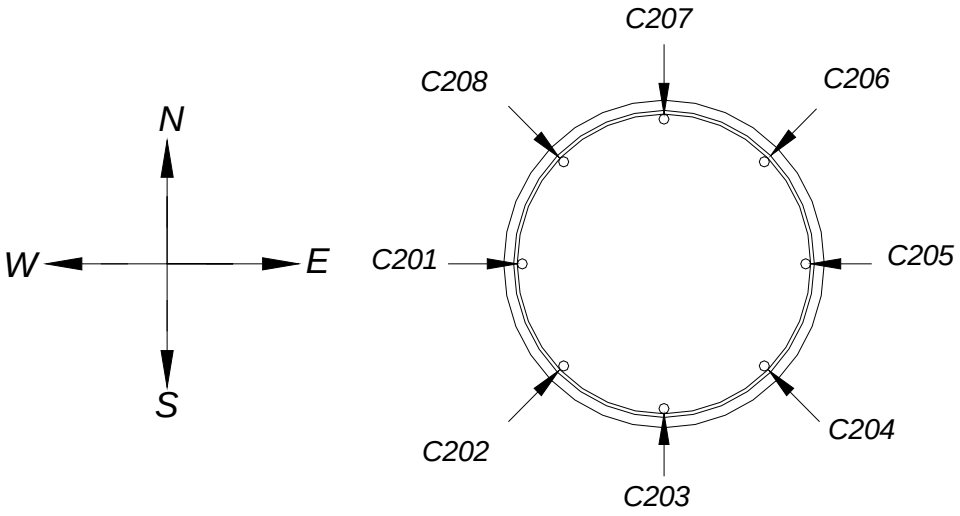

Figure 4.7 Cross section of TS-2 showing the reference numbers of the eight #5 stainless steel longitudinal rebar.

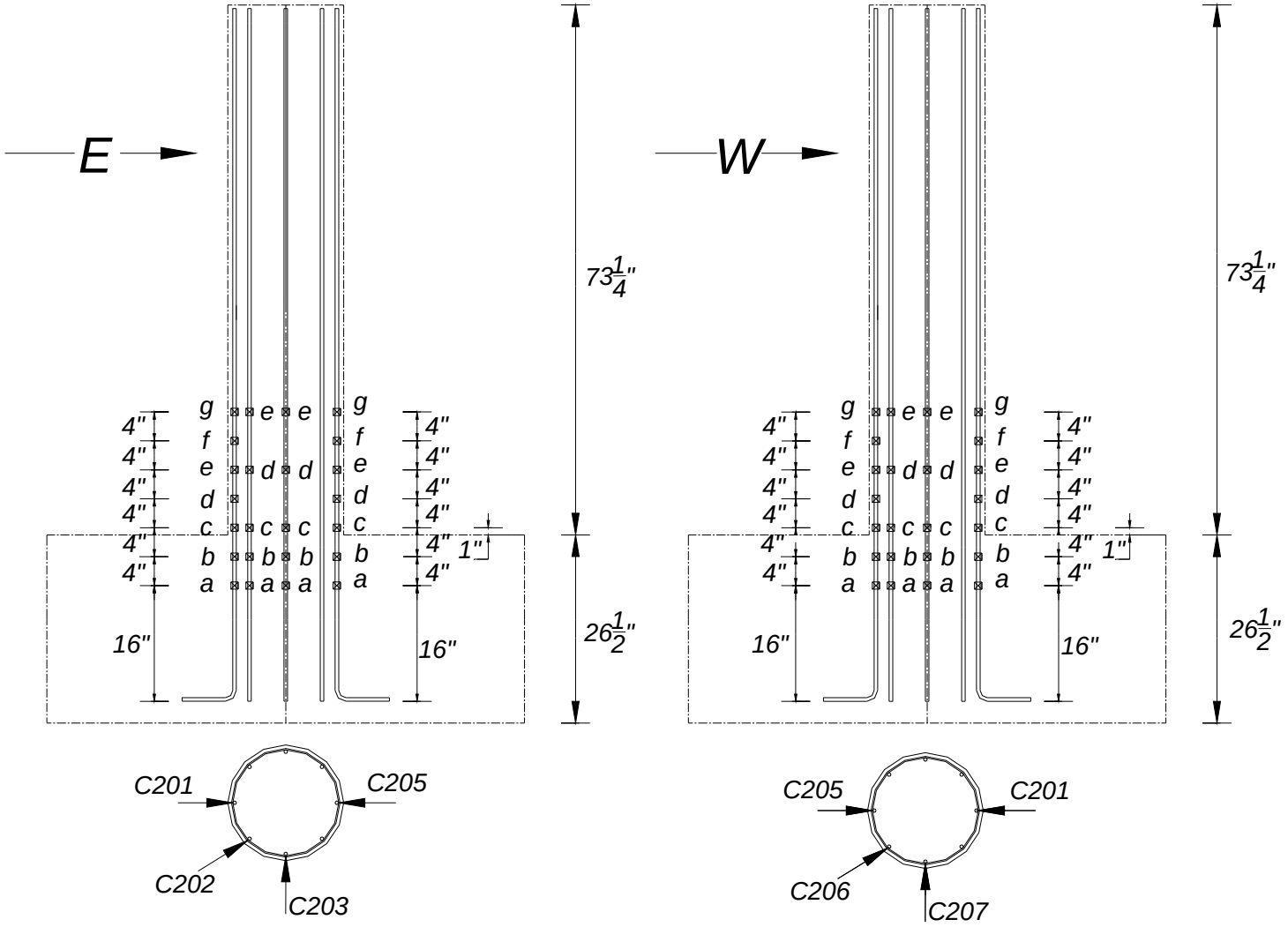

Figure 4.8 Elevation view of strain gauges location on the longitudinal rebar of TS-2.

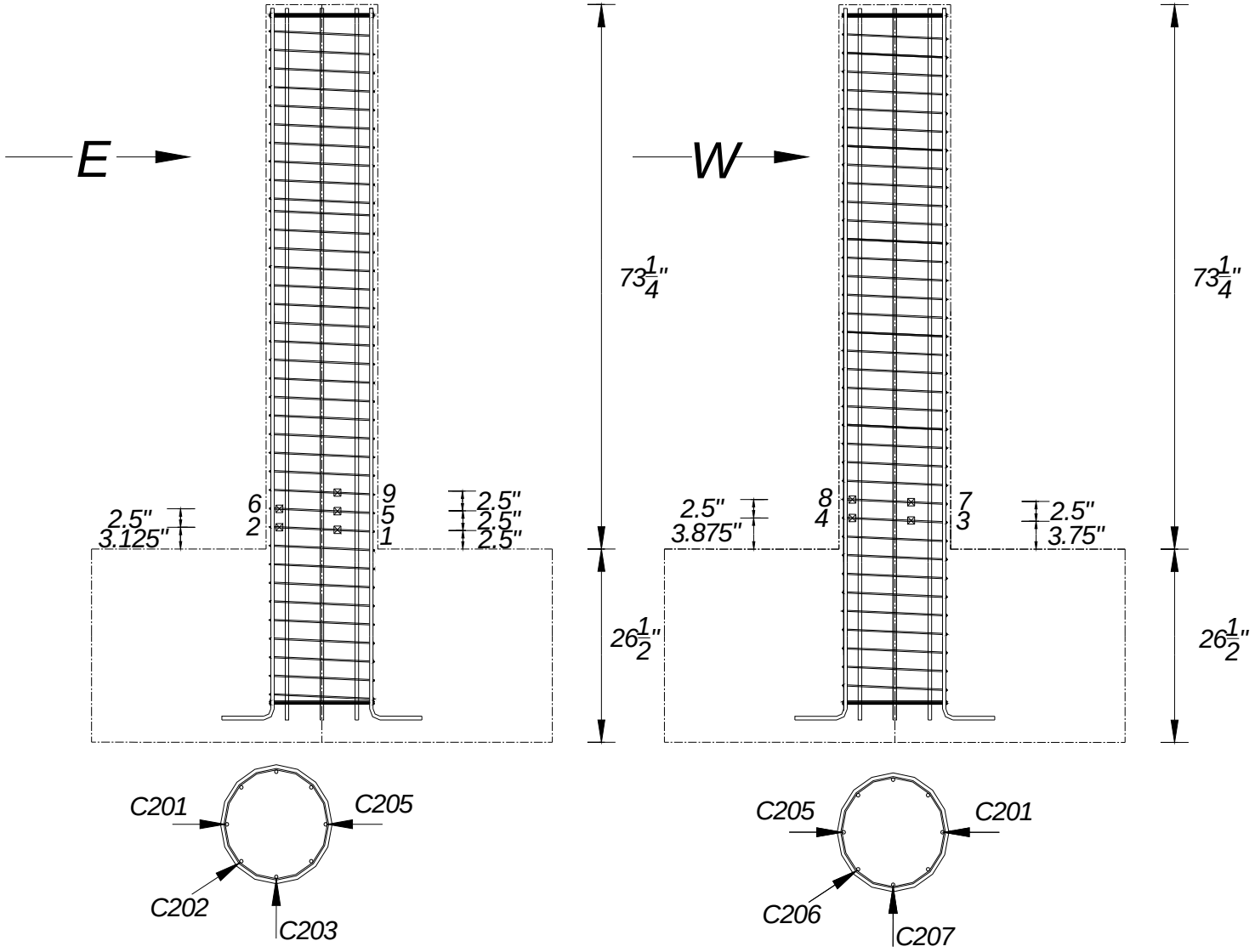

Figure 4.9 Locations of strain gauges on the spiral reinforcement of TS-2.

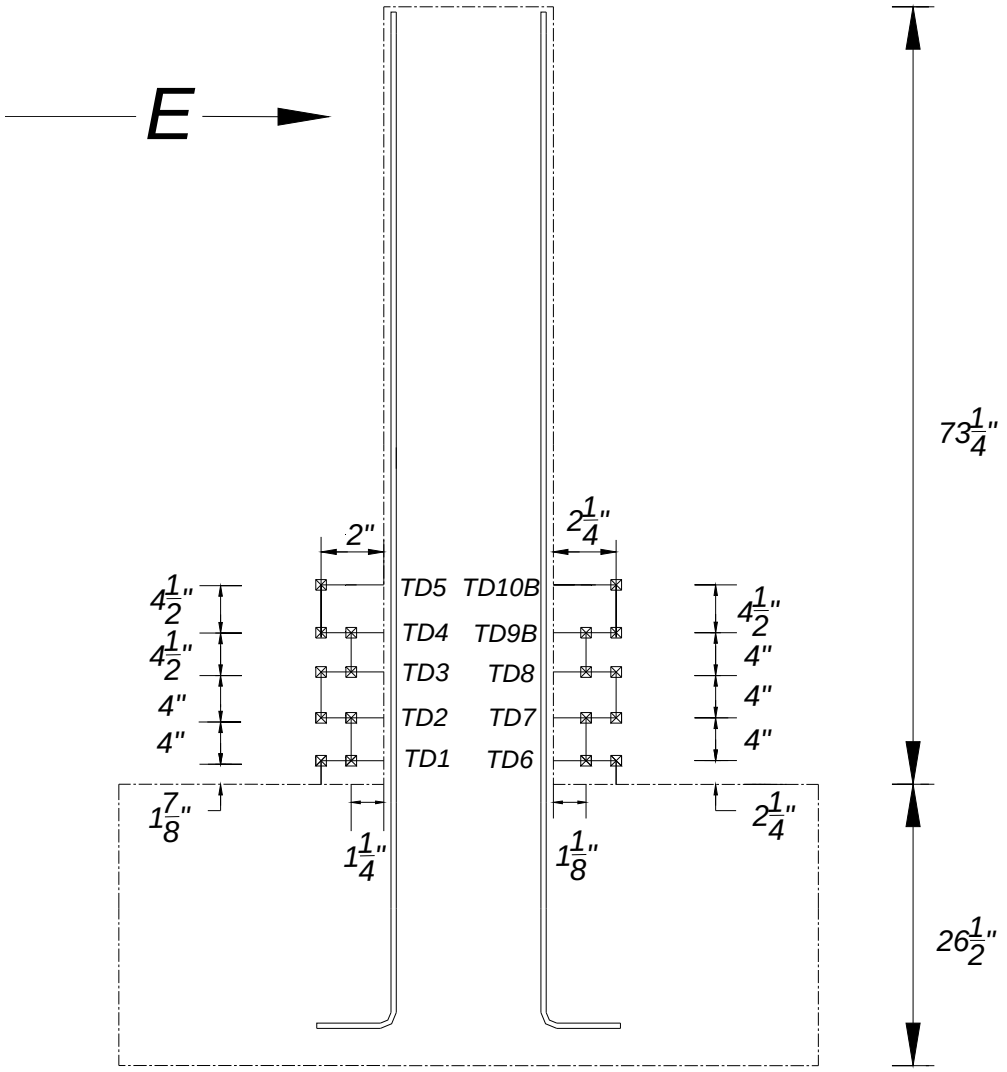

Figure 4.10 Locations of vertical transducers of TS-2 (west-east).

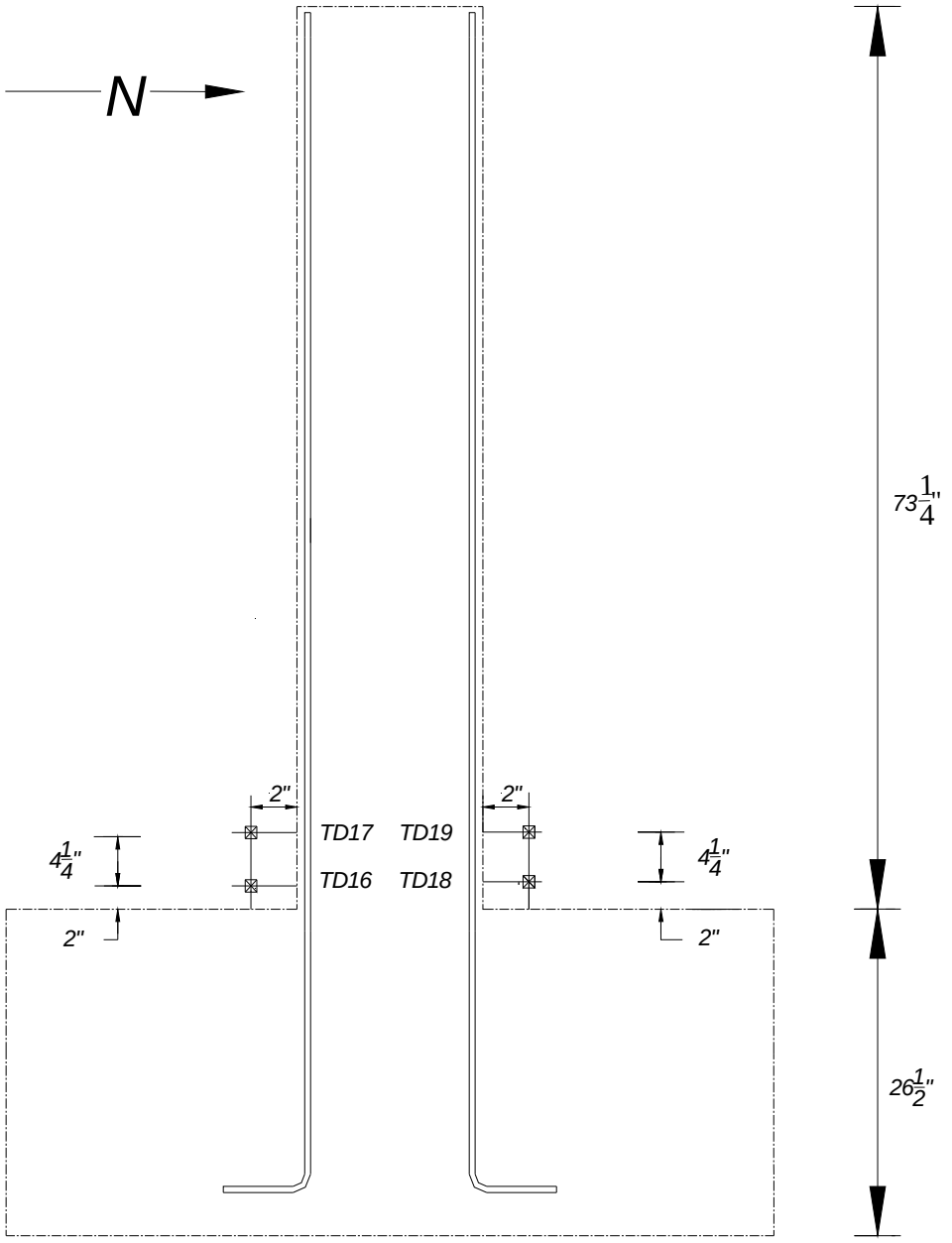

Figure 4.11 Locations of vertical transducers of TS-2 (south-north).

4.3 LOADING PROTOCOL

Table 4.1 lists the characteristics of the load protocols, and Figure 4.12 plots their histories. Table 4.1 also includes the number of cycles at each displacement amplitude and gives the drift

ratios $\theta_r = \Delta / H$, where Δ is the applied lateral displacement at height H = 67.25 in. The protocols for both specimens were identical up to top displacements equal to Δ = 1.6 in., corresponding to a drift ratio θ_r = 2.4%. Up to this displacement, three cycles occurred for each amplitude level. The protocols differed for drift ratios larger than 2.4%. For drift ratios of 4.2% and larger, the protocol of TS-1 had only one cycle at each level of displacement whereas TS-2 included two cycles up to a drift ratio of 7.1%. The last cycle of both protocols had a peak displacement equal to 7.6 in., corresponding to a drift ratio of 11.3%.

Table 4.1 Number of cycles at various drift ratios (H = 67.25 in.).

Top Displacement, Δ (in.)	**Drift Ratio, (θ_r) %**	**Number of Cycles**	
		TS-1	**TS-2**
0.1	0.15	3	3
0.2	0.30	3	3
0.3	0.44	3	3
0.4	0.60	3	3
0.8	1.2	3	3
1.2	1.8	3	3
1.6	2.4	3	3
2.0	3.0	0	3
2.4	3.6	3	3
2.8	4.2	1	2
3.2	4.8	1	2
4.0	6.0	1	2
4.8	7.1	1	2
5.6	8.3	1	1
6.4	9.5	1	1
7.6	11.3	1	1

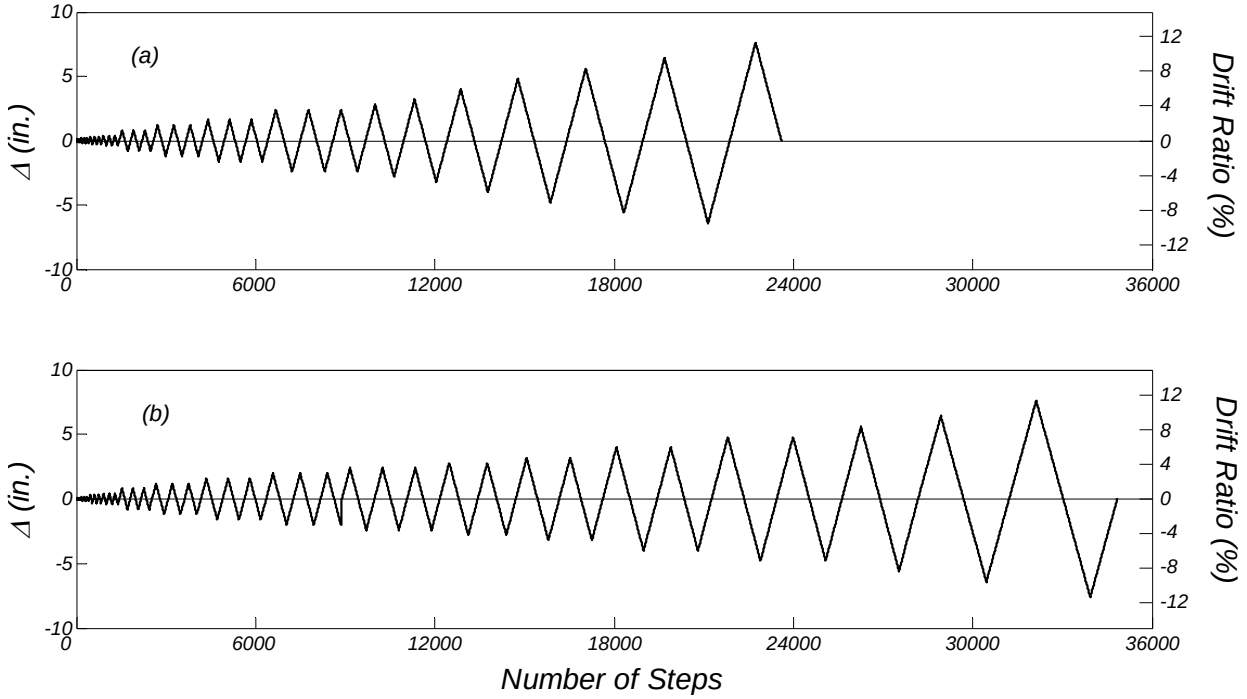

Figure 4.12 Lateral displacement protocol: (a) TS-1; and (b) TS-2.

5 Experimental Results and Discussion

5.1 OVERVIEW

This chapter presents the experimental results of the two test specimens. First, the observed test response is described in terms of visual damage at different stages of the specimens' response. Next, the measured response based on the external and internal instrumentation is presented, and the performance of the two SC-HyFRC columns is compared to a conventional RC bridge column with the same dimensions and longitudinal reinforcement but double transverse reinforcement.

5.2 OBSERVED TEST RESPONSE

5.2.1 Testing of Specimen TS-1

To recap, TS-1 was designed so that the column rocked at its interface with the foundation. Cracking of the concrete was first observed at the column foundation interface on the east face of the column for the westward response when the test specimen reached θ_r = 0.44%. Up to a drift ratio of θ_r = 1.2% no new cracks developed. Shown in Figure 5.1(a), the crack at the column-foundation at θ_r = 1.2%. For drift ratios between θ_r = 1.2% and 1.8% hairline flexural cracks appeared up to 24 in. above the foundation top [see Figure 5.1(b)].

The crack opening at the column-foundation interface increased during the first cycle of θ_r = 2.4%. On the west face of the column, the spiral reinforcement became visible [see Figure 5.2(a)], and more cracking was observed on the east column face up to 4 in. above the top of the foundation. The gap opening on the east column face increased to 0.5 in. [see Figure 5.2(b)]. At θ_r = 3.6%, a 0.75-in. gap opened up at the column base on the west column face Localized spalling was observed on the east side of the column at a height of 14 in. above the foundation top [see Figure 5.2(c)]. The measured thickness of the concrete cover at this location was

discovered to be less than the designed 0.5 in. due to a construction flaw. Longitudinal bar C107 buckled at the same location where the localized spalling was first observed. During the cycle θ_r = 4.8%, buckling of longitudinal bar C107 became more prominent [see Figure 5.2(d)].

During the cycle θ_r = 6.0% the longitudinal bar C107, which started to buckle at θ_r = 3.6%, fractured during the westward response [see Figure 5.3(a)]. In the same cycle during the eastward response the longitudinal bar C106 buckled, preceded by spalling of cover concrete, at 2.5 in. above the foundation top [see Figure 5.3(b)]. At θ_r = 7.1%, for the eastward response, the crack opening measured 1.125 in. and more extensive crushing of concrete near the column's base was observed [see Figure 5.3(c)]. During this cycle for the eastward response, the longitudinal bar C108 buckled preceded by spalling of cover concrete near column base [see Figure 5.3(d)]. Buckling of longitudinal rebar C101 on the west face of the column was observed at 6 in. above the foundation top during the cycle θ_r = 7.1% for the eastward response. During the cycle θ_r = 8.3% and the westward response, the longitudinal bar C106 fractured at 2.5 in. above the foundation top. Longitudinal bar C108 fractured during the cycle θ_r = 9.5%, at 5 in. from the foundation top [see Figure 5.4(a)]. During this cycle, buckling of longitudinal bars C102 and C112 occurred along with crushing of concrete on both the east and the west face of specimen's base. At θ_r = 11.3%, the measured base crack width was 2 in. During this cycle longitudinal bars C101, C102 and C112 fractured and extensive crushing of concrete at the column base was observed [see Figure 5.4(b)].

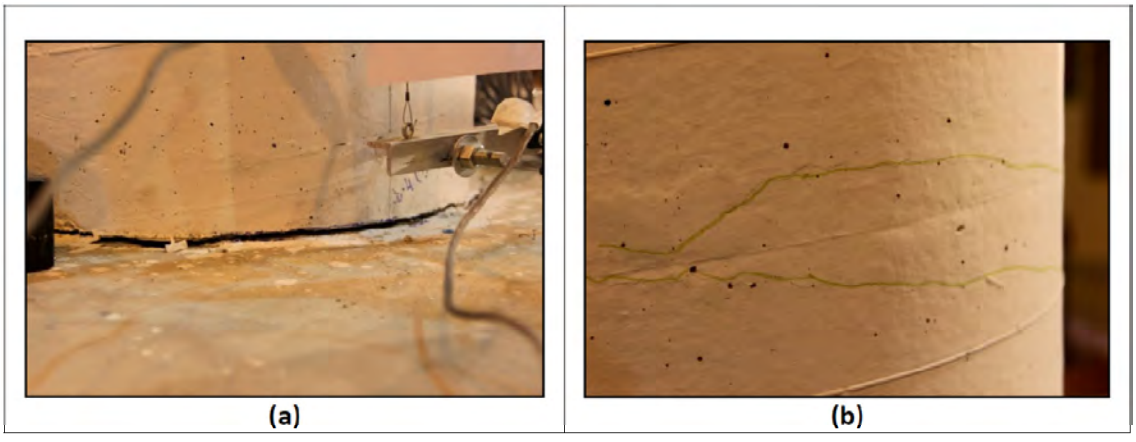

Figure 5.1 **(a) Crack at column-foundation interface at θ_r = 1.2%; and (b) thin hairline flexural cracks at 22 in. and 24 in. above the foundation top at θ_r = 1.8% on the east face of the column.**

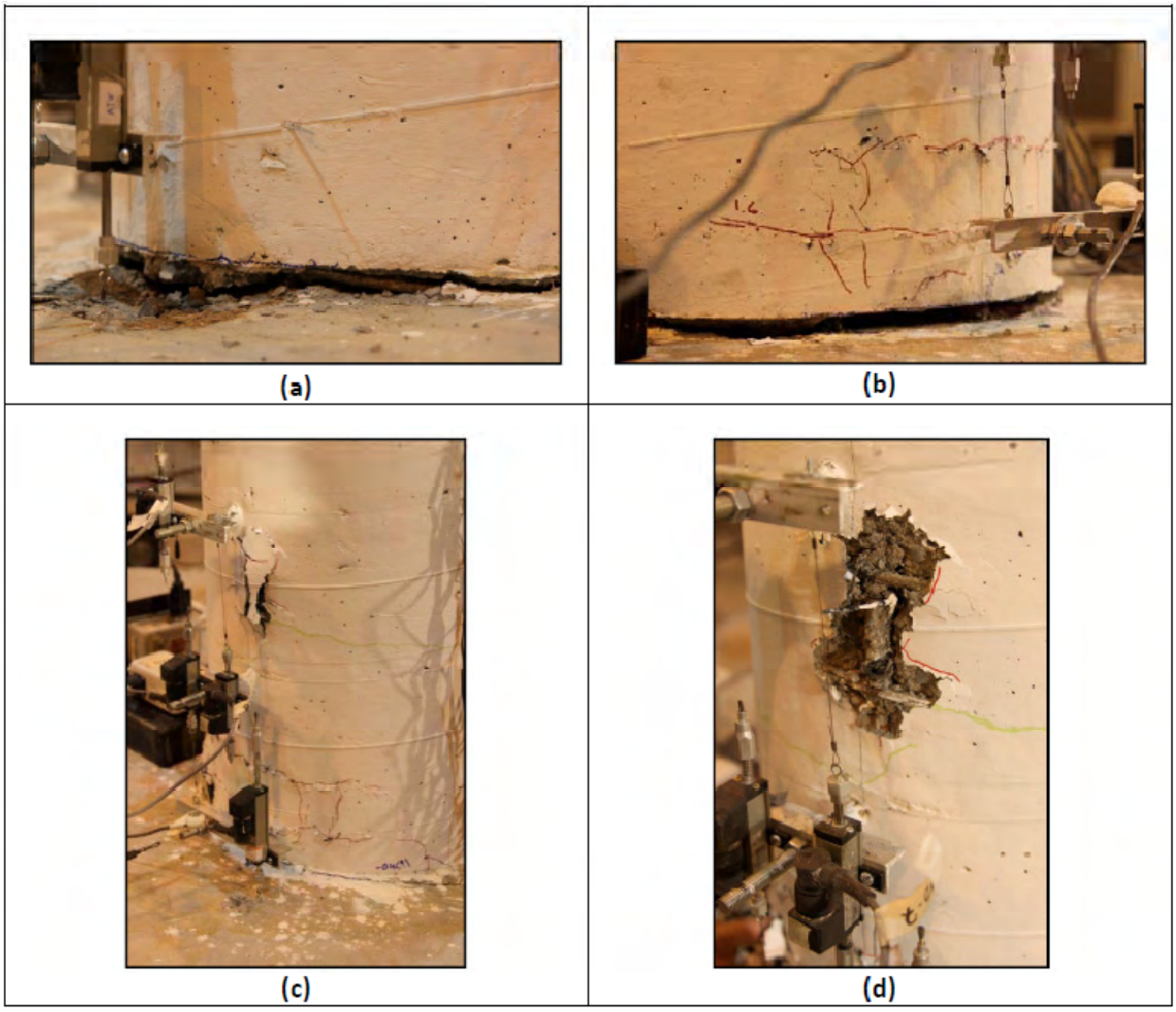

Figure 5.2 **(a) Crack opening at column-foundation interface at θ_r = 2.4% on the west face of the column during eastward response; (b) crack opening at column-foundation interface at θ_r = 2.4% of the east face of the column during westward response; (c) damage state of the east column face for eastward response at θ_r = 3.6% where buckling of C107 bar was first observed; and (d) buckled bar C107 at θ_r = 4.8% on the east column face.**

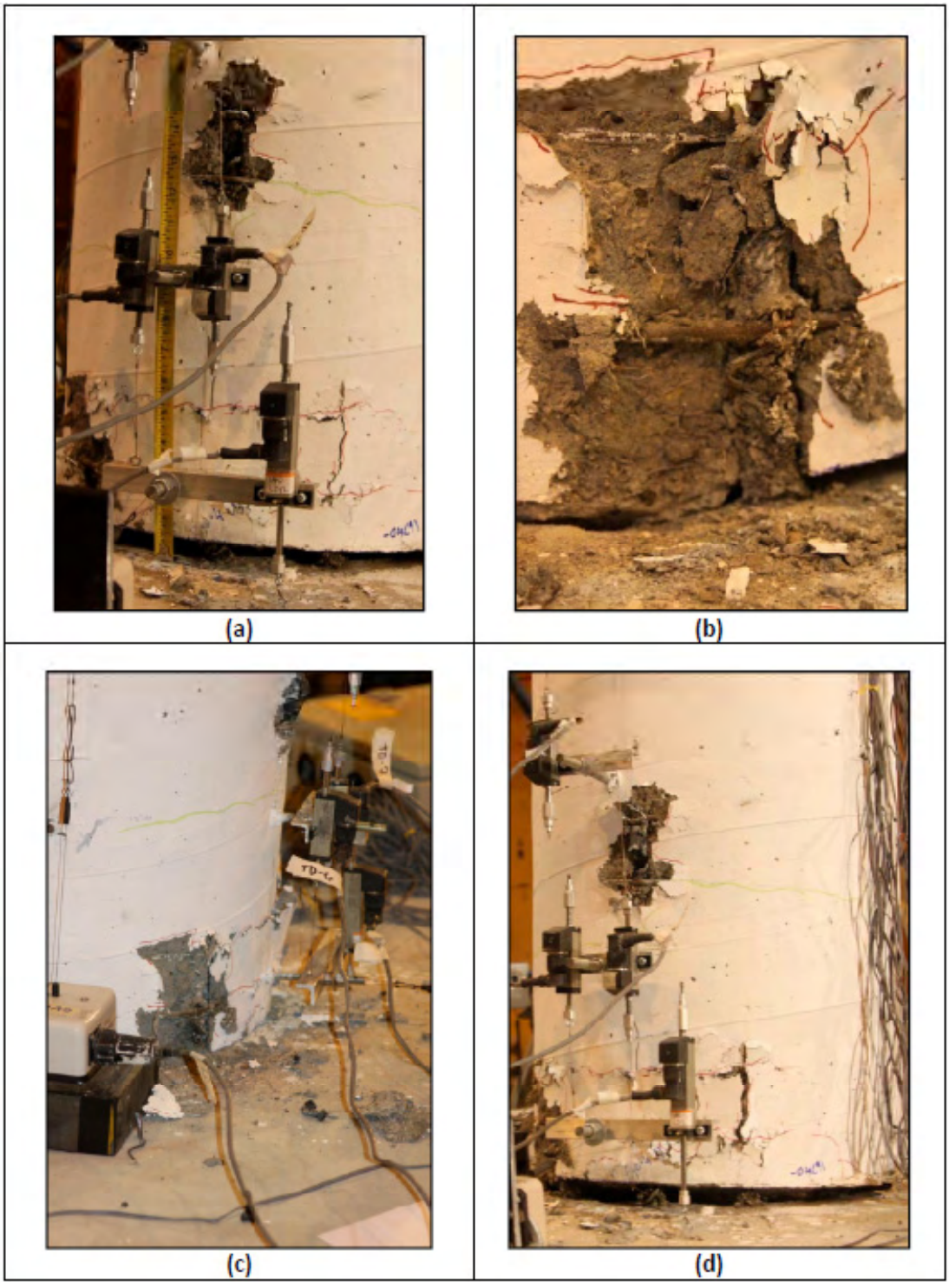

Figure 5.3 **(a) Fracture of longitudinal bar C107 at θ_r = 6.0% on the east face of the column; (b) buckling of longitudinal bar C106 at θ_r = 6.0%, east face of the column; (c) damage state of specimen's base at θ_r = 7.1%, east face of the column for eastward response; and (d) damage state of specimen and buckling of longitudinal bar C108 at θ_r = 7.1%, east face of the column.**

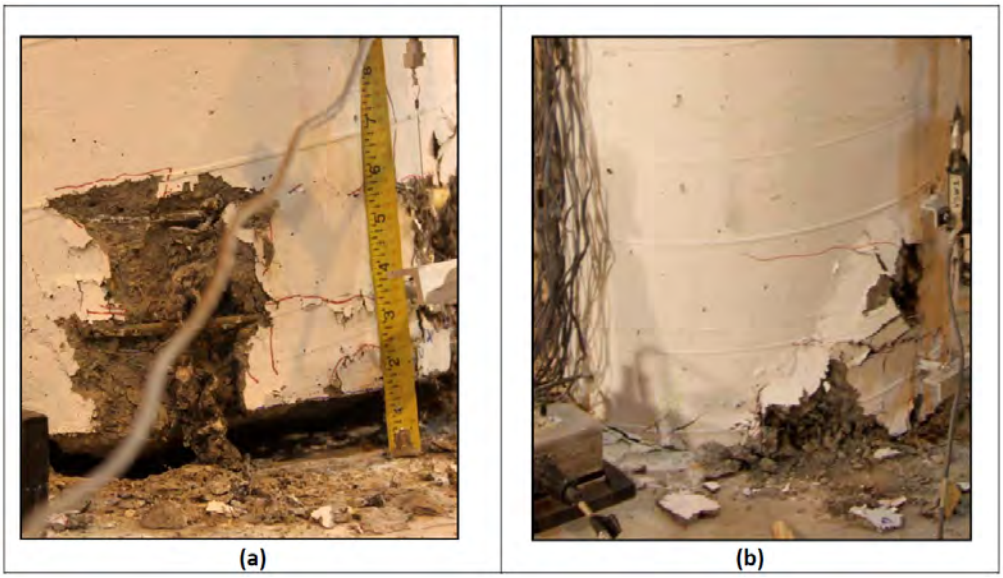

Figure 5.4 **Damage state of column's base: (a) θ_r = 9.5%, east face of the column; and (b) the final cycle of θ_r = 11.3%, west face of the column.**

5.2.2 Testing of Specimen TS-2

This specimen was designed to form a flexural plastic hinge at the column base. Flexural cracking was observed for the first time during the cycle of θ_r = 0.44% at 1.75 in. and 5.75 in. above the foundation on the west face of the column, and at 5.5 in. above the foundation on the east face of the column. During the cycle θ_r = 0.60%, new flexural cracks formed 17 in., 22 in., and 27 in. above the foundation top. Figure 5.5through Figure 5.9show the damage state of the column at various drift ratios ranging from 1.2% to 11.3%. During the cycle θ_r = 1.2%, hairline flexural cracks spread up to a height of 27.5 in. above the foundation on the east face of the column [see Figure 5.5(a)] and up to a height of 29.5 in. on the west face of the column. During the cycle θ_r = 1.8%, three prominent cracks formed at 1.25 in., 3 in., and 5.75 in. above the foundation at the east face of the column [see Figure 5.5(b)]. More cracks formed at θ_r = 2.4% along both the west and east face of the column, as shown in Figure 5.6(a) and (b), respectively.

During the cycle θ_r = 3.0%, concrete bulged on the west face of the column at 3.4 in from the foundation top [see Figure 5.7(a)], with crack widths of 1.25 in., 3 in., and 5.75 in. from the foundation top on the east side increased between θ_r = 1.2% to 3.0% and are shown at a drift ratio of 3.0% in Figure 5.7(b). During the cycle θ_r = 3.6%, the crack width at 1.25 in. from the top of foundation, was measured at 0.375 in. Figure 5.7(c) and (d) shows the damage state of the west- and east face column's base at θ_r = 3.6%, respectively.

At θ_r = 4.8%, the crack width at the bottom measured 0.625 in. [see Figure 5.8(a)]. During the cycle θ_r = 6.0%, the concrete began to bulge on the east face, 5 in. from the foundation top. Spalling of concrete increased on the west face of the column [see Figure 5.8(b)] At this drift ratio, the spiral reinforcement fractured on the east face of the column 2.5 in. above the foundation, and rebar C205 buckled during the reverse cycle [see Figure 5.8(c)]. During the cycle θ_r = 7.1%, the bottom crack width on the west column face measured 0.75 in. Figure 5.8(d) shows the damage state at the base of the column at the east face of the column.

During the cycle θ_r = 8.3%, crushing of concrete at foundation and column interface was quite extensive [see Figure 5.9(a)], and longitudinal bar C202, C204, C206 on the east face of the column buckled [see Figure 5.9(b)]. Longitudinal Bar C201 on west face of the column buckled with fracture of the spiral at height of 2.5 in. from the top of foundation. During the cycle θ_r = 9.5%, longitudinal bar C205 and C201 fractured at height of 2 in. and 2.75 in. respectively, from top of foundation [see Figure 5.9(c)]. The damage state at the final cycle of θ_r = 11.3%, is shown in Figure 5.9(d). Figure 5.10 shows the global view of TS-2 at θ_r = 11.3%.

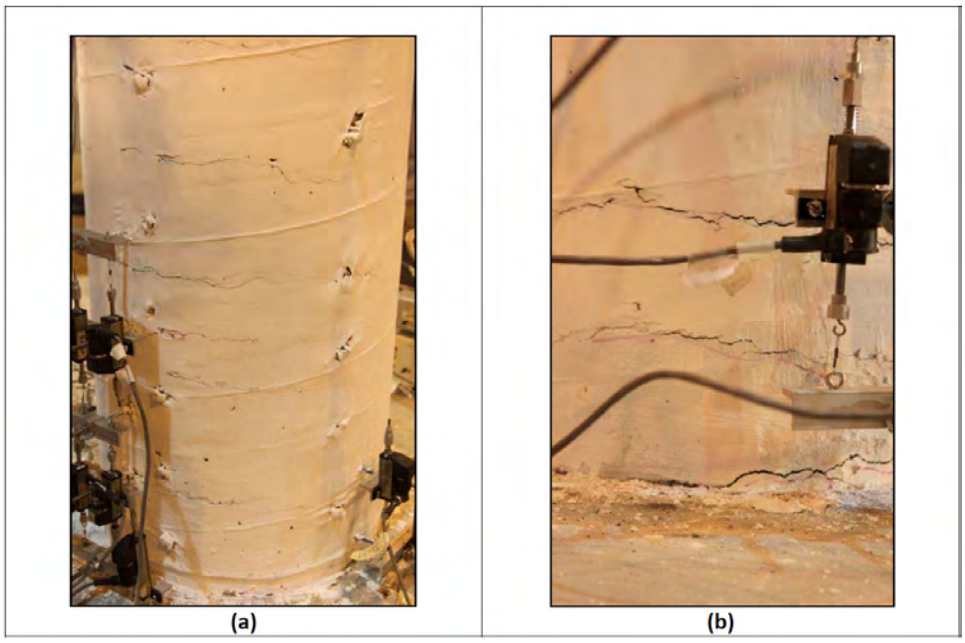

Figure 5.5 **(a) Spreading of hairline flexural cracks up to a height of 27.5 in. at θ_r = 1.2% on the east face of the column; and (b) formation of cracks at 1.25 in., 3 in., and 5.75 in. at θ_r = 1.8% on the east face of the column.**

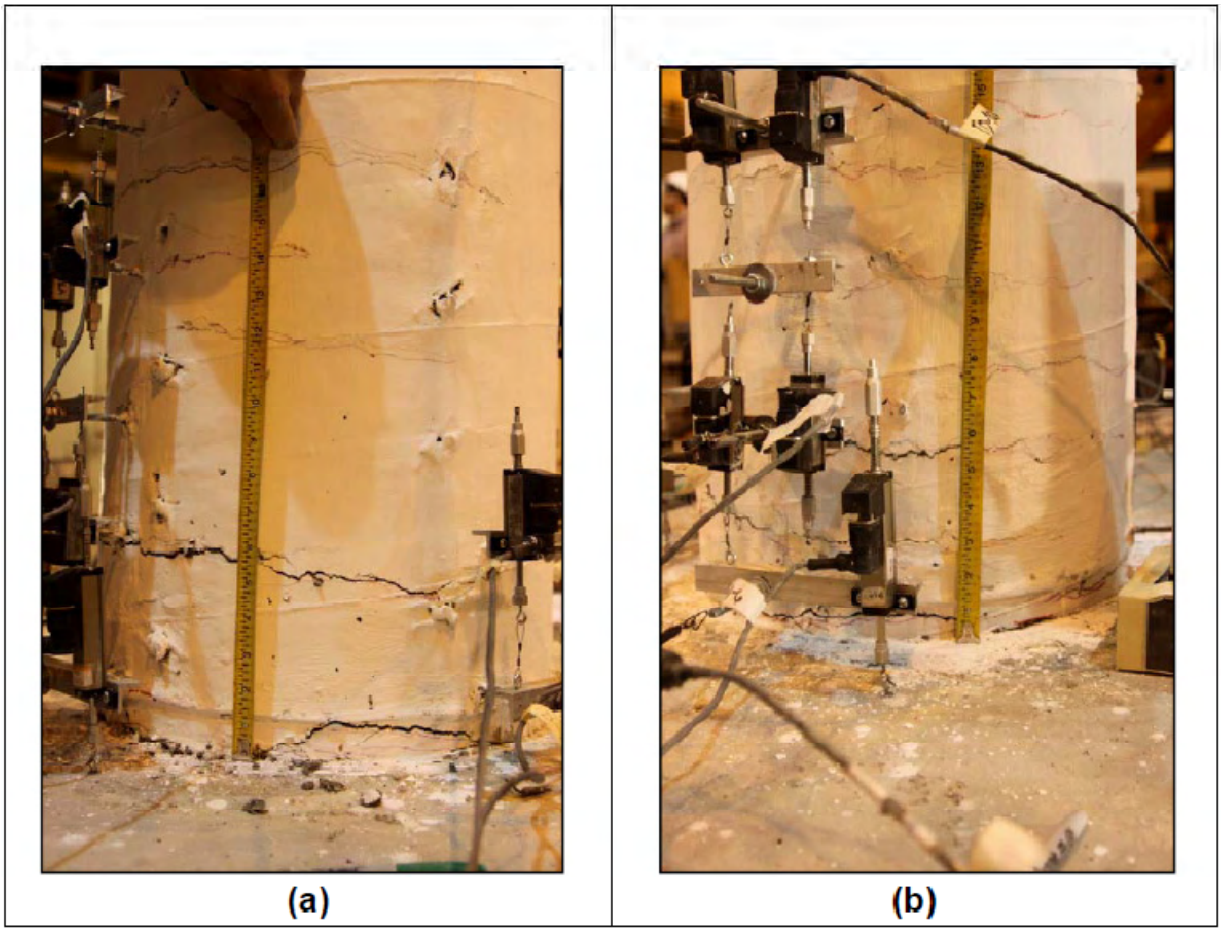

Figure 5.6 **Elevation view showing locations of cracks at θ_r = 2.4%: (a) west face of the column during the eastward response; and (b) east face of the column during the westward response.**

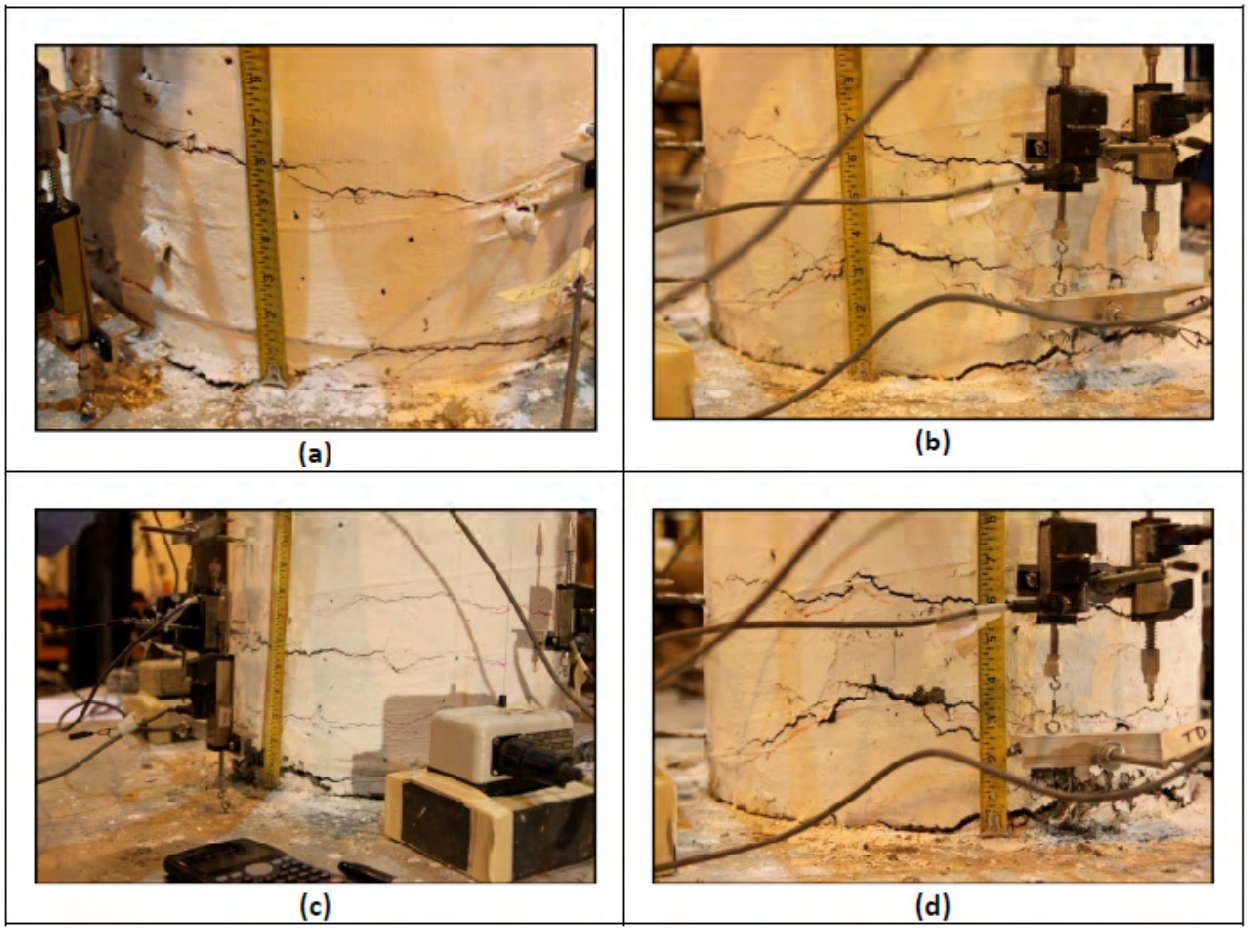

Figure 5.7 **(a) Damage state at θ_r = 3.0% on the west column face during eastward response; (b) damage state at θ_r = 3.0% on the east column face during westward response; (c) damage state at θ_r = 3.6% on the west face of the column; and (d) damage state at θ_r = 3.6% on the east column face.**

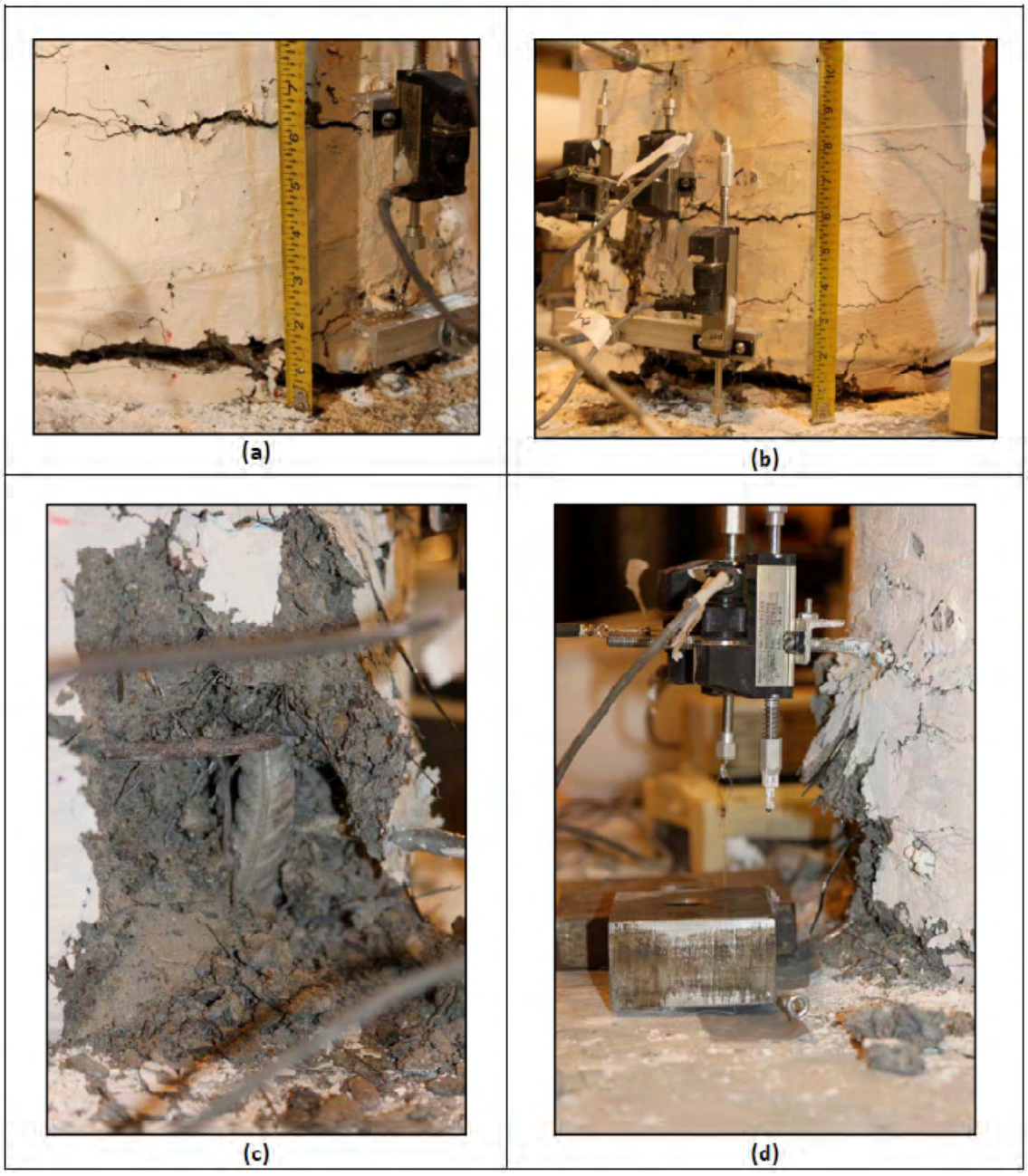

Figure 5.8 **(a) Damage state at column base on the west column face at θ_r = 4.8%; (b) damage state at column base on the west column face at θ_r = 6.0%; (c) spiral fracture and buckling of longitudinal bar C205 at θ_r = 6.0% on the east face of the column; and (d) concrete crushed state at θ_r = 7.1% on the east face of the column.**

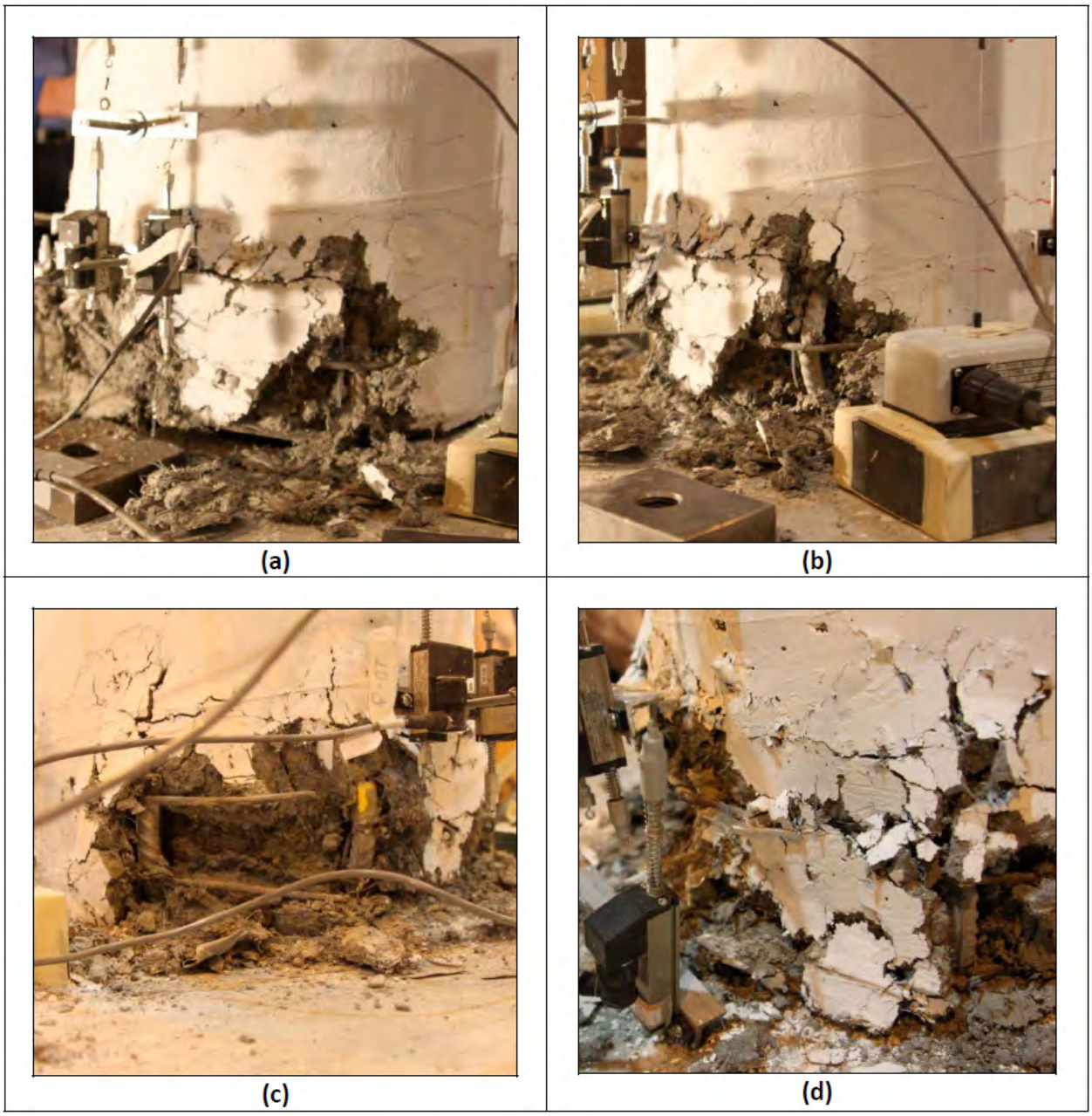

Figure 5.9 **(a) Crushed concrete at the base of the east column face at θ_r = 8.3%; (b) buckling of longitudinal bar C206 at θ_r = 8.3%; (c) fracture of longitudinal bar C205 at θ_r = 9.5%; and (d) damage at the base of the west face of the column at θ_r = 11.3%.**

Figure 5.10 Global view of TS-2 at θ_r = 11.3%.

5.3 MEASURED TEST RESPONSE

This section presents the measured response of the two test specimens using both external and internal instrumentation. Force-displacement and strain response quantities are discussed.

5.3.1 TS-1

Figure 5.11 plots the measured lateral-force versus lateral-displacement response of the TS-1 in the east-west direction. The force-displacement hysteretic response of this specimen was highly nonlinear and quite symmetric in terms of direction of displacement. The hysteretic response did not demonstrate significant strength degradation for drift ratios up to θ_r = 4%. An increase in both the stiffness and the strength was observed at θ_r = 2.4% for both sides of the response. As shown in Figure 5.11, points 1 to 6 delineate the fracture points of longitudinal bars C107, C106, C108, C101, C102, and C110, respectively. The first longitudinal bar, C107, fractured at θ_r = 4%. By the end of the test, half of the longitudinal bars had fractured. The specimen reached a maximum drift ratio of 11.3%. Even at this level of lateral displacement, the specimen remained stable and was able to resist its axial load. Figure 5.12 plots the lateral-force versus the lateral displacement response of TS-1 for θ_r up to 5.0%.

Figure 5.13 plots the measured displacement of the two vertical displacement transducers – TD1 and TD5 – versus drift ratio. Installed at the bottom of the east and west face of the column [see Figure 4.10 and Figure 4.11], respectively these transducers measured the crack opening at the column-foundation interface, which was nearly symmetric for the two sides of response. Both these transducers failed before the peak drift ratio was reached for each side of the response.

Figure 5.14(a) plots the computed smeared strain of the west face of the column along the unbonded length of the rebar using the displacement measurement of TD1 divided by the unbonding length, L_d = 18 in. This strain is compared with the strain measured by strain gauge SG102d, located in the unbonding length near the west face of the column, 12 in. above the foundation top. Figure 5.14(b) plots the corresponding smeared strain of the east face of the column using the displacement transducer TD5 versus the strain measured by strain gauge C108d, located near the east face of the column 12 in. above the foundation top. The computed smeared strains based on TD1 and TD5 are larger than the strains measured with SG102d and SG108d, respectively. A main reason for this is that use of L_d = 18 in. does not account for the strain penetration that occurred outside the unbonding region at both ends; in addition, instruments TD1 and TD5 were placed at 1.125 in. and 1 in. from the column face, respectively [see Figure 4.6].

Figure 5.15 plots the computed base rotation (θ_b) based on measurements of TD1 and TD5 versus the drift ratio with, $\theta_b = \frac{TD1 - TD5}{d}$, where d = 20.1 in. is the horizontal distance between the point of measurement of TD1 and TD5 [see Figure 4.6]. As shown, the base rotation is close to the drift ratio, indicating that the main contribution to the lateral deformation mechanism of this specimen was due to rocking of the column at its interface with the foundation.

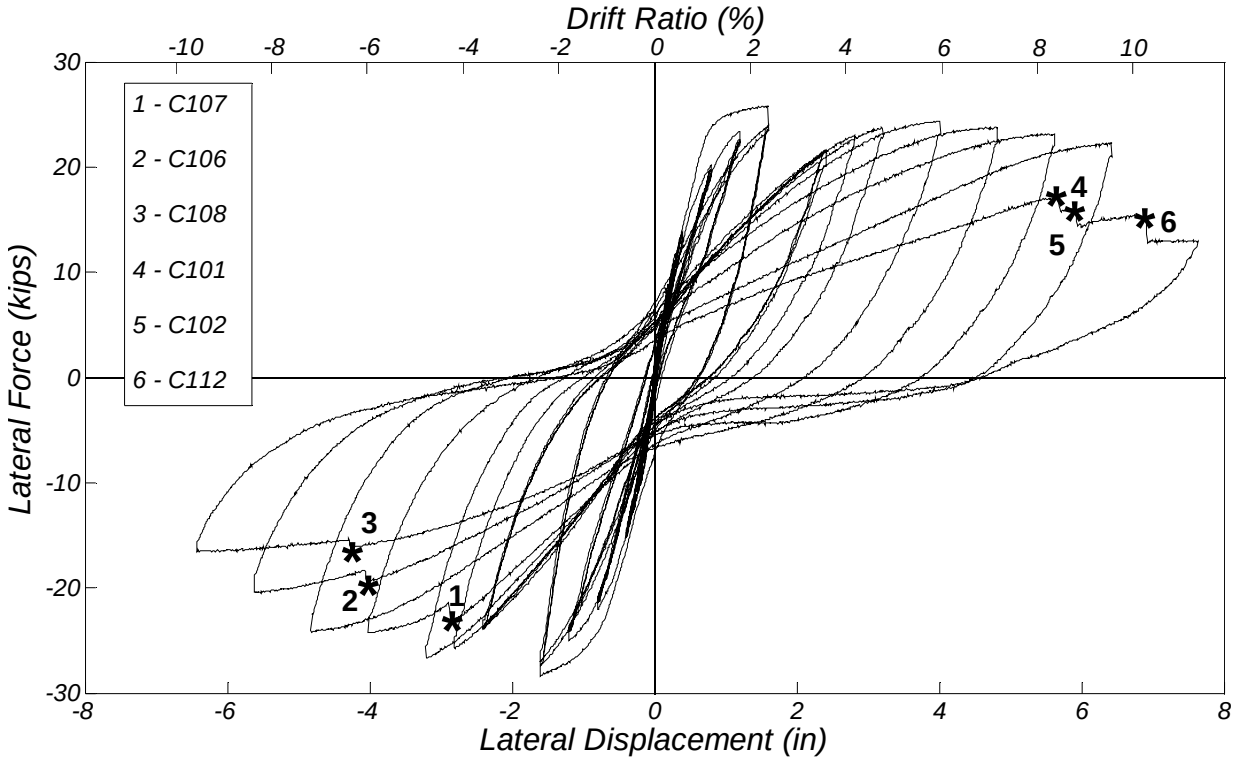

Figure 5.11 Lateral-force versus lateral-displacement response of TS-1.

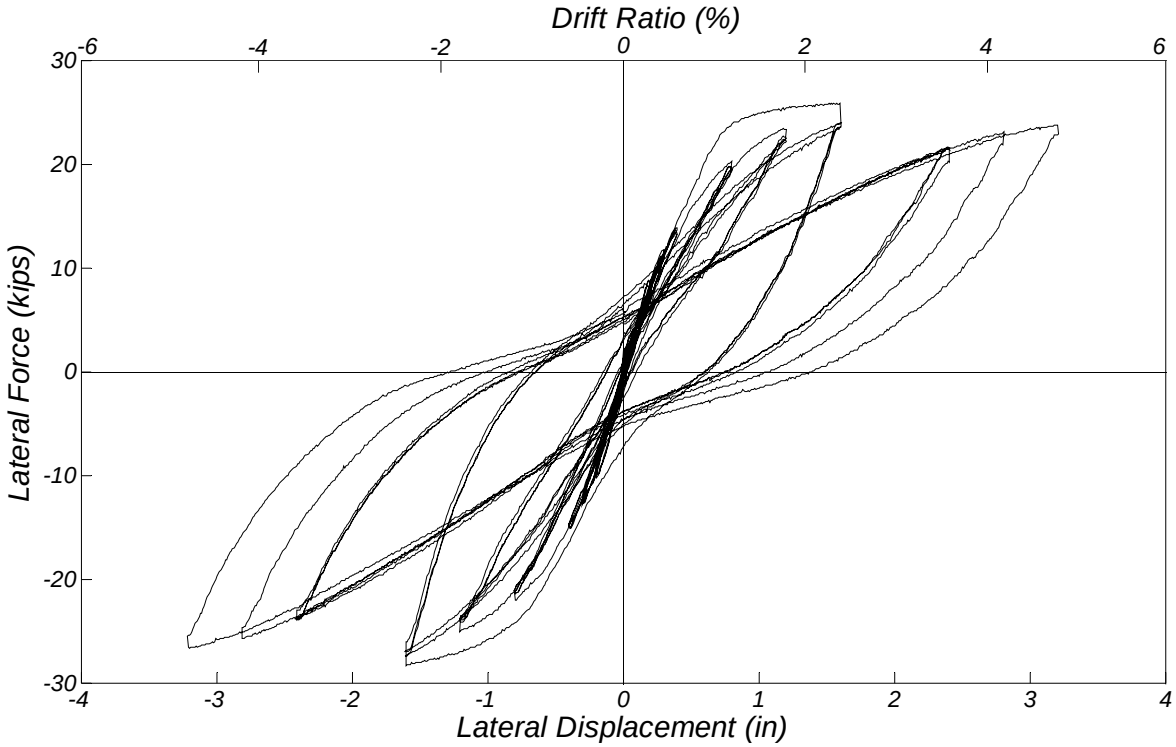

Figure 5.12 Lateral-force versus lateral-displacement response of TS-1 up to θ_r = 5%.

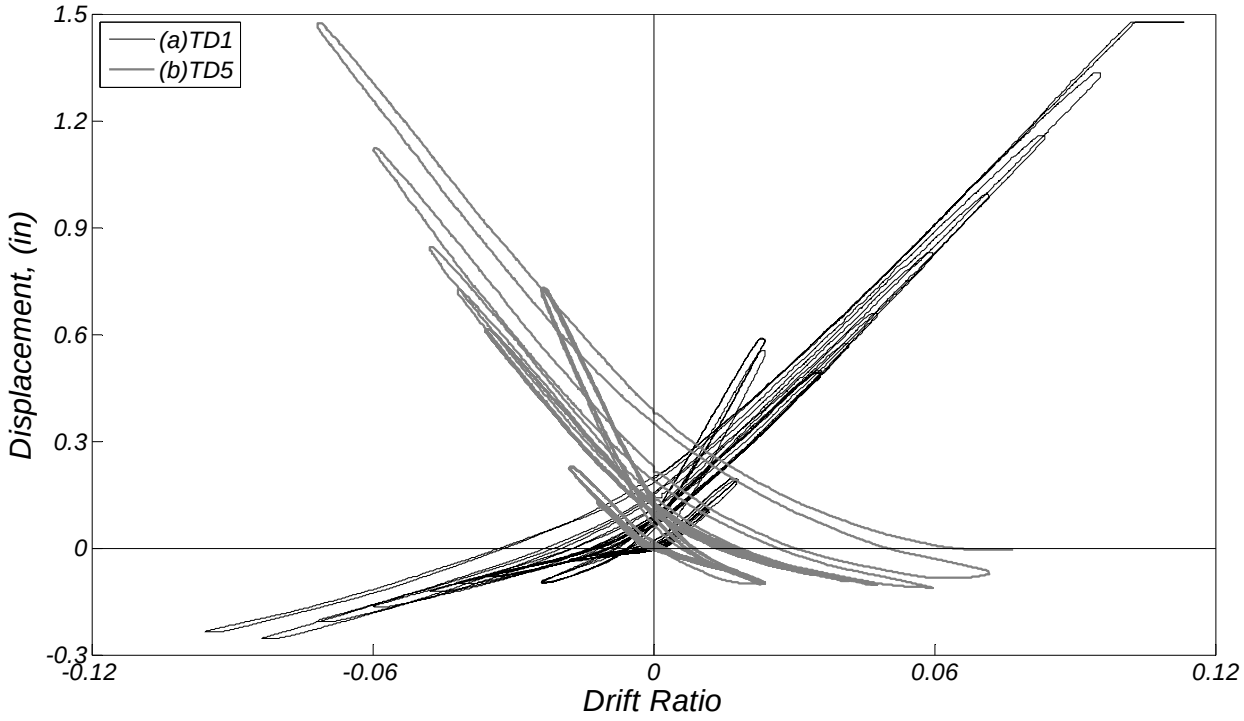

Figure 5.13 **Displacement measured using TD1 and TD5 at column's base versus drift ratio.**

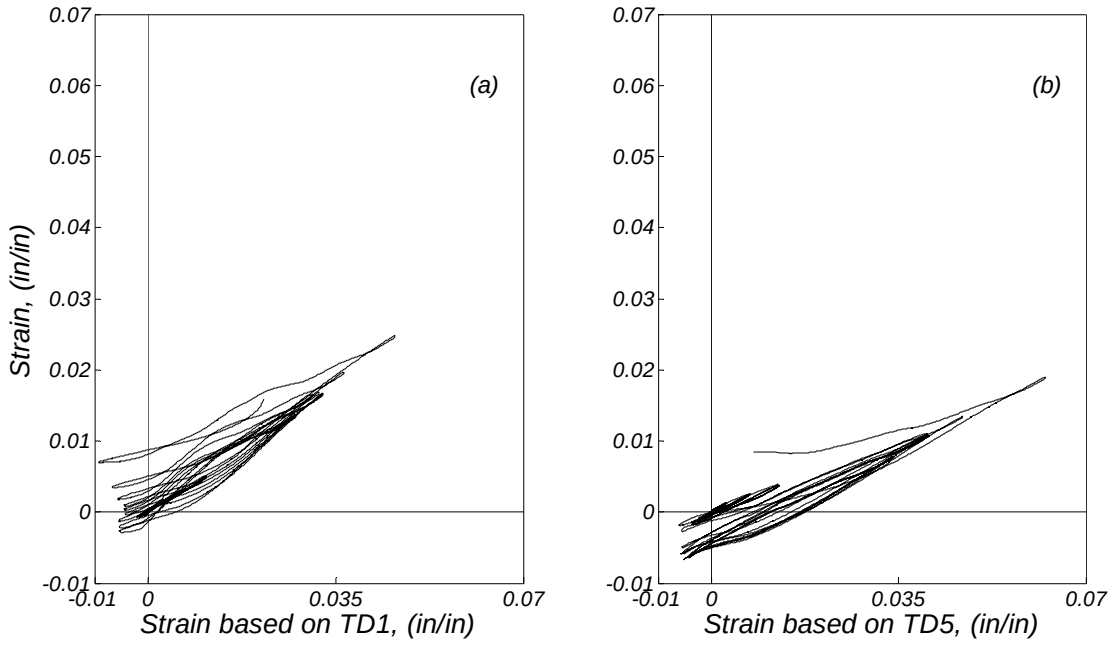

Figure 5.14 **(a) Strain measured by strain gauge SG102d versus smeared strain along the unbonded length on the west face of the column, based on TD1 measurements; (b) strain measured by strain gauge SG108d versus smeared strain, along the unbonded length, at the east face of the column–based on TD5 measurements.**

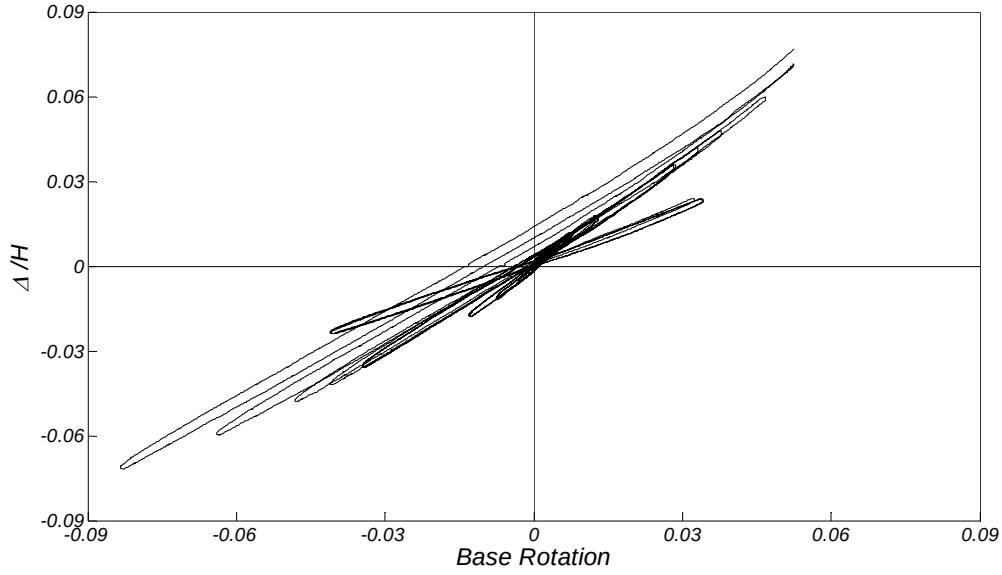

Figure 5.15 Computed base rotation using the measurements of TD1 and TD5 versus drift ratio.

Figure 5.16 plots the strain profiles of the east and west faces of the column based on the displacement transducers' measurements. Figure 5.16(a) plot the strain profiles of the west face for the eastward response, Figure 5.16(b) plots the strain profile of the east column face for westward response. Figure 5.16(c) plots the strain profile of the west face for the westward response, and Figure 5.16(d) plots the strain profiles of the of the east column face for eastward response. The profiles are plotted at six distinct drift ratios (θ_r) equal to 0.6%, 1.2% 2.4%, 3.6%, 4.8%, and 6.0%, respectively. At each drift ratio the profile during the last cycle of these drift ratios is plotted. As shown in Figure 5.16(a) and (b), for both column faces at drift ratios larger than 1.2%, the strain measured 5.5 in. above the column's base is compressive even if the corresponding face of the column's base uplifts. This location falls within the unbonded region of the rebar, therefore the steel-concrete strain compatibility does not hold. Note that significant compressive strains were measured at both sides of the column even if the bottom of this side uplifts.

Figure 5.17 plots the strain measurements of four strain gauges located in the unbonding length region versus the drift ratio. As shown in Figure 5.17(a) and (b), similar values of strains were measured at both sides of the column 12 in. from the foundation top. As expected, the strain measured for positive displacement response at 12 in. from the top of foundation of bar C110 is smaller than the corresponding of bar C102, which is closer to the west face of the column [see

Figure 5.17(c)]. Figure 5.17(d) shows that the strain measured for negative displacement response at bar C107 6 in. above the column's base exceeded the strain measured at bar C108 12 in. from the column base.

Figure 5.18 plots the spiral reinforcement tensile strain profiles, based on the spiral strain gauge measurements at six drift ratios θ_r = 0.6%, 1.2% 2.4%, 3.6%, 4.8%, and 6.0%, respectively. At each drift ratio, the profile corresponds to the last cycle of this specific drift ratio. As expected, highest amplitude strains were measured at these gauges located near to the east and west faces of the column (see Figure 4.6 for a schematic of the gauge locations). Note that the strain measured in the spiral reinforcement remains less than 0.3% for drift ratios up to 6.0%. Figure 5.19 plots the spiral reinforcement strains using TSG3 and TSG9 versus drift ratio.

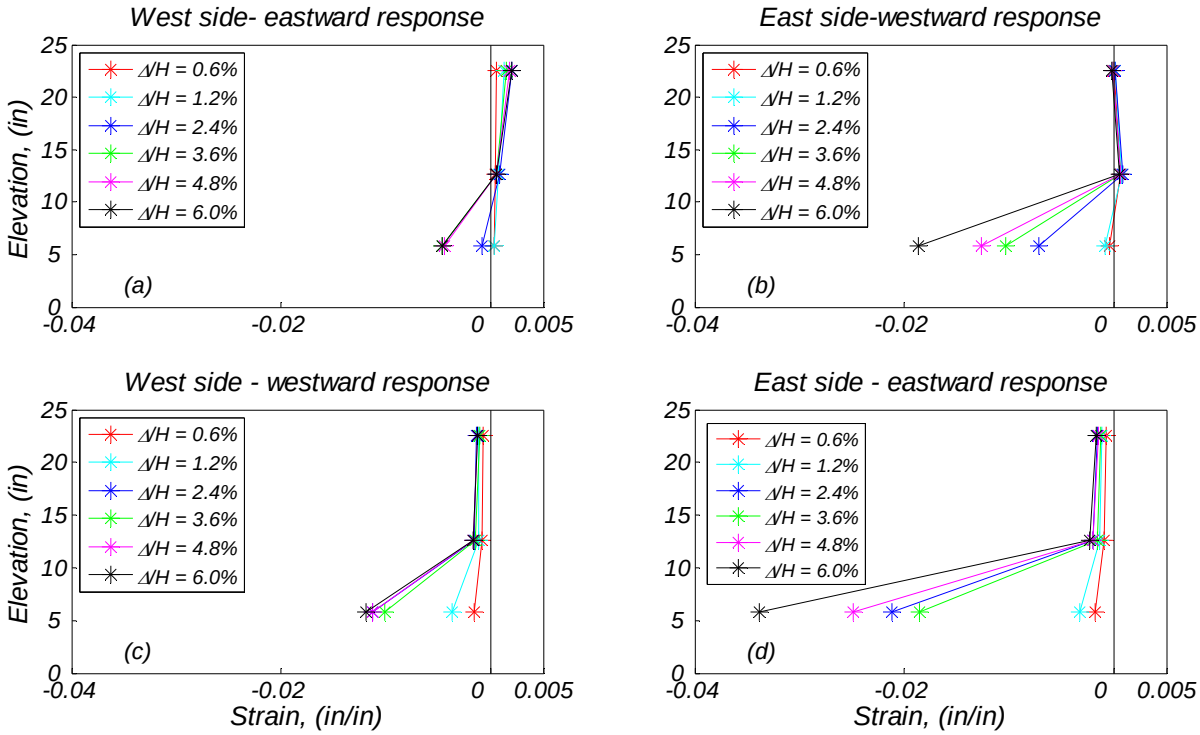

Figure 5.16 **Strain profiles based on displacement transducers: (a) west face for eastward response; (b) east face for westward response; (c) west face for westward response; and (d) east face for eastward response.**

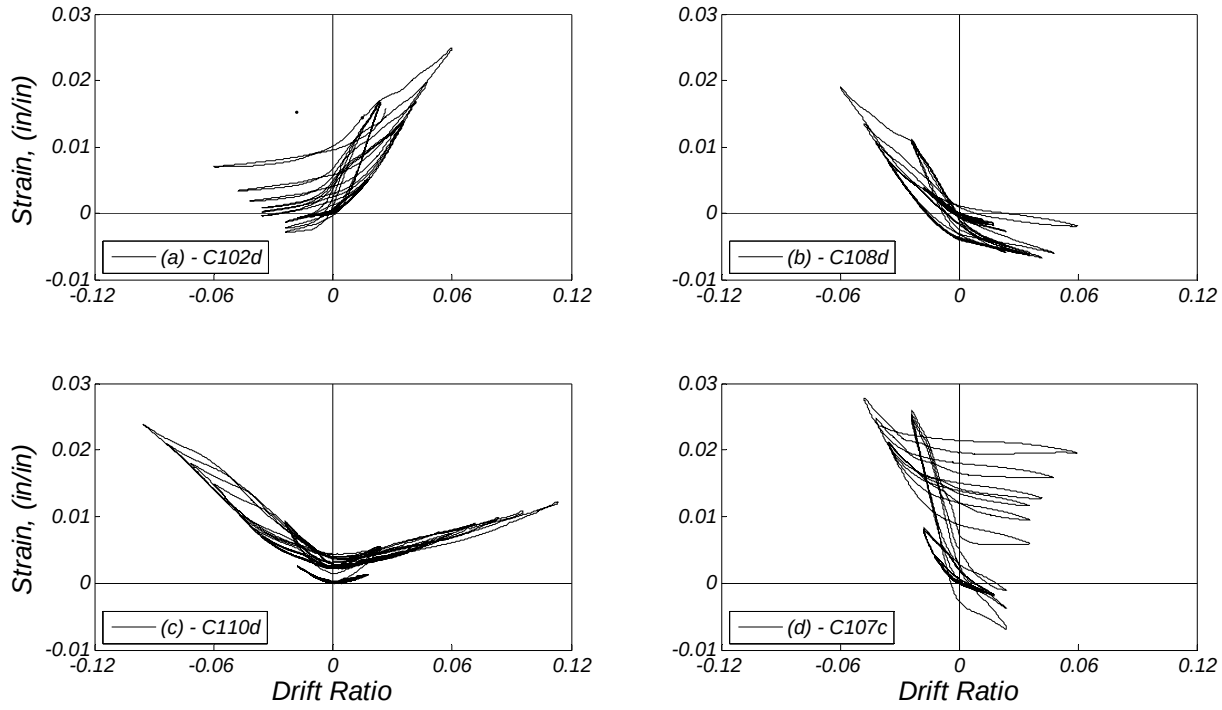

Figure 5.17 Longitudinal reinforcement strains versus drift ratio.

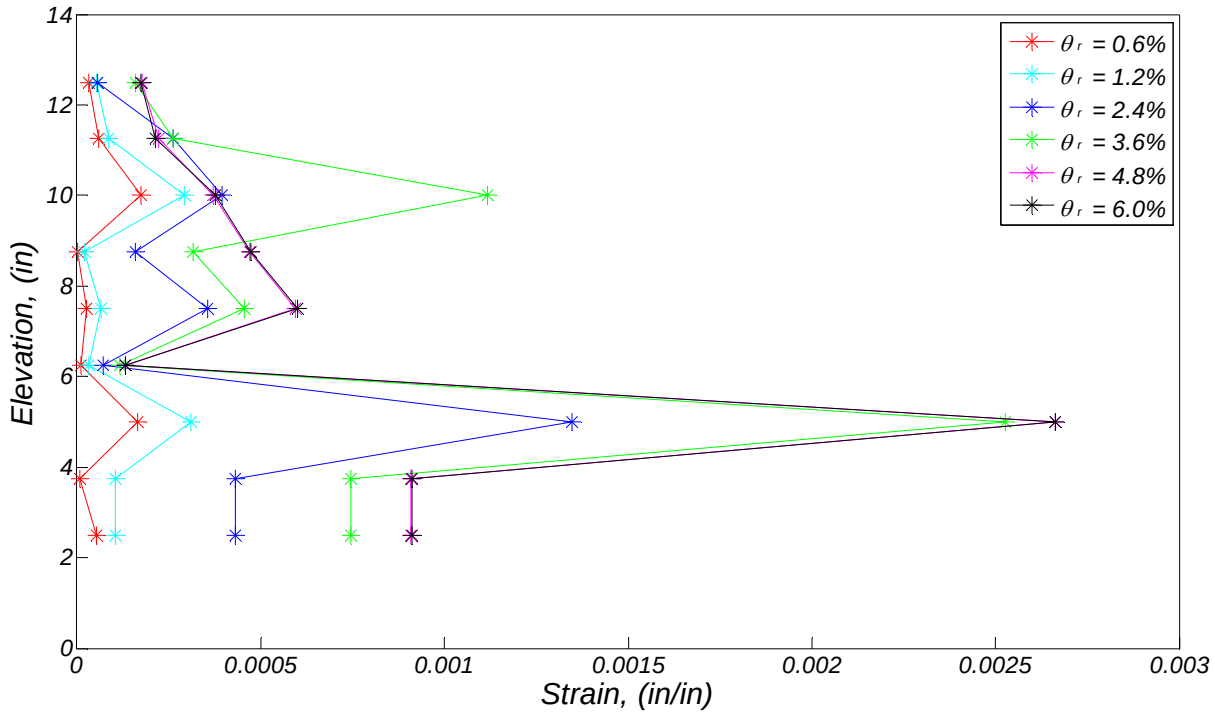

Figure 5.18 Strain profiles of spiral reinforcement of TS-1.

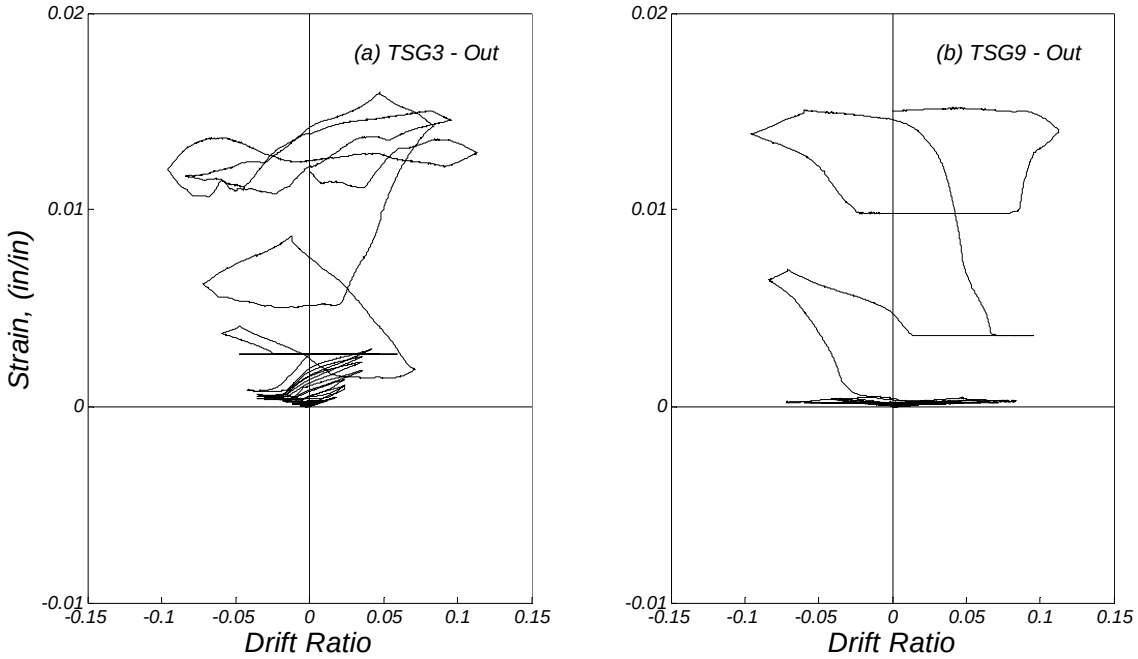

Figure 5.19 Spiral reinforcement strain gauge measurements versus drift ratio.

5.3.2 Specimen TS-2

Figure 5.20 plots the measured lateral-force versus lateral-displacement response of the TS-2. The force-displacement hysteretic response of this specimen was highly nonlinear and quite symmetric in terms of direction of displacement. The hysteretic response was stable and did not demonstrate significant strength degradation for drift ratios up to 4% for both sides of the response. Points 1 and 2 in Figure 5.20 correspond to the instants where the longitudinal bars C201 and C205 fractured. Both bars fractured during the cycle θ_r = 9.5%. The specimen reached a maximum drift ratio of 11.3%; it was stable and able to resist its axial load. This specimen formed a flexural plastic hinge at its bottom. Figure 5.21 shows in more detail the measured lateral-force versus the lateral-displacement response for θ_r up to 5%.

Figure 5.22 plots the measurements of the displacement transducers TD1 and TD6 [see Figure 4.10] versus drift ratio. Large values of displacements were measured on both faces, especially on the west face of the column. This was due to a major crack that formed at 1.2 in. from the column's base on both faces.

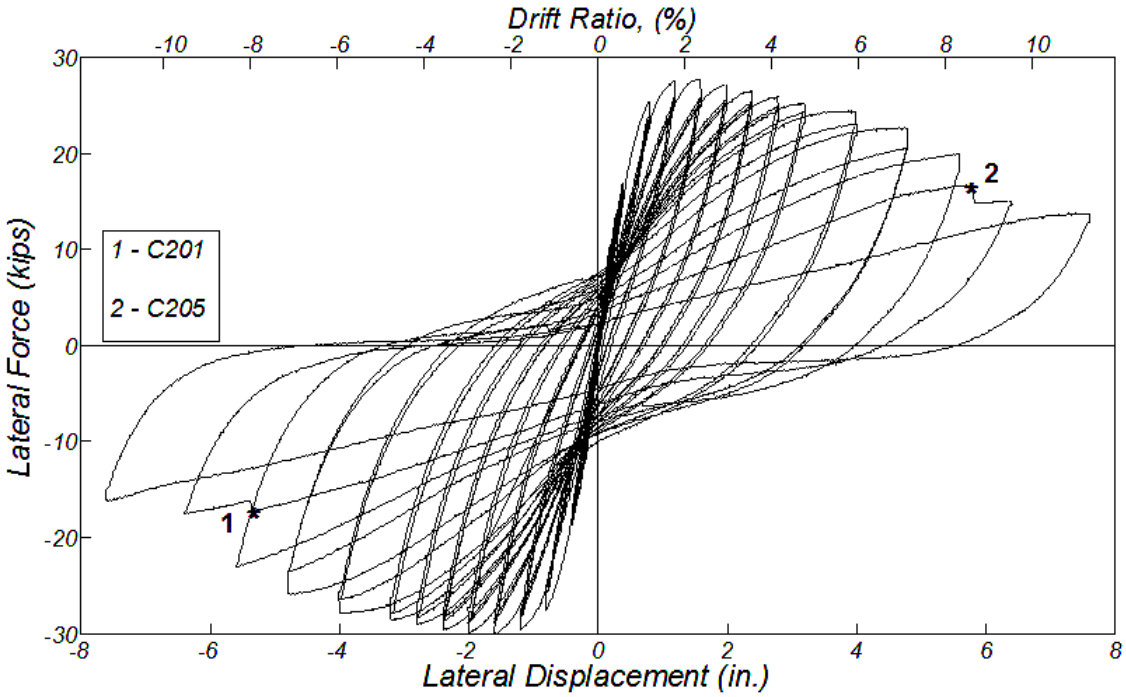

Figure 5.20 Lateral-force versus lateral-displacement response of TS-2.

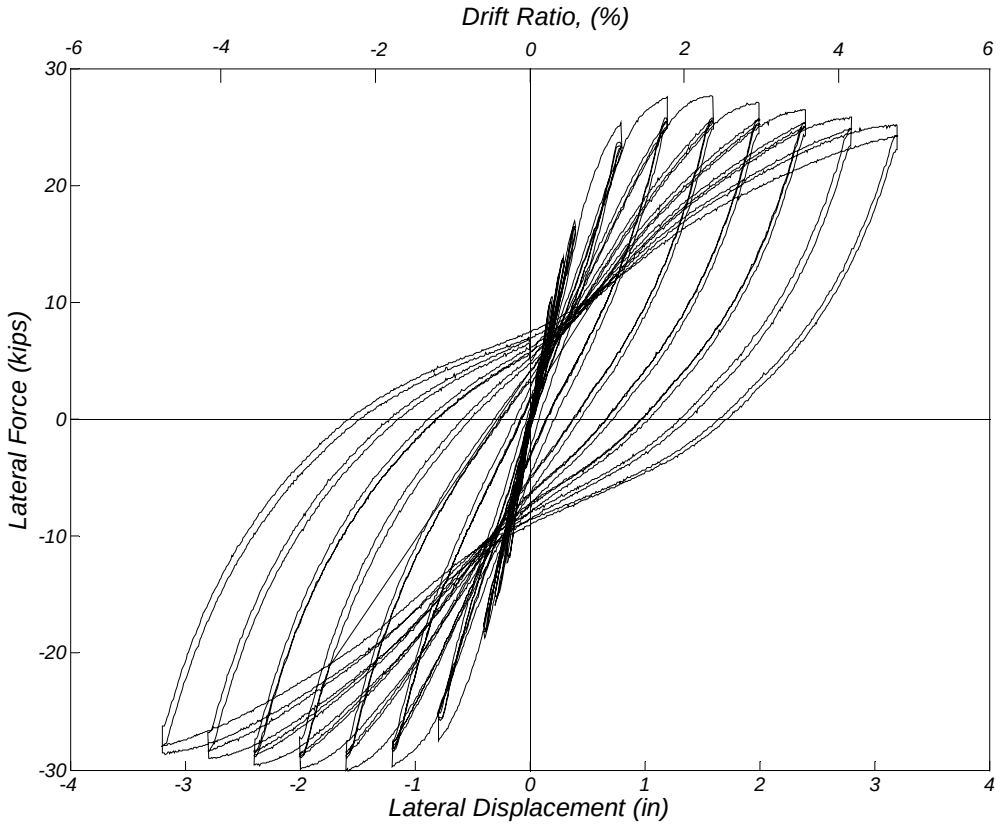

Figure 5.21 Lateral-force versus lateral-displacement response of TS-2 for θ_r up to 5%.

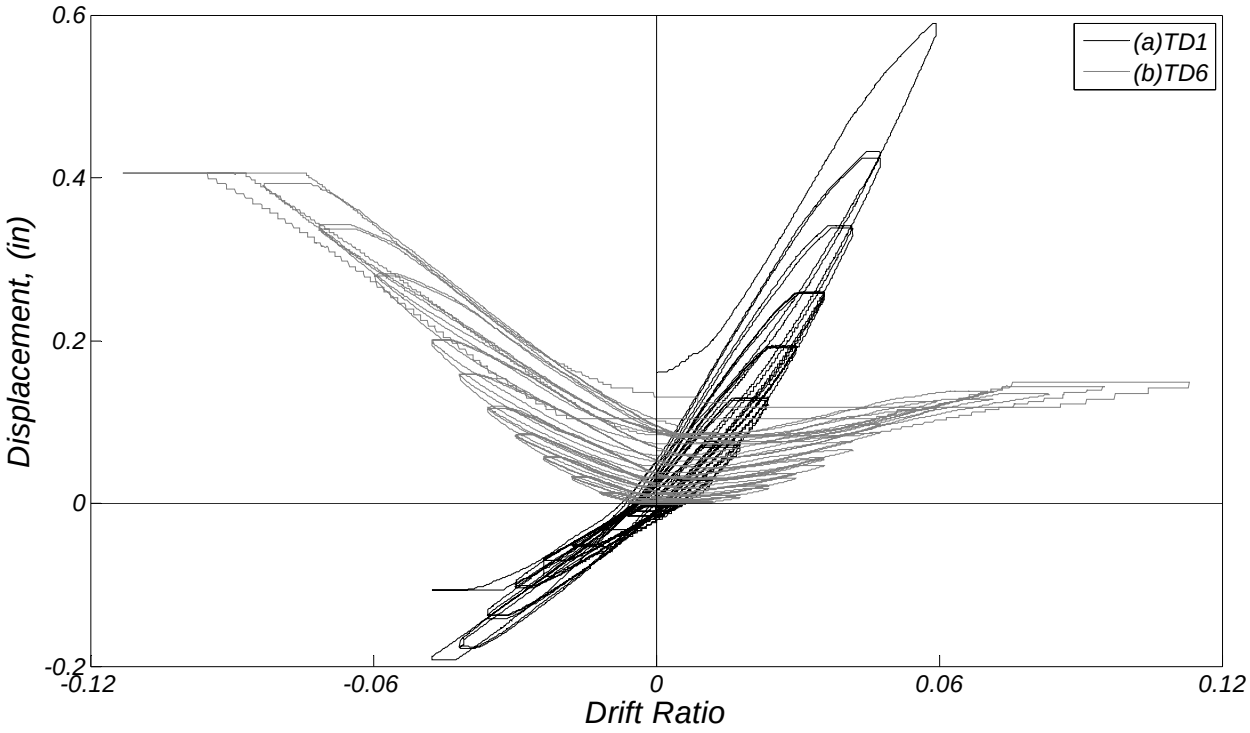

Figure 5.22 Displacements measured using TD1 and TD6 at column's base versus drift ratio.

Figure 5.23 plots the strain profiles of the west and east faces of the column based on the displacement transducer measurements. Profiles are shown for six drift ratios (θ_r) equal to 0.6%: 1.2% 2.4%, 3.6%, 4.8%, and 6.0%, respectively. For the west face and eastward response, Figure 5.23(a) shows that strains were localized in the bottom 4 in. of the column, especially within the bottom 2 in. of the column where a single crack formed. In this region, the measured strains were 7%, 14%, and 24 % for drift ratios 2.4%, 3.6% and 4.8%, respectively. It is assumed that such large values of strain developed without fracture of the longitudinal rebar because of the large strain ductility of the stainless steel rebar. As shown in the Figure 5.23(b), for the east face of the column and westward response, the strains were more uniform at the bottom 12 in. of the column compared to the west face of the column due to the presence of multiple cracks.

Figure 5.23(c) plots the strain profiles of the west face of the column for the westward response, demonstrating that up to θ_r = 4.8 % compressive strains were measured 1 in. above the column's base. For the east face of the column and eastward response, the largest compressive strains were measured at 8 in. above the column base for almost all drift ratios [see Figure

5.23(d)]. Figure 5.24 plots measurements of strain gauges versus drift ratio; large strains of 7% were measured for C 202c [see Figure 5.24(a)].

Figure 5.25 plots the strain profiles of the spiral reinforcement at six distinct drift ratios: θ_r = 0.6%, 1.2% 2.4%, 3.6%, 4.8%, and 6.0%, respectively. The profile at the last cycle of each θ_r is plotted. The peak strain measured with the inner and outer strain gauge at each location is presented. Peak strains were measured on those strain gauges located closer to the east and west face of the column. Figure 5.26 shows the crack locations along the column height on west and east face of the column, which are in agreement with these strain profiles. Strains larger than 1% and up to 4.3% were measured for drift ratios between 2.4% and 6.0%. Figure 5.26 plots the strains measured with TSG2 and TSG6 versus drift ratio.

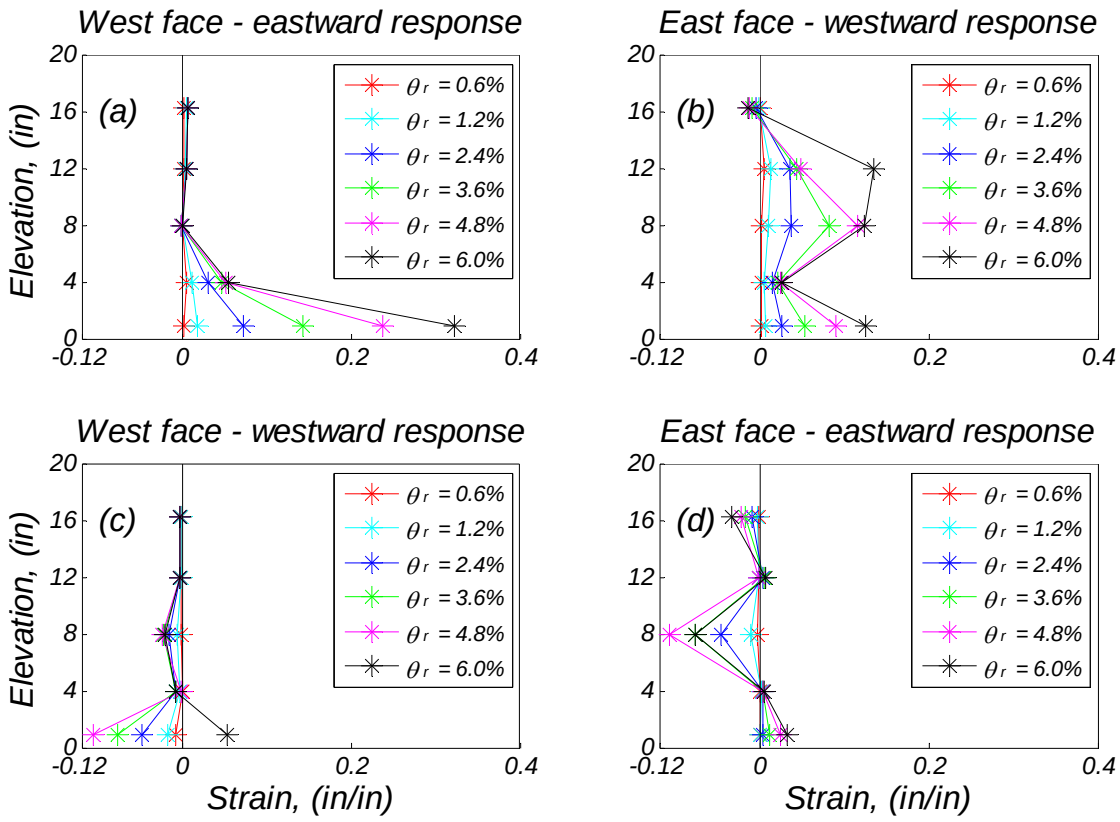

Figure 5.23 **Strain profiles based on displacement transducers: (a) west face for eastward response; (b) east face for westward response; (c) west face for westward response; and (d) east face for eastward response.**

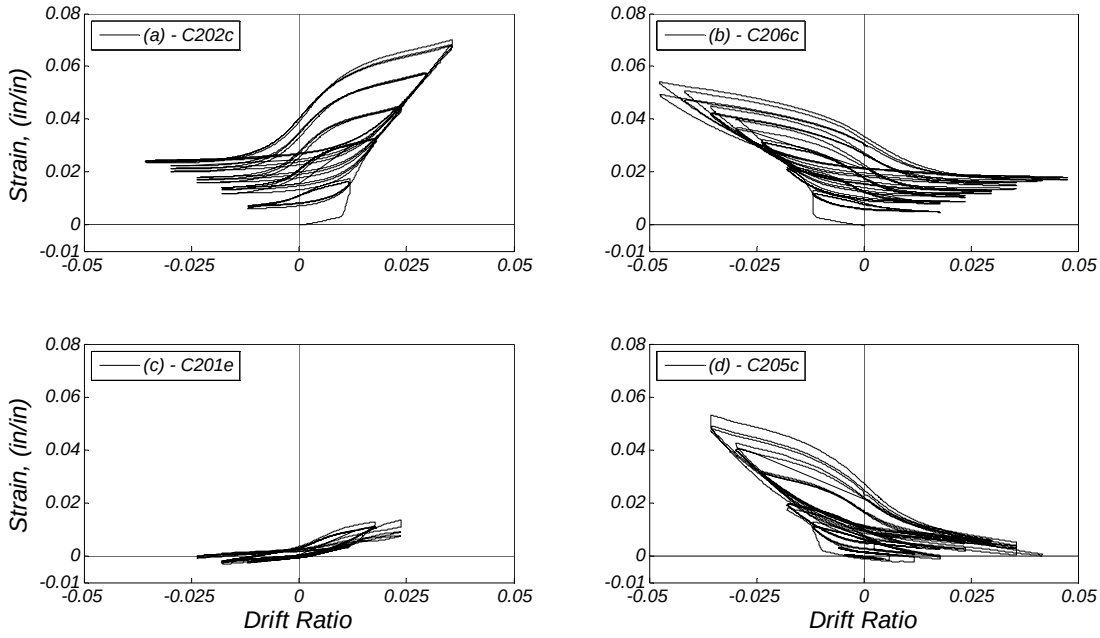

Figure 5.24 Longitudinal reinforcement strains versus drift ratio.

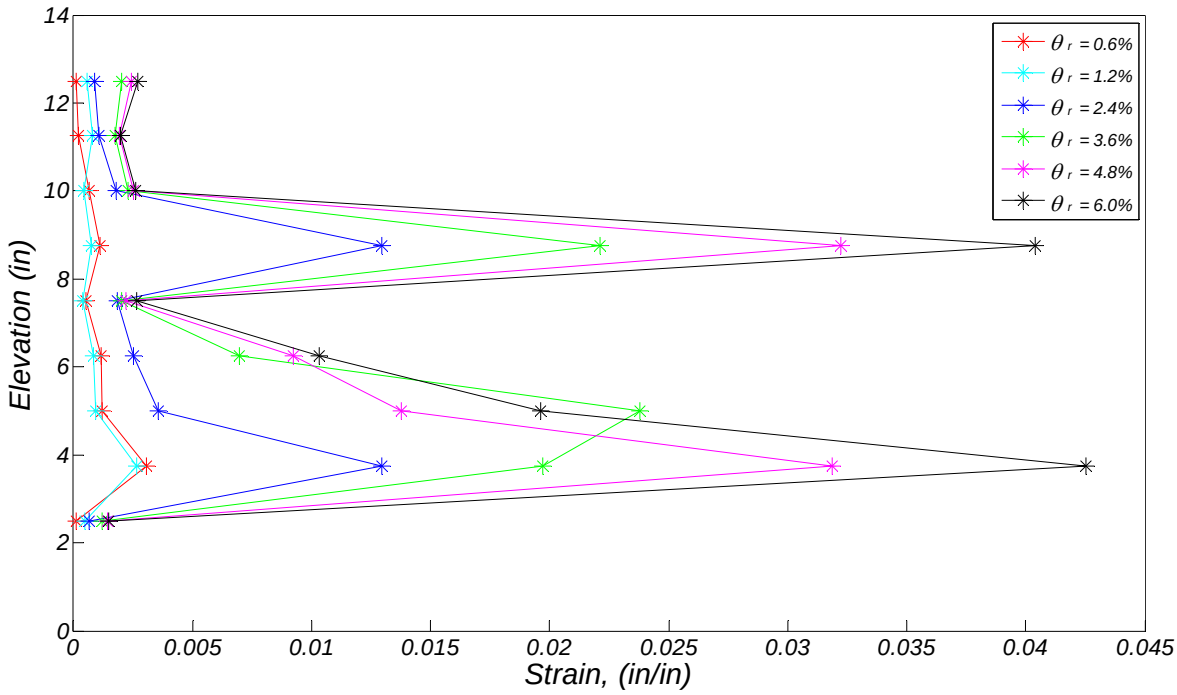

Figure 5.25 Strain profile of spiral reinforcement of TS-2.

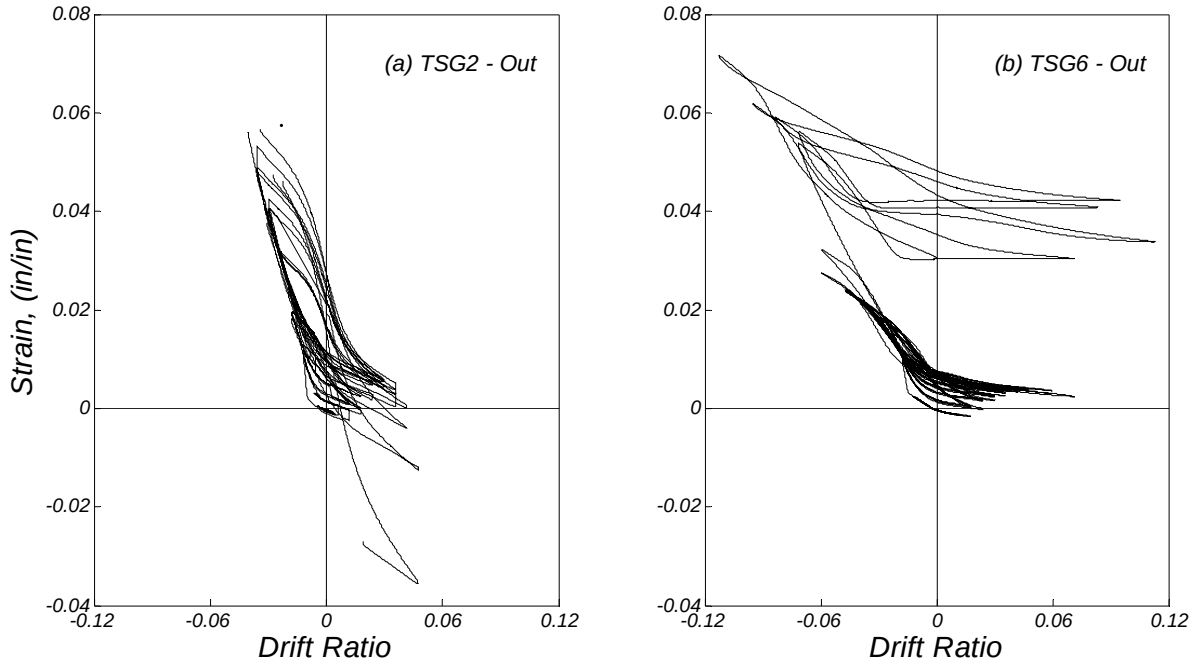

Figure 5.26 Spiral reinforcement strain measurements versus drift ratio.

5.4 COMPARISON OF FORCE DISPLACEMENT RELATIONSHIP OF TS-1 AND TS-2

Figure 5.27 and Figure 5.28 compare the lateral-force versus lateral-displacement response of TS-1 and TS-2 for drift ratios up to 11% and 5%, respectively. For drift ratios up to 6%, both specimens demonstrated similar behavior [see Figure 5.28]. The hysteretic behavior of TS-2 was characterized by about 10% greater strength, while TS-1 was characterized by more pinching. At drift ratios larger than 6%, TS-1 demonstrated less strength degradation for positive displacement response compared to TS-2. In addition, TS-1 was more economical to construct compared to TS-2, which used stainless steel for the longitudinal bars.

Deformation at zero lateral force of TS-1 was less than TS-2 at the same drift ratio. Also Figure 5.27 shows that there is more energy dissipation in TS-2 response compared to TS-1, which is due to the spread of plasticity in TS-2.

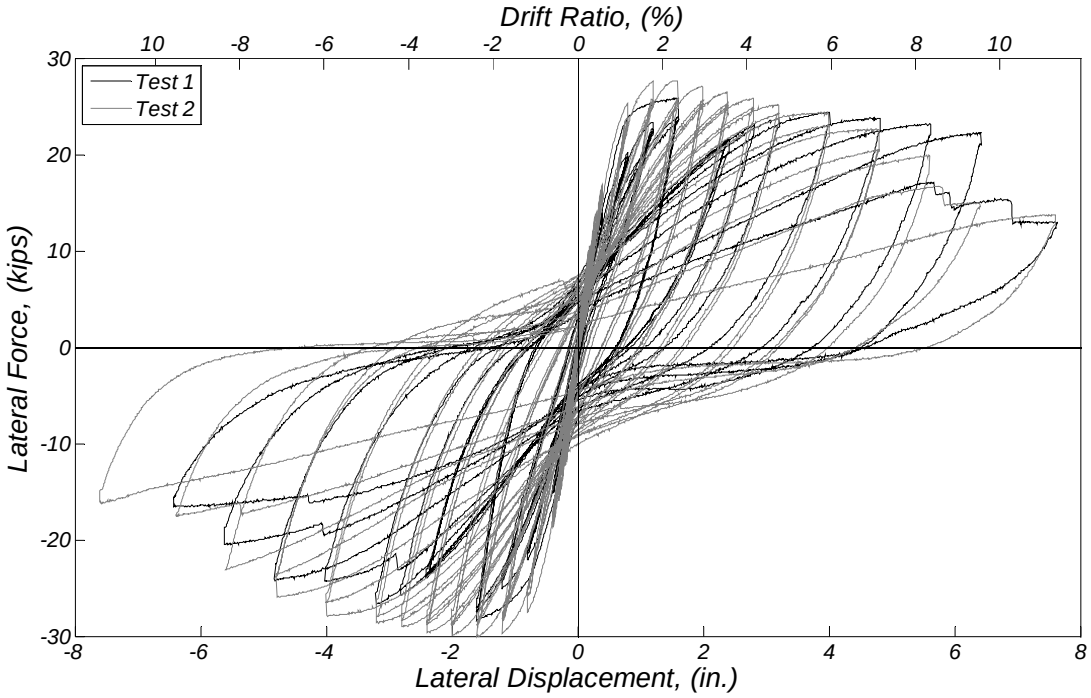

Figure 5.27 Comparison of lateral-force versus lateral-displacement relation for TS-1 and TS-2.

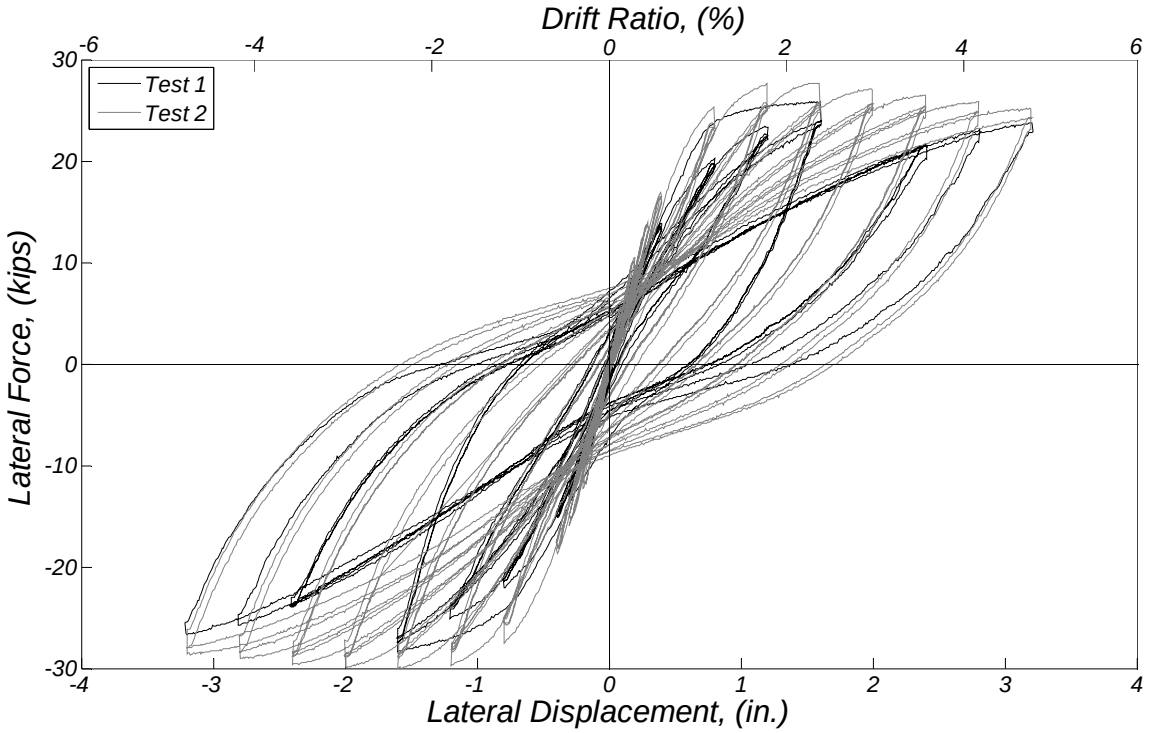

Figure 5.28 Comparison of lateral-force versus lateral-displacement relation for TS-1 and TS-2 for a drift ratio up to 5%.

5.5 COMPARISON OF FORCE DISPLACEMENT RELATIONSHIP OF TS-1 AND TS-2 WITH A CONVENTIONAL REINFORCED CONCRETE COLUMN

Terzic recently carried out an experimental investigation of RC bridge columns, with column dimensions identical to those of the present study (2009).The specimens were tested under biaxial loading in two perpendicular directions (*x*-axis and *y*-axis) with the same boundary conditions as presented herein. Although Terzic's specimens had the same ρ_l of 1.2%, they had a ρ_v of 0.75%, which was two times larger compared to the specimens reported here.

One of the major differences in performance between Terzic's specimens and the current test specimens was in the spalling resistance of the concrete cover. Whereas extensive spalling was observed in Terzic's Base 45 specimen at a drift ratio of 4%—with concrete spalling up to a height equal to the diameter of the column above the top of the foundation—very limited spalling was observed at a similar drift ratio of 3.6% in both TS-1 and TS-2 (see Figure 5.29. Specifically, in TS-1, spalling was only observed locally in close vicinity to the longitudinal bar C107 [see Figure 5.29(a)].

The difference in lateral-force verses lateral-displacement behavior for drift ratios up to 5% for TS-1, TS-2, and Terzic's Base 45 specimen is shown in Figure 5.30. As expected, the lateral force of TS-1 and TS-2 exceeded the corresponding force of Terzic's specimen because of the enhanced tension ductility of SC-HyFRC. Both TS-1 and TS-2 performed very well despite half the transverse reinforcing ratio compared to Terzic's Base 45 specimen. Figure 5.31 is similar to Figure 5.30 but with the lateral force of each test now normalized to their peak loads. This was done to better compare the hysteretic characteristics of the response. For both TS-1 and TS-2 a more pinched behavior is observed compared to the Base45 specimen.The pinching in TS-1 is a result of the different mechanism of nonlinear deformation that relies on a single crack formation and rocking of the column at its interface with the foundation. In TS-2, the pinching may possibly be due to the less extent of spread of plasticity in the plastic hinge region.

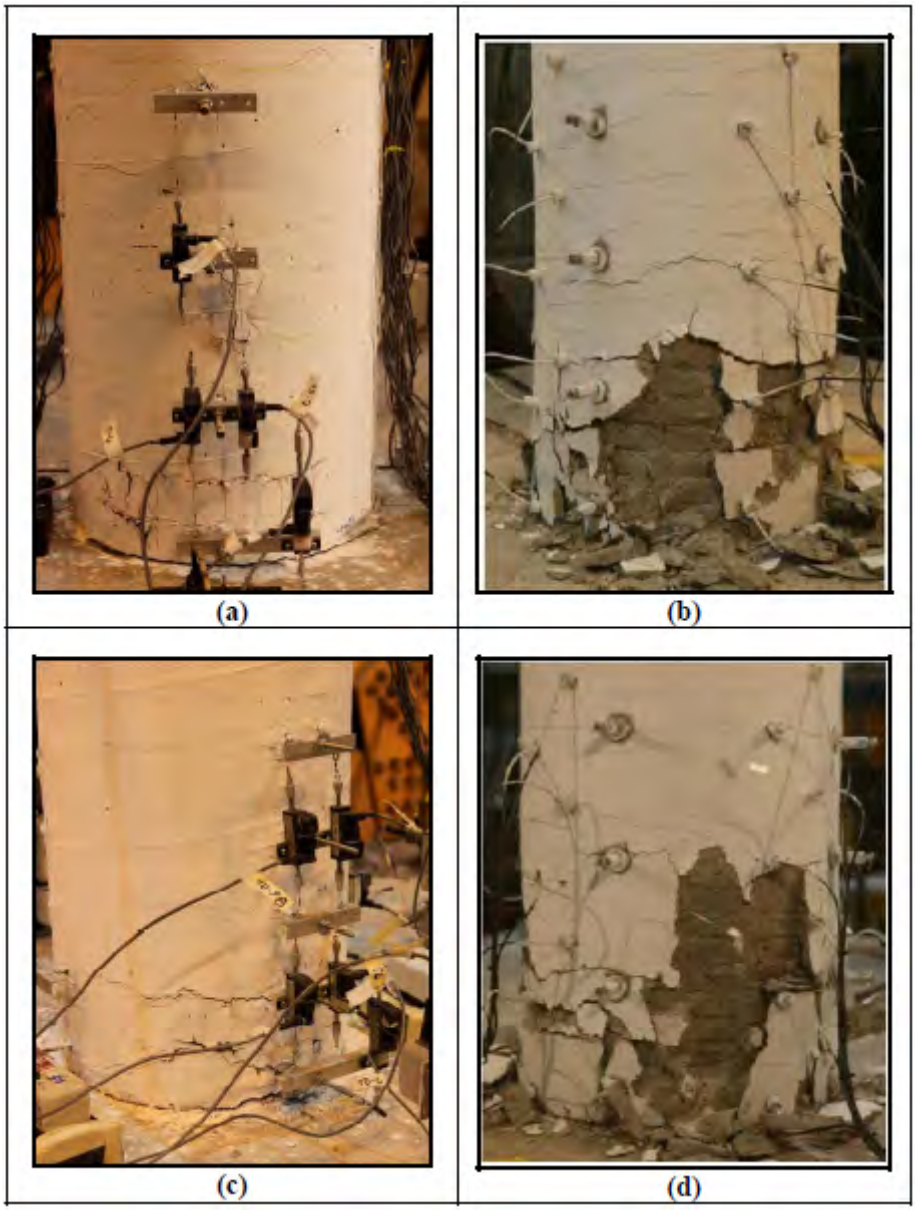

Figure 5.29 **Damage states of bridge columns at similar drift ratio: (a) east face of TS-1 at drift ratio of 3.6%; (b) north-west face of Terzic's test Base45 at drift ratio of 4%; (c) east face of TS-2 at drift ratio of 3.6%; and (d) south-east face of Terzic's test Base45 at 4%.**

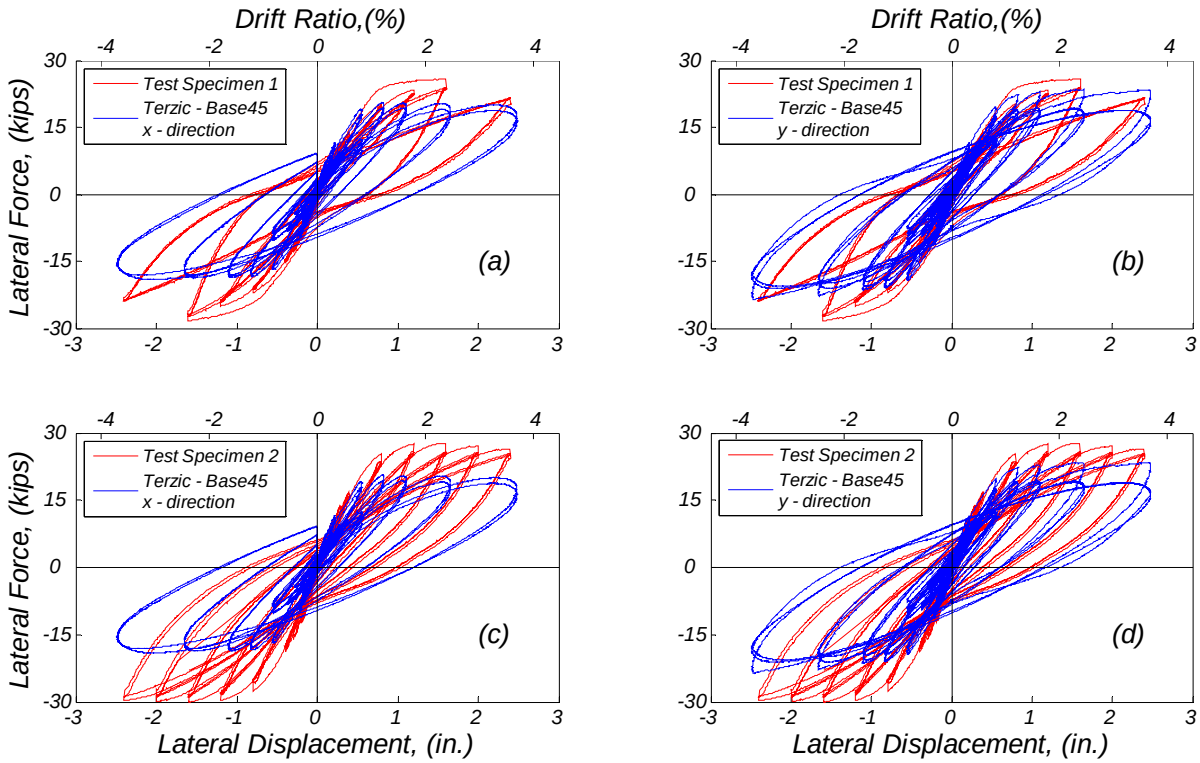

Figure 5.30 **Lateral-force and lateral-displacement compares the results for: (a) TS-1 compared with Terzic's response along the *x*-axis; (b) TS-1 compared with Terzic's response along the *y*-axis; (c) TS-2 compared with Terzic's response along *x*-axis; and (d) TS-2 compared with Terzic's response along *y*-axis.**

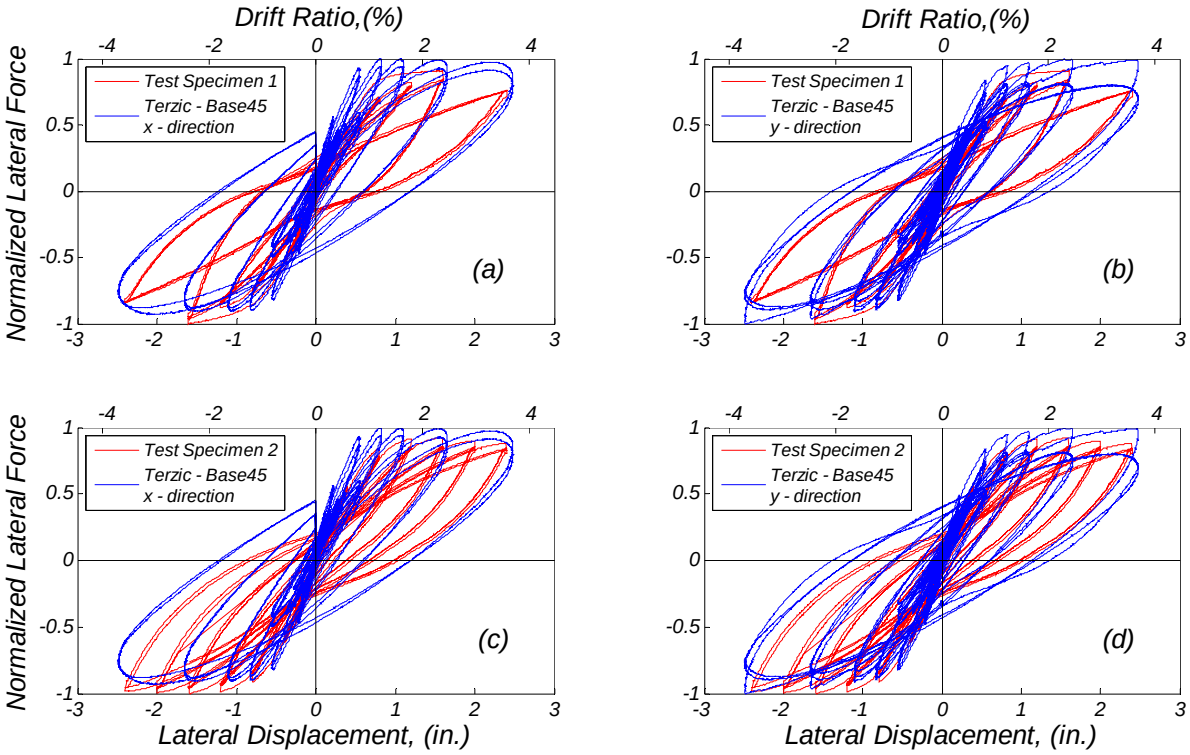

Figure 5.31 **Normalized lateral-force and lateral-displacement compares the results for: (a) TS-1 compared with Terzic's response along the *x*-axis; (b) TS-1 compared with Terzic's response along the *y*-axis; (c) TS-2 compared with Terzic's response along *x*-axis; and (d) TS-2 compared with Terzic's response along *y*-axis.**

6 Summary and Conclusions

An experimental study of the cyclic response of bridge piers built using self-compacting hybrid fiber reinforced concrete was conducted. Two 1:4.5 scale column specimens were built using SC-HyFRC and were tested statically under uni-directional cyclic loading. The design of the two specimens differed in terms of the location where the nonlinear deformations were accommodated. The first specimen was designed to rock at the column's base–foundation interface. The second specimen, which incorporated stainless steel for the longitudinal reinforcement, was designed to form a flexural plastic hinge at its base. Both specimens had half the transverse reinforcement ratio of conventional RC columns.

In comparison with conventional RC, SC-HyFRC combines the advantages of self compaction, resulting in improved constructability, and enhanced material properties compared to conventional fiber reinforced composites, resulting in a more ductile behavior in both tension and compression.

The response of both test specimens was very satisfactory. Both attained large drift ratios equal to 11% without losing axial load carrying capacity and both resisted spalling of the concrete cover up to a drift ratio of 3.6%. Thus, not only does SC-HyFRC result in enhanced constructability of bridge columns but also enhanced seismic performance at different performance levels.

REFERENCES

AASHTO (1998). LRFD Bridge Design Specifications, second edition. American Association of State Highway and Transportation Officials, Washington DC,

ACI Committee, 318 (2002). Building Code Requirements for Structural Concrete (ACI 318 – 02) and Commentary (318R – 02), American Concrete Institute, Farmington Hills, Michigan.

Aoude, H., Cook W., Mitchell, D. (2009). Behavior of columns constructed with fibers and self-consolidating concrete. ACI Struct.l J. 106(3):349–357.

ASTM Standard C1609 (2006). Standard Test Method for Flexural Performance of Fiber-Reinforced Concrete. West Conshohocken, PA, 2003, DOI: 10.1520/C1609, www.astm.org: ASTM International.

ASTM Standard C1611 (2009). Standard Test Method for Slump Flow of Self-Consolidating Concrete. West Conshohocken, PA, 2003, DOI: 10.1520/C1611, www.astm.org: ASTM International.

ASTM Standard C1621 (2009). Standard Test Method for Passing Ability of Self-Consolidating Concrete by J-Ring. West Conshohocken, PA, 2003, DOI: 10.1520/C1621, www.astm.org: ASTM International.

Aviram A., Stojadinovic, B., Parra-Montesinos, G.J., Mackie, K.R. (2010). Structural response and cost characterization of bridge construction using seismic performance enhancement strategies, PEER Report No. 2010/01, Pacific Earthquake Engineering Research Center, University of California, Berkeley, CA.

Banthia, N., Nandakumar, N. (2003). Crack growth resistance of hybrid fiber reinforced cement composites. Cem. Concr. Composites, 25:3–9.

Bayasi, Z., Gebman, M. (2002). Reduction of lateral reinforcement in seismic beam-column connection via application of steel fibers, ACI Struct. J., 99(6):772–780.

Billington, S.L., Yoon, J.K. (2004). Cyclic response of unbonded post-tensioned precast columns with ductile fiber-reinforced concrete, ASCE, J. Bridge Engrg., 4:353–363.

Blunt, J., Ostertag, C.P. (2009a). A performance based approach for the design of a deflection hardened hybrid Fiber reinforced concrete, ASCE, J. Engrg. Mech., 135:978–986.

Blunt, J., Ostertag, C.P. (2009b). Deflection hardening and workability of hybrid fiber composites, ACI Mat. J., 106:265–272.

Buckle, I.G., Constantinou, M.C., Dicleli, M., Ghasemi, H. (2006). Seismic isolation of highway bridges, Technical Report MCEER-06-SP07, Multidisciplinary Center for Earthquake Engineering Research, State University of New York at Buffalo, Buffalo, NY.

California Department of Transportation (2006). Seismic Design Criteria – version 1.4. Sacramento, CA.

CHBDC (2001). Canadian Highway Bridge Design Code. CAN/CSA-S6-00, CSA International Toronto, Ontario, Canada.

Cormack, L.G. (1998). The design and construction of the major bridges on the Mangaweka rail deviation. Trans. Institute of Professional Engineers of New Zealand, 15:6–23.

Espinoza, A., Mahin, S. (2006). Rocking of bridges piers subjected to multi-directional earthquake loading, Proc., Fifth Natl. Seismic Conf. Bridges & Highways. San Francisco, CA.

Filiatrault, A., Pineau, Houde, J. 1995. Seismic behavior of steel fiber reinforced concrete interior beam column joints, ACI Struct. J., 92(5):543–552.

Grubb, J., Ostertag, C.P., Devine, T. (2007). Effect of crack control on corrosion, Cem. Concr. Res., 37:1115–1126.

Henager, C.H. (1977). Steel fibrous, ductile concrete joint for seismic-resistant structures. In: Reinforced Concrete Structures in Seismic Zones, SP-53, N. M. Hawkins and D. Mitchell, eds., American Concrete Institute, Farmington Hills, Michigan, pp. 371–379.

Hewes, J. T. (2007). Seismic tests on precast segmental concrete columns with unbonded tendons, Bridge Struct., 3(3)215–227. London: Taylor and Francis.

Japan Road Association (2002). Specifications for Highway Bridges, Part V: Seismic Design.

Ketchum, M., Chang, V., Shantz, T. (2004). Influence of design ground motion level on highway bridge costs, PEER Report 6D01, Pacific Earthquake Engineering Research Center, University of California, Berkeley, CA.

Lawler, J.S., Zampini, D., Shah, S.P. (2005). Microfiber and macrofiber hybrid fiber reinforced concrete. J. Mat. Civil Engrg., ASCE, 17:595–604.

Mahin, S., Sakai,J., Jeong, H. (2006). Use of partially pre-stressed reinforced concrete columns to reduce post-earthquake residual displacements of bridges, Proc., Fifth Natl. Seismic Conf. on Bridges & Highways, Paper No. B25, San Francisco, CA.

Mander, J.B., Cheng, C.T. (1997a). Seismic design of bridge columns based on control and repairability of damage, Technical Report NCEER-97-0013, National Center for Earthquake Engineering Research, State University of New York, Buffalo, NY.

Mander, J.B., Cheng, C.T. (1997b). Seismic resistance of bridge piers based on damage avoidance design, Technical Report NCEER-97-0014. National Center for Earthquake Engineering Research, State University of New York, Buffalo, NY.

Mergos P.E., Kawashima, K. (2005). Rocking isolation of typical bridge pier on spread foundation, J. Earthq. Engrg., 9(2):395–414.

NCHRP 12-74 Research Project (2010). Development of Precast Bent Cap Systems for Seismic Region.

Nehdi, M., Ladanchuk, J. (2004). Fiber synergy in fiber-reinforced self-consolidating concrete, ACI Mat. J., 101(6):508–517.

Okamura, H., Ouchi, M. (1998). Self-compacting high performance concrete, Progress in Struct. Engrg. Mat., 1(4):378-383.

Ostertag, C.P., Blunt, J. (2010). Effect of crack control in hybrid fiber reinforced composites on corrosion rate of steel reinforcing bars, In: Fracture Mechanics of Concrete and Concrete Structures, 1:415–422.

Ostertag, C.P., Blunt, J. (2008). Use of fiber reinforced concrete in bridge approach slabs, Caltrans Report No. CA09-0632, pp. 1–74.

Ostertag, C.P., Blunt, J., Grubb, J. (2007). Mitigation of expansive deterioration processes through crack control, In: Fracture Mechanics of Concrete and Concrete Structures, 3:1843-1849.

Ou Y. Chiewanichakorn, C.M., Aref, A.J., Lee, G.C. (2007). Seismic performance of segmental precast unbonded post-tensioned concrete bridge columns, J. Struct. Engrg., ASCE, 133(11):1636–1647.

Ouchi, M., Hibino, M., Okamura, H. (1996). Effect of superplasticizer on self-compactablility of fresh concrete, Transportation Research Record, 1574:37–40.

Park, R., Paulay, T. (1975). Reinforced Concrete Structures. New York: John Wiley & Sons.

Parra-Montesinos, G., Wight J.K. (2002). Prediction and shear distortion in R/C beam column joints, S. M. Uzumeri Symposium: Behavior and Design of Concrete Structures for Seismic Performance, SP-197, S. A. Shiekh and O. Bayrak, eds., American Concrete Institute, Farmington Hills, Mich., 191–214.

Qian, C., Stroeven, P. (2000). Fracture properties of concrete reinforced with steel-propylene hybrid fibres, Cem. Concr. Composites, 22:343–351.

Rossie, P. (1997). High performance multimodal fiber reinforced cement composites (HPMFRCC): The LCPC experience, ACI Mat. J., 94:478–483.

Saiidi, S., O'Brien, M., Sadrossadat-Zadeh, M. (2009). Cyclic response of concrete bridge columns using superelastic nitinol and bendable concrete, ACI Struct. J., 106:67–77.

Sritharan, S., Priestley, M.J.N., Seible (1999). Enhancing seismic performance of bridge cap beam-to-column joints using prestressing. PCI J., 44(4):74–91.

Terzic, V. (2009). Experimental evaluation of the residual axial load capacity of circular bridge columns, CE299 Report, Dept. of Civil and Enrviron. Engrg., University of California, Berkeley, CA.

Vasconez, R. M., Naaman, A.E., Wight, J.K. (1998). Behavior of HPFRC connections for precast concrete frames under reversed cyclic loading, PCI J., 43(6):58–71.

Yi, C.K., Ostertag, C.P. (2005). Mechanical approach in mitigating alkali-silica reaction, Cem. Concr. Res., 35(1):67-75.

Yoon, J.K., Billington, S.L. (2002). Experimental and numerical studies of precast unbonded post-tensioned bridge columns with engineered cementitious composites, Research Report 02–03, Cornell University, Ithaca, NY.

Appendix A: Development of SC-HyFRC; Batching Process, Flow Characteristics, and Mechanical Properties

The initial batching and testing was performed on plain concrete to investigate the proper ratio of superplasticizers and VMA to produce self-compacting properties without fibers. The concrete mix without fibers (given in Table A.1) was successful in achieving a non-segregated flow, with measured flow diameters of 28 in. (710 mm) in both directions, as shown in Figure A.1.

Table A.1 SCC mix composition (lb / yd^3).

Cement	Fly Ash	Water	FA	CA	SP (wt.%)	VMA (wt.%)
670	220	400	1695	837	0.42	0.40

Figure A.1 Flow diameter of SCC mix without fibers.

To achieve the required flow properties of a self-compacting HyFRC with target flow diameters of 24 in., the following parameters were investigated and optimized:

- Chemical admixtures and SP / VMA ratios
- Fiber types and volume fractions
- Paste/aggregate volume ratios
- Aggregate content and FA / CA ratios

(i) Chemical Admixtures and SP / VMA Ratios

Following the manufacturer's recommendation for both minimum and maximum dosages of SP and VMA (Table A.2) produced non-consolidating mixes and segregated mixes, respectively. Fiber inclusion drastically limited the fresh state fluidity with low chemical dosages (Mix #3 in Table A.2), resulting in a lack of fiber dispersion. Under maximum recommended dosages of admixtures (Mix #4 in Table A.2), segregation was exhibited as shown in Figure A.2.

Table A.2 SC-FRC mix compositions with minimum and maximum chemical dosages (lb/yd^3).

Cement	Fly Ash	Water	FA	CA	SP (wt.%)	VMA (wt.%)	S2 (V_f)	S1 (V_f)	PVA (V_f)
670	220	400	1650	815	0.42	0.40	0.8	0.5	0.2
670	220	400	1650	815	1.22	0.66	0.8	0.5	0.2

Figure A.2 Lack of fiber dispersion due to maximum dosage of chemical admixtures (Mix #2).

When using Glenium 3030 NS and Rheomac VMA 358, subsequent testing showed that superplasticizer dosage must be limited to 0.69 weight percent of binder materials, and VMA dosage must be limited to 2.22 weight percent of binder materials, otherwise the probability of experiencing concrete segregation was noticeably higher. The initial trail batching and testing incorporated Rheomac VMA 358. However, due to a product update by BASF, a switch was made mid-project to the next generation VMA product, Rheomac VMA 362. The Rheomac VMA 362 was more effective in keeping the mix cohesive, even at higher dosages of superplasticizers.

(ii) Fiber Types and Volume Fractions

Over the course of the project three types of steel fibers and their effect on the flow properties were investigated. The manufacturer product designations of the fibers were Dramix RC 80/60 BN, Dramix ZP 305, and Dramix RC 80/30 BP with the 80/60 being a 60mm fiber, and the ZP

305 and RC 80/30 being 30mm in length. The aspect ratios of the different steel fibers were 80, 55, and 80, respectively.

The initial HyFRC mix with slump flow of 6.5 in. shown in Table 2.1 incorporated 0.8 volume percent of the S2 type steel fibers (Dramix RC 80/60 BN), however, early mix iterations revealed a tendency for these long fibers to clump, reducing the slump flow and a lack of long fibers present in the perimeter of the slump flow diameters. In addition, the volume fraction of the S2 fibers had to be reduced to ensure sufficient flowability and homogenous fiber dispersion due to the close rebar spacing of the bridge columns simulated by the modified J-ring test, described in Section 2.2.2 and shown in Figure A.3.

Figure A.3 Modified J-ring test reveals reduced flow and fiber pile up around rebar due to S2 fibers.

In order to prevent severe fiber clumping, the maximum volume of long fibers that could be successfully incorporated into the mix was 0.2%. Of the two 30 mm length fibers, the Dramix RC 80/30 was quickly discarded due to difficulty in getting the fibers to mix without clumping, resulting in and severely limited workability. When referencing 30 mm steel fiber all mixes discussed in this report refer to the Dramix ZP305 fiber type. The trial batches with the adjusted SP/VMA ratio, Dramix ZP 305, and S2 fibers for 0%, 0.1%, and 0.2% are given in Table A.3. The flow diameters of the different fiber mixes were 24 in. (610 mm), 22 in. (550 mm) and 21 in. (530 mm) for mixes 15, 17, and 18, respectively.

Microfibers have a large impact on the workability of fresh concrete due to the large number present even at low volume percentages. In order to quantify the effect of PVA fibers on the flow properties of the mix, several iterations were made to investigate if there was any relationship between PVA volume percentage and flow diameter at low volume fractions. The different mixes with PVA fiber adjustments are given in Table A.4. The measured flow

diameters for mixes 15, 16, 21, and 18 were 610, 510, 730, and 530, respectively. The results reveal that that for each 0.1 volume percent increase in PVA fibers, the slump flow diameter decreases by approximately 100 mm. While the benefit of PVA fiber in terms of controlling microcracking behavior can be significant, these results would suggest that their use should be minimized as much as possible if high workability is required.

Table A.3 SC-FRC mix compositions with S2 fiber adjustments (lb / yd3).

	Cement	Fly Ash	Water	FA	CA	SP (wt.%)	VMA (wt.%)	S2 (V_f)	S1 (V_f)	PVA (V_f)
Mix (#15)	670	220	400	1665	822	0.69	2.22	-	0.8	0.2
Mix (#17)	670	220	400	1662	820	0.69	2.22	0.1	0.8	0.2
Mix (#18)	670	220	400	1659	819	0.69	2.66	0.2	0.8	0.2

Table A.4 SC-FRC mix compositions with PVA fiber adjustments (lb / yd^3).

	Cement	Fly Ash	Water	FA	CA	SP (wt.%)	VMA (wt.%)	S2 (V_f)	S1 (V_f)	PVA (V_f)
Mix (#15)	670	220	400	1665	822	0.69	2.22	-	0.8	0.2
Mix (#16)	670	220	400	1662	820	0.69	2.22	-	0.8	0.3
Mix (#18)	670	220	400	1659	819	0.69	2.66	0.2	0.8	0.2
Mix (#21)	670	220	400	1665	822	0.69	2.66	0.2	0.8	-

(iii) Paste/Aggregate Volume Ratios

To ensure deflection hardening behavior, the target volume percent of the fibers were kept at 1.5%. Recognizing that cement paste provides the most fluid-like component to self-compacting

concrete, the next step of mixing investigated whether it would be beneficial to increase the cement paste volume fraction despite the increase in material cost. All of the previous mixes had used a cement paste to aggregate volume ratio of 0.76 to 1. When increasing the cement paste content to a ratio of 1 volume of cement paste for every 1 volume of aggregate, there was no measurable difference in slump flow properties between Mix #33 and Mix #34 (Table A.5). Moreover, the increased cement paste content made the high cement content mixes more prone to segregation. This line of mix iterations was soon abandoned.

Table A.5 SC-FRC mix compositions with cement content adjustments (lb / yd^3).

	Cement	**Fly Ash**	**Water**	**FA**	**CA**	**SP (wt.%)**	**VMA (wt.%)**	**S2 (V_f)**	**S1 (V_f)**	**PVA (V_f)**
Mix (#33)	670	220	400	1650	815	0.69	2.22	-	1.3	0.2
Mix (#34)	781	260	469	1421	715	0.69	2.22	-	1.3	0.2
Mix (#35)	670	220	400	1650	815	0.69	2.22	0.2	1.1	0.2

(iv) Aggregate Content and FA/CA Ratios

Following the adjustments made to chemical admixture content, fiber content, and cement paste content, the next parameter to investigate was the aggregate content. An extensive literature search found that research to date on self-consolidating FRC eliminated the coarse aggregate content from the mix design. Not wanting to completely remove the coarse aggregate content because of issues pertaining to dimensional stability, the effect of increasing the fine to coarse aggregation ratio was explored. The mix designs that were investigated are shown in Table A.6. While earlier testing always included a fine to coarse aggregate ratio of 2 to 1, a fine to coarse aggregate ratio of 2.5 to 1 was attempted.

Table A.6 SC-FRC mix compositions with aggregate ratio adjustments (lb / yd^3).

	Cement	Fly Ash	Water	FA	CA	SP (wt.%)	VMA (wt.%)	S2 (V_f)	S1 (V_f)	PVA (V_f)
Mix (#57)	670	220	400	1650	815	0.46	2.22	-	1.3	0.2
Mix (#58)	670	220	400	1760	705	0.46	2.22	-	1.3	0.2
Mix (#59)	670	220	400	1760	705	0.46	2.22	0.2	1.1	0.2

While Mix #57—representing the old fine to coarse ratio—had a flow diameter of 410 mm and a clump height of 130 mm, Mix #58 preformed much better with flow diameters of 560 mm and 620 mm, and clump heights of 60 mm and 40 mm when processed in a small batch (0.01 yd^3) and large batch (0.1 yd^3), respectively. Due to these increased flow properties all following mixes were designed to incorporate a fine to coarse aggregate ratio of 2.5 to 1.

Appendix B: Finalized Column Mix Designs (SSD Mix Design and Batch Weights)

Table B.1 SC-HyFRC SSD mix proportions (1 yd^3).

Material	Weight
Cement (lb)	670
Fly ash (lb)	220
Replacement (%)	0.25
FA (lb)	1760
CA (lb)	705
(fiber + agg) / binder	2.97
FA / CA	2.50
Wwater (lb)	400
w / binder	0.45
60 mm SF (lb)	0
30 mm SF (lb)	173
8 mm PVA (lb)	4
SP (lb)	8.24
SP wt% binder	0.93
VMA (lb)	19.65
VMA wt% binder	2.21

Table B.2 Column 1 SC-HyFRC mixes.

	Mix 1	**Mix 2**
Volume (yd^3)	0.237	0.227
$FA_{Free\ Moisture}$ (%)	+0.4	+0.4
$CA_{Free\ Moisture}$ (%)	+0.1	+0.1
Cement (lb)	158.8	152.1
Fly ash (lb)	52.1	49.9
FA (lb)	418.8	401.1
CA (lb)	167.3	160.2
Water (lb)	87.0	83.3
60mm SF (lb)	0.00	0.00
30mm SF (lb)	41.00	39.27
8mm PVA (lb)	0.95	0.91
SP (ml)	844	808
VMA (ml)	2109	2020

Table B.3 Column 2 SC-HyFRC mixes.

	Mix 3	**Mix 4**	**Mix 5**
Volume (yd^3)	0.153	0.396	0.227
$FA_{Free\ Moisture}$ (%)	+1.6	+0.1	-0.2
$CA_{Free\ Moisture}$ (%)	0	0	0
Cement (lb)	102.5	265.3	152.1
Fly ash (lb)	33.7	87.1	49.9
FA (lb)	273.7	697.7	398.7
CA (lb)	107.9	279.2	160.0
Water (lb)	53.0	147.7	85.9
60 mm SF (lb)	0.00	0.00	0.00
30 mm SF (lb)	26.47	68.51	39.27
8 mm PVA (lb)	0.61	1.58	0.91
SP (ml)	545	1410	808
VMA (ml)	1362	3524	2020

Appendix C: Response History of Vertical Displacement Transducers and Strain Gauges

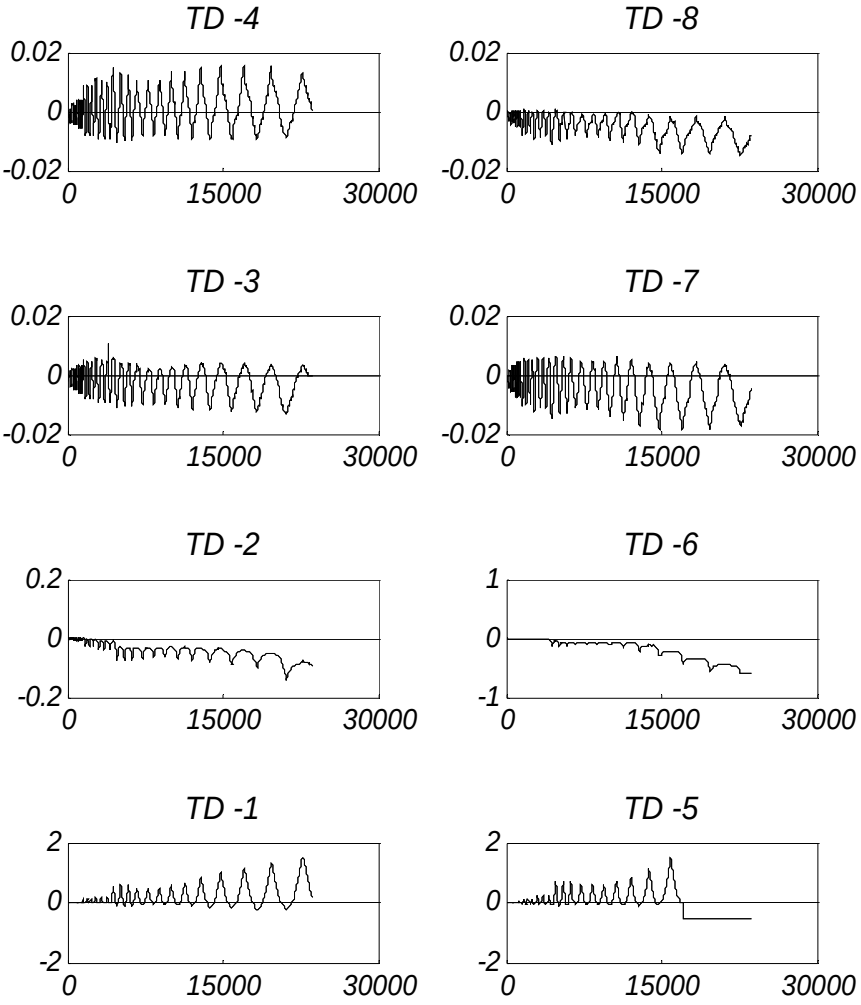

Figure C.1 **Measured response history of displacement transducers of TS-1 (*x*-axis shows number of steps and *y*-axis displacement in inches).**

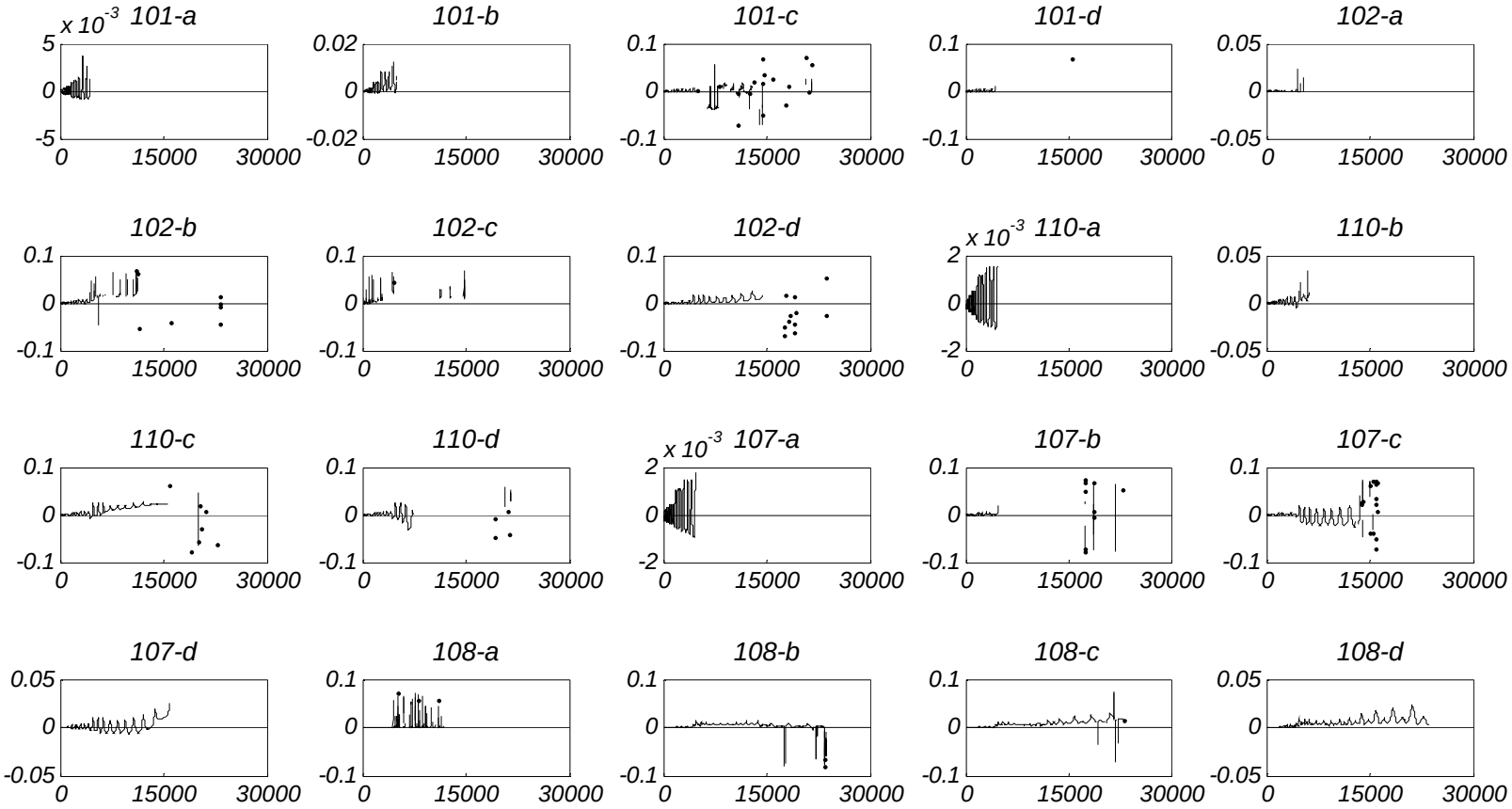

Figure C.2 **Measured response history of strain gauges of TS-1 (*x*-axis shows number of steps and *y*-axis displacement in inches).**

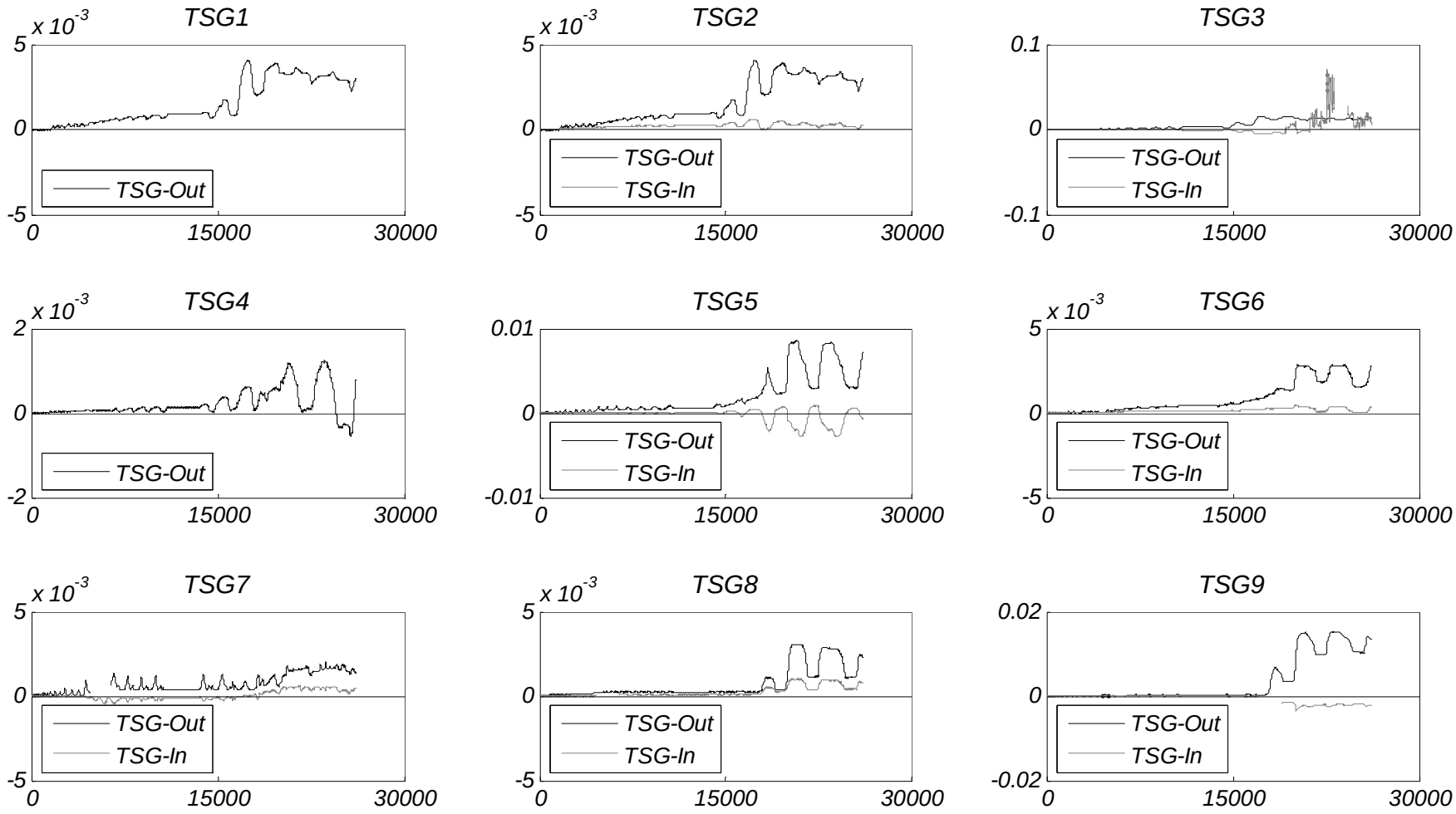

Figure C.3 Response history of strain gauges of spiral reinforcement of TS-1 (*x*-axis shows number of steps and *y*-axis displacement in inches).

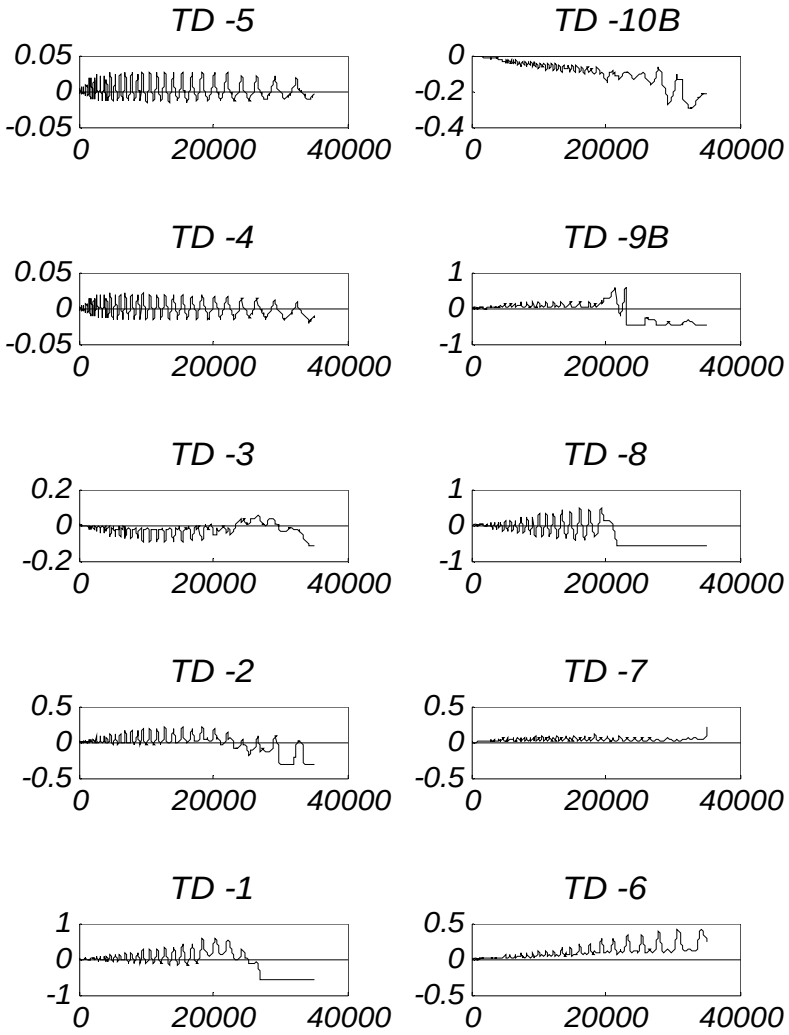

Figure C.4 Measured response history of displacement transducers of TS- 2 (*x*-axis shows number of steps and *y*-axis displacement in inches).

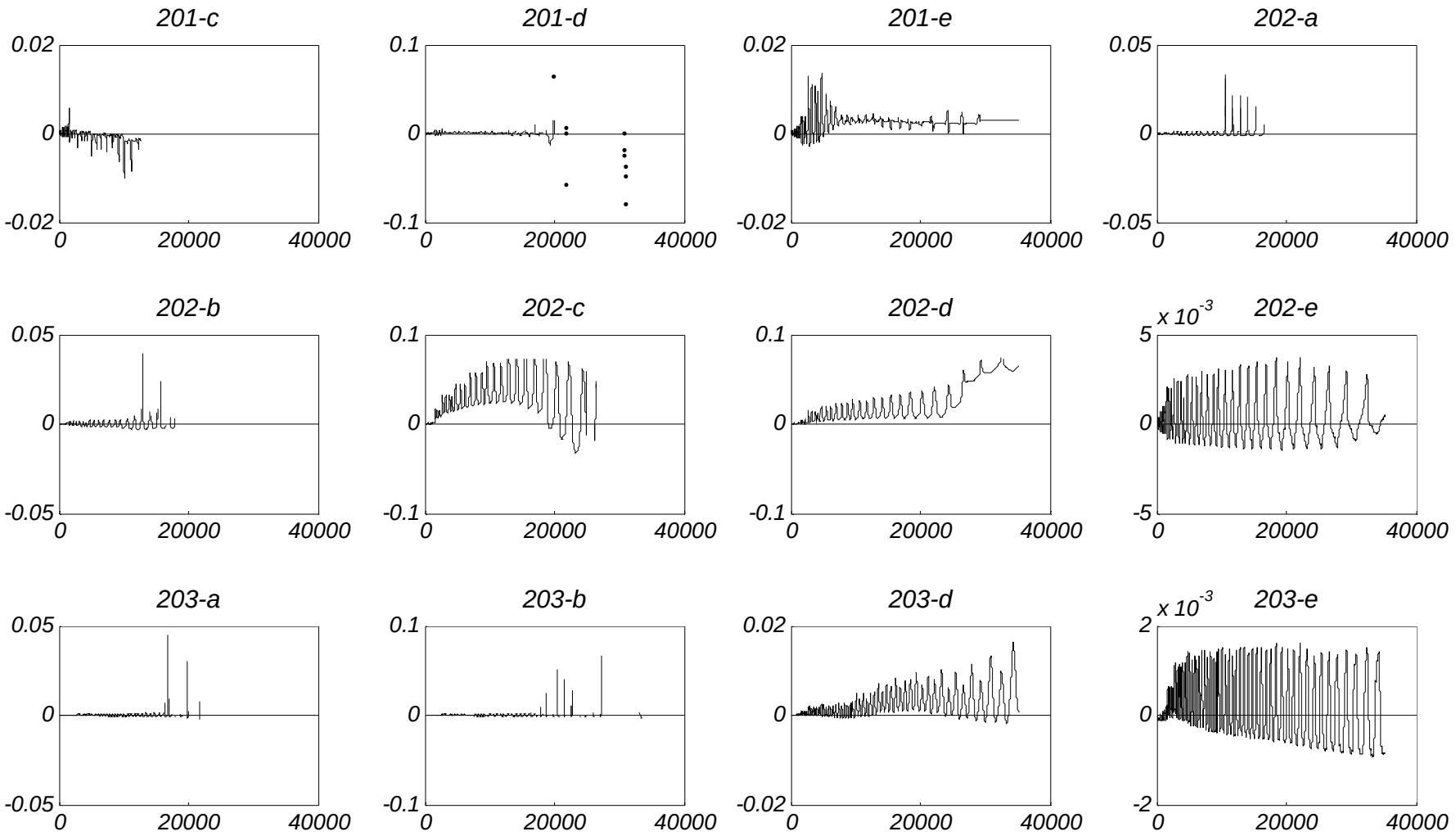

Figure C.5 **Measured response history of strain gauges of TS-2 (*x*-axis shows number of steps and *y*-axis displacement in inches).**

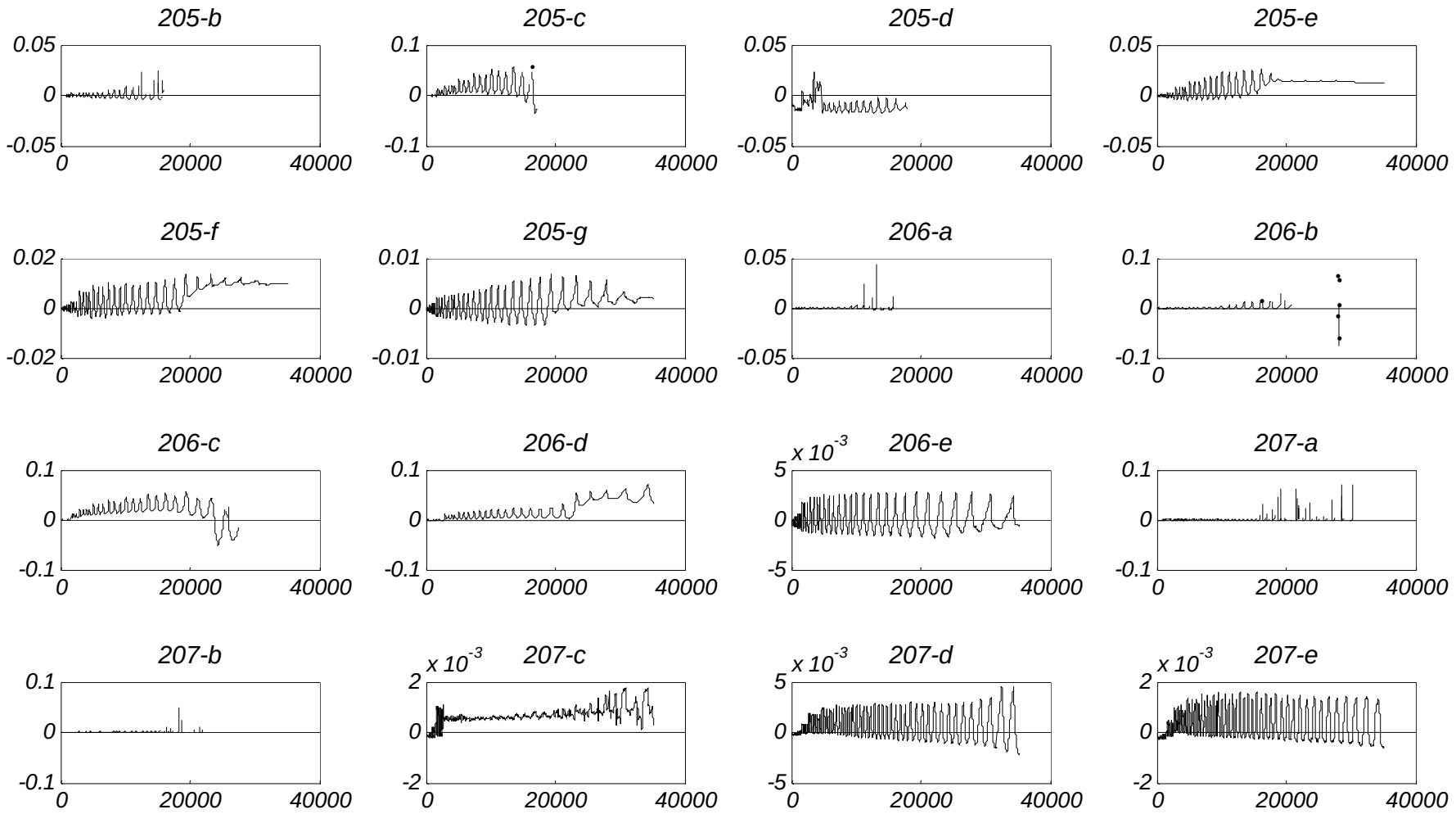

Figure C.6 **Measured response history of strain gauges of TS- 2 (*x*-axis shows number of steps and *y*-axis displacement in inches).**

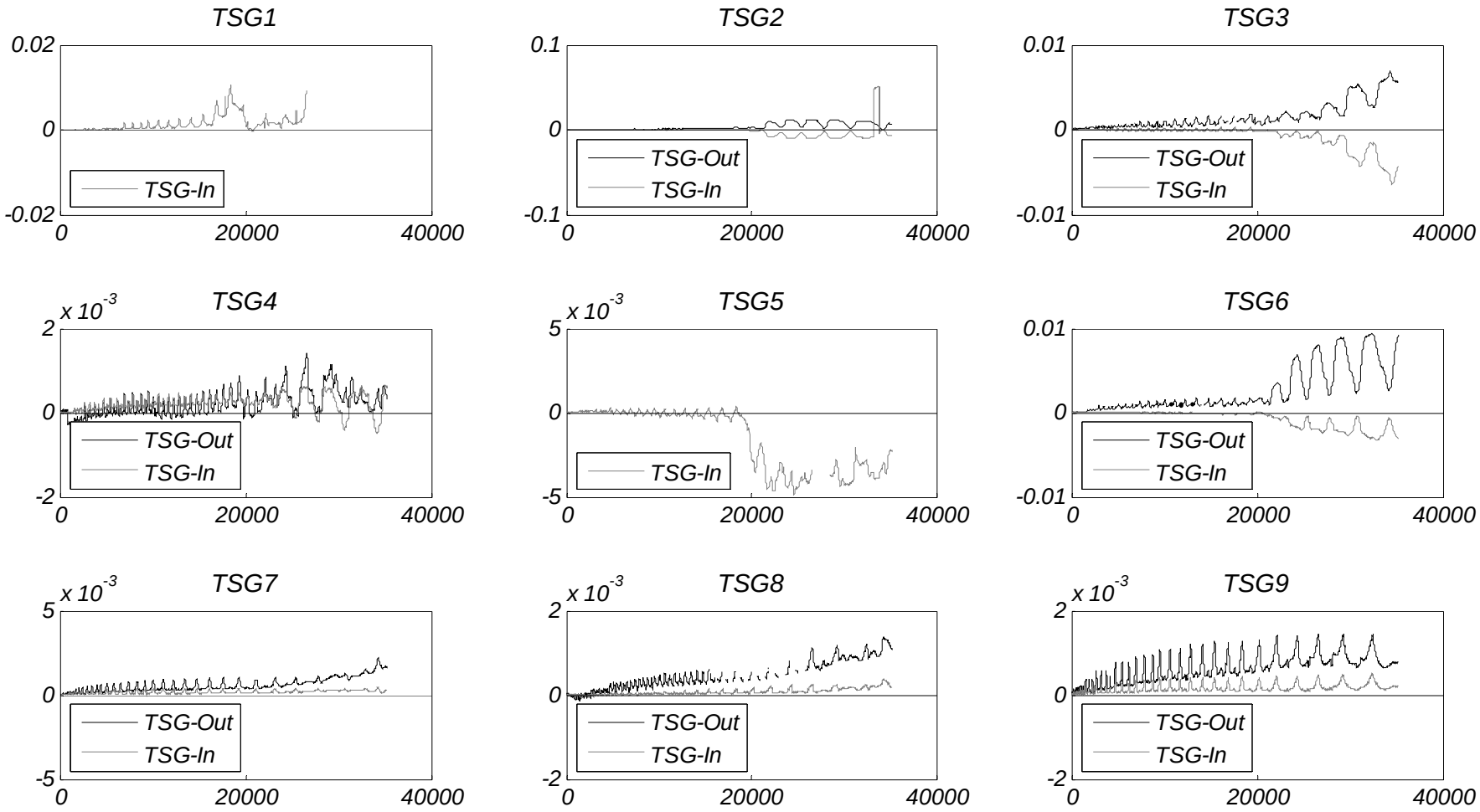

Figure C.7 **Response history of strain gauges of spiral reinforcement of TS-2 (*x*-axis shows number of steps and *y*-axis displacement in inches).**

PEER REPORTS

PEER reports are available individually or by yearly subscription. PEER reports can be ordered at http://peer.berkeley.edu/publications/peer_reports.html or by contacting the Pacific Earthquake Engineering Research Center, 325 Davis Hall mail code 1792, Berkeley, CA 94720. Tel.: (510) 642-3437; Fax: (510) 665-1655; Email: peer_editor@berkeley.edu

PEER 2011/06 *The Use of Base Isolation Systems to Achieve Complex Seismic Performance Objectives.* Troy A. Morgan and Stephen A. Mahin. July 2011.

PEER 2011/05 *Case Studies of the Seismic Performance of Tall Buildings Designed by Alternative Means.* Task 12 Report for the Tall Buildings Initiative. Jack Moehle, Yousef Bozorgnia, Nirmal Jayaram, Pierson Jones, Mohsen Rahnama, Nilesh Shome, Zeynep Tuna, John Wallace, Tony Yang, and Farzin Zareian. July 2011.

PEER 2011/04 *Recommended Design Practice for Pile Foundations in Laterally Spreading Ground.* Scott A. Ashford, Ross W. Boulanger, and Scott J. Brandenberg. June 2011.

PEER 2011/03 *New Ground Motion Selection Procedures and Selected Motions for the PEER Transportation Research Program.* Jack W. Baker, Ting Lin, Shrey K. Shahi, and Nirmal Jayaram. March 2011.

PEER 2011/02 *A Bayesian Network Methodology for Infrastructure Seismic Risk Assessment and Decision Support.* Michelle T. Bensi, Armen Der Kiureghian, and Daniel Straub. March 2011.

PEER 2011/01 *Demand Fragility Surfaces for Bridges in Liquefied and Laterally Spreading Ground.* Scott J. Brandenberg, Jian Zhang, Pirooz Kashighandi, Yili Huo, and Minxing Zhao. March 2011.

PEER 2010/05 *Guidelines for Performance-Based Seismic Design of Tall Buildings.* Developed by the Tall Buildings Initiative. November 2010.

PEER 2010/04 *Application Guide for the Design of Flexible and Rigid Bus Connections between Substation Equipment Subjected to Earthquakes.* Jean-Bernard Dastous and Armen Der Kiureghian. September 2010.

PEER 2010/03 *Shear Wave Velocity as a Statistical Function of Standard Penetration Test Resistance and Vertical Effective Stress at Caltrans Bridge Sites.* Scott J. Brandenberg, Naresh Bellana, and Thomas Shantz. June 2010.

PEER 2010/02 *Stochastic Modeling and Simulation of Ground Motions for Performance-Based Earthquake Engineering.* Sanaz Rezaeian and Armen Der Kiureghian. June 2010.

PEER 2010/01 *Structural Response and Cost Characterization of Bridge Construction Using Seismic Performance Enhancement Strategies.* Ady Aviram, Božidar Stojadinović, Gustavo J. Parra-Montesinos, and Kevin R. Mackie. March 2010.

PEER 2009/03 *The Integration of Experimental and Simulation Data in the Study of Reinforced Concrete Bridge Systems Including Soil-Foundation-Structure Interaction.* Matthew Dryden and Gregory L. Fenves. November 2009.

PEER 2009/02 *Improving Earthquake Mitigation through Innovations and Applications in Seismic Science, Engineering, Communication, and Response. Proceedings of a U.S.-Iran Seismic Workshop.* October 2009.

PEER 2009/01 *Evaluation of Ground Motion Selection and Modification Methods: Predicting Median Interstory Drift Response of Buildings.* Curt B. Haselton, Ed. June 2009.

PEER 2008/10 *Technical Manual for Strata.* Albert R. Kottke and Ellen M. Rathje. February 2009.

PEER 2008/09 *NGA Model for Average Horizontal Component of Peak Ground Motion and Response Spectra.* Brian S.-J. Chiou and Robert R. Youngs. November 2008.

PEER 2008/08 *Toward Earthquake-Resistant Design of Concentrically Braced Steel Structures.* Patxi Uriz and Stephen A. Mahin. November 2008.

PEER 2008/07 *Using OpenSees for Performance-Based Evaluation of Bridges on Liquefiable Soils.* Stephen L. Kramer, Pedro Arduino, and HyungSuk Shin. November 2008.

PEER 2008/06 *Shaking Table Tests and Numerical Investigation of Self-Centering Reinforced Concrete Bridge Columns.* Hyung IL Jeong, Junichi Sakai, and Stephen A. Mahin. September 2008.

PEER 2008/05 *Performance-Based Earthquake Engineering Design Evaluation Procedure for Bridge Foundations Undergoing Liquefaction-Induced Lateral Ground Displacement.* Christian A. Ledezma and Jonathan D. Bray. August 2008.

PEER 2008/04 *Benchmarking of Nonlinear Geotechnical Ground Response Analysis Procedures.* Jonathan P. Stewart, Annie On-Lei Kwok, Yousseff M. A. Hashash, Neven Matasovic, Robert Pyke, Zhiliang Wang, and Zhaohui Yang. August 2008.

PEER 2008/03 *Guidelines for Nonlinear Analysis of Bridge Structures in California.* Ady Aviram, Kevin R. Mackie, and Božidar Stojadinović. August 2008.

PEER 2008/02 *Treatment of Uncertainties in Seismic-Risk Analysis of Transportation Systems.* Evangelos Stergiou and Anne S. Kiremidjian. July 2008.

PEER 2008/01 *Seismic Performance Objectives for Tall Buildings.* William T. Holmes, Charles Kircher, William Petak, and Nabih Youssef. August 2008.

PEER 2007/12 *An Assessment to Benchmark the Seismic Performance of a Code-Conforming Reinforced Concrete Moment-Frame Building.* Curt Haselton, Christine A. Goulet, Judith Mitrani-Reiser, James L. Beck, Gregory G. Deierlein, Keith A. Porter, Jonathan P. Stewart, and Ertugrul Taciroglu. August 2008.

PEER 2007/11 *Bar Buckling in Reinforced Concrete Bridge Columns.* Wayne A. Brown, Dawn E. Lehman, and John F. Stanton. February 2008.

PEER 2007/10 *Computational Modeling of Progressive Collapse in Reinforced Concrete Frame Structures.* Mohamed M. Talaat and Khalid M. Mosalam. May 2008.

PEER 2007/09 *Integrated Probabilistic Performance-Based Evaluation of Benchmark Reinforced Concrete Bridges.* Kevin R. Mackie, John-Michael Wong, and Božidar Stojadinović. January 2008.

PEER 2007/08 *Assessing Seismic Collapse Safety of Modern Reinforced Concrete Moment-Frame Buildings.* Curt B. Haselton and Gregory G. Deierlein. February 2008.

PEER 2007/07 *Performance Modeling Strategies for Modern Reinforced Concrete Bridge Columns.* Michael P. Berry and Marc O. Eberhard. April 2008.

PEER 2007/06 *Development of Improved Procedures for Seismic Design of Buried and Partially Buried Structures.* Linda Al Atik and Nicholas Sitar. June 2007.

PEER 2007/05 *Uncertainty and Correlation in Seismic Risk Assessment of Transportation Systems.* Renee G. Lee and Anne S. Kiremidjian. July 2007.

PEER 2007/04 *Numerical Models for Analysis and Performance-Based Design of Shallow Foundations Subjected to Seismic Loading.* Sivapalan Gajan, Tara C. Hutchinson, Bruce L. Kutter, Prishati Raychowdhury, José A. Ugalde, and Jonathan P. Stewart. May 2008.

PEER 2007/03 *Beam-Column Element Model Calibrated for Predicting Flexural Response Leading to Global Collapse of RC Frame Buildings.* Curt B. Haselton, Abbie B. Liel, Sarah Taylor Lange, and Gregory G. Deierlein. May 2008.

PEER 2007/02 *Campbell-Bozorgnia NGA Ground Motion Relations for the Geometric Mean Horizontal Component of Peak and Spectral Ground Motion Parameters.* Kenneth W. Campbell and Yousef Bozorgnia. May 2007.

PEER 2007/01 *Boore-Atkinson NGA Ground Motion Relations for the Geometric Mean Horizontal Component of Peak and Spectral Ground Motion Parameters.* David M. Boore and Gail M. Atkinson. May. May 2007.

PEER 2006/12 *Societal Implications of Performance-Based Earthquake Engineering.* Peter J. May. May 2007.

PEER 2006/11 *Probabilistic Seismic Demand Analysis Using Advanced Ground Motion Intensity Measures, Attenuation Relationships, and Near-Fault Effects.* Polsak Tothong and C. Allin Cornell. March 2007.

PEER 2006/10 *Application of the PEER PBEE Methodology to the I-880 Viaduct.* Sashi Kunnath. February 2007.

PEER 2006/09 *Quantifying Economic Losses from Travel Forgone Following a Large Metropolitan Earthquake.* James Moore, Sungbin Cho, Yue Yue Fan, and Stuart Werner. November 2006.

PEER 2006/08 *Vector-Valued Ground Motion Intensity Measures for Probabilistic Seismic Demand Analysis.* Jack W. Baker and C. Allin Cornell. October 2006.

PEER 2006/07 *Analytical Modeling of Reinforced Concrete Walls for Predicting Flexural and Coupled–Shear-Flexural Responses.* Kutay Orakcal, Leonardo M. Massone, and John W. Wallace. October 2006.

PEER 2006/06 *Nonlinear Analysis of a Soil-Drilled Pier System under Static and Dynamic Axial Loading.* Gang Wang and Nicholas Sitar. November 2006.

PEER 2006/05 *Advanced Seismic Assessment Guidelines.* Paolo Bazzurro, C. Allin Cornell, Charles Menun, Maziar Motahari, and Nicolas Luco. September 2006.

PEER 2006/04 *Probabilistic Seismic Evaluation of Reinforced Concrete Structural Components and Systems.* Tae Hyung Lee and Khalid M. Mosalam. August 2006.

PEER 2006/03 *Performance of Lifelines Subjected to Lateral Spreading.* Scott A. Ashford and Teerawut Juirnarongrit. July 2006.

PEER 2006/02 *Pacific Earthquake Engineering Research Center Highway Demonstration Project.* Anne Kiremidjian, James Moore, Yue Yue Fan, Nesrin Basoz, Ozgur Yazali, and Meredith Williams. April 2006.

PEER 2006/01 *Bracing Berkeley. A Guide to Seismic Safety on the UC Berkeley Campus.* Mary C. Comerio, Stephen Tobriner, and Ariane Fehrenkamp. January 2006.

PEER 2005/16 *Seismic Response and Reliability of Electrical Substation Equipment and Systems.* Junho Song, Armen Der Kiureghian, and Jerome L. Sackman. April 2006.

PEER 2005/15 *CPT-Based Probabilistic Assessment of Seismic Soil Liquefaction Initiation.* R. E. S. Moss, R. B. Seed, R. E. Kayen, J. P. Stewart, and A. Der Kiureghian. April 2006.

PEER 2005/14 *Workshop on Modeling of Nonlinear Cyclic Load-Deformation Behavior of Shallow Foundations.* Bruce L. Kutter, Geoffrey Martin, Tara Hutchinson, Chad Harden, Sivapalan Gajan, and Justin Phalen. March 2006.

PEER 2005/13 *Stochastic Characterization and Decision Bases under Time-Dependent Aftershock Risk in Performance-Based Earthquake Engineering.* Gee Liek Yeo and C. Allin Cornell. July 2005.

PEER 2005/12 *PEER Testbed Study on a Laboratory Building: Exercising Seismic Performance Assessment.* Mary C. Comerio, editor. November 2005.

PEER 2005/11 *Van Nuys Hotel Building Testbed Report: Exercising Seismic Performance Assessment.* Helmut Krawinkler, editor. October 2005.

PEER 2005/10 *First NEES/E-Defense Workshop on Collapse Simulation of Reinforced Concrete Building Structures.* September 2005.

PEER 2005/09 *Test Applications of Advanced Seismic Assessment Guidelines.* Joe Maffei, Karl Telleen, Danya Mohr, William Holmes, and Yuki Nakayama. August 2006.

PEER 2005/08 *Damage Accumulation in Lightly Confined Reinforced Concrete Bridge Columns.* R. Tyler Ranf, Jared M. Nelson, Zach Price, Marc O. Eberhard, and John F. Stanton. April 2006.

PEER 2005/07 *Experimental and Analytical Studies on the Seismic Response of Freestanding and Anchored Laboratory Equipment.* Dimitrios Konstantinidis and Nicos Makris. January 2005.

PEER 2005/06 *Global Collapse of Frame Structures under Seismic Excitations.* Luis F. Ibarra and Helmut Krawinkler. September 2005.

PEER 2005//05 *Performance Characterization of Bench- and Shelf-Mounted Equipment.* Samit Ray Chaudhuri and Tara C. Hutchinson. May 2006.

PEER 2005/04 *Numerical Modeling of the Nonlinear Cyclic Response of Shallow Foundations.* Chad Harden, Tara Hutchinson, Geoffrey R. Martin, and Bruce L. Kutter. August 2005.

PEER 2005/03 *A Taxonomy of Building Components for Performance-Based Earthquake Engineering.* Keith A. Porter. September 2005.

PEER 2005/02 *Fragility Basis for California Highway Overpass Bridge Seismic Decision Making.* Kevin R. Mackie and Božidar Stojadinović. June 2005.

PEER 2005/01 *Empirical Characterization of Site Conditions on Strong Ground Motion.* Jonathan P. Stewart, Yoojoong Choi, and Robert W. Graves. June 2005.

PEER 2004/09 *Electrical Substation Equipment Interaction: Experimental Rigid Conductor Studies.* Christopher Stearns and André Filiatrault. February 2005.

PEER 2004/08 *Seismic Qualification and Fragility Testing of Line Break 550-kV Disconnect Switches.* Shakhzod M. Takhirov, Gregory L. Fenves, and Eric Fujisaki. January 2005.

PEER 2004/07 *Ground Motions for Earthquake Simulator Qualification of Electrical Substation Equipment.* Shakhzod M. Takhirov, Gregory L. Fenves, Eric Fujisaki, and Don Clyde. January 2005.

PEER 2004/06 *Performance-Based Regulation and Regulatory Regimes.* Peter J. May and Chris Koski. September 2004.

PEER 2004/05 *Performance-Based Seismic Design Concepts and Implementation: Proceedings of an International Workshop.* Peter Fajfar and Helmut Krawinkler, editors. September 2004.

PEER 2004/04 *Seismic Performance of an Instrumented Tilt-up Wall Building.* James C. Anderson and Vitelmo V. Bertero. July 2004.

PEER 2004/03 *Evaluation and Application of Concrete Tilt-up Assessment Methodologies.* Timothy Graf and James O. Malley. October 2004.

PEER 2004/02 *Analytical Investigations of New Methods for Reducing Residual Displacements of Reinforced Concrete Bridge Columns.* Junichi Sakai and Stephen A. Mahin. August 2004.

PEER 2004/01 *Seismic Performance of Masonry Buildings and Design Implications.* Kerri Anne Taeko Tokoro, James C. Anderson, and Vitelmo V. Bertero. February 2004.

PEER 2003/18 *Performance Models for Flexural Damage in Reinforced Concrete Columns.* Michael Berry and Marc Eberhard. August 2003.

PEER 2003/17 *Predicting Earthquake Damage in Older Reinforced Concrete Beam-Column Joints.* Catherine Pagni and Laura Lowes. October 2004.

PEER 2003/16 *Seismic Demands for Performance-Based Design of Bridges.* Kevin Mackie and Božidar Stojadinović. August 2003.

PEER 2003/15 *Seismic Demands for Nondeteriorating Frame Structures and Their Dependence on Ground Motions.* Ricardo Antonio Medina and Helmut Krawinkler. May 2004.

PEER 2003/14 *Finite Element Reliability and Sensitivity Methods for Performance-Based Earthquake Engineering.* Terje Haukaas and Armen Der Kiureghian. April 2004.

PEER 2003/13 *Effects of Connection Hysteretic Degradation on the Seismic Behavior of Steel Moment-Resisting Frames.* Janise E. Rodgers and Stephen A. Mahin. March 2004.

PEER 2003/12 *Implementation Manual for the Seismic Protection of Laboratory Contents: Format and Case Studies.* William T. Holmes and Mary C. Comerio. October 2003.

PEER 2003/11 *Fifth U.S.-Japan Workshop on Performance-Based Earthquake Engineering Methodology for Reinforced Concrete Building Structures.* February 2004.

PEER 2003/10 *A Beam-Column Joint Model for Simulating the Earthquake Response of Reinforced Concrete Frames.* Laura N. Lowes, Nilanjan Mitra, and Arash Altoontash. February 2004.

PEER 2003/09 *Sequencing Repairs after an Earthquake: An Economic Approach.* Marco Casari and Simon J. Wilkie. April 2004.

PEER 2003/08 *A Technical Framework for Probability-Based Demand and Capacity Factor Design (DCFD) Seismic Formats.* Fatemeh Jalayer and C. Allin Cornell. November 2003.

PEER 2003/07 *Uncertainty Specification and Propagation for Loss Estimation Using FOSM Methods.* Jack W. Baker and C. Allin Cornell. September 2003.

PEER 2003/06 *Performance of Circular Reinforced Concrete Bridge Columns under Bidirectional Earthquake Loading.* Mahmoud M. Hachem, Stephen A. Mahin, and Jack P. Moehle. February 2003.

PEER 2003/05 *Response Assessment for Building-Specific Loss Estimation.* Eduardo Miranda and Shahram Taghavi. September 2003.

PEER 2003/04 *Experimental Assessment of Columns with Short Lap Splices Subjected to Cyclic Loads.* Murat Melek, John W. Wallace, and Joel Conte. April 2003.

PEER 2003/03 *Probabilistic Response Assessment for Building-Specific Loss Estimation.* Eduardo Miranda and Hesameddin Aslani. September 2003.

PEER 2003/02 *Software Framework for Collaborative Development of Nonlinear Dynamic Analysis Program.* Jun Peng and Kincho H. Law. September 2003.

PEER 2003/01 *Shake Table Tests and Analytical Studies on the Gravity Load Collapse of Reinforced Concrete Frames.* Kenneth John Elwood and Jack P. Moehle. November 2003.

PEER 2002/24 *Performance of Beam to Column Bridge Joints Subjected to a Large Velocity Pulse.* Natalie Gibson, André Filiatrault, and Scott A. Ashford. April 2002.

PEER 2002/23 *Effects of Large Velocity Pulses on Reinforced Concrete Bridge Columns.* Greg L. Orozco and Scott A. Ashford. April 2002.

PEER 2002/22 *Characterization of Large Velocity Pulses for Laboratory Testing.* Kenneth E. Cox and Scott A. Ashford. April 2002.

PEER 2002/21 *Fourth U.S.-Japan Workshop on Performance-Based Earthquake Engineering Methodology for Reinforced Concrete Building Structures.* December 2002.

PEER 2002/20 *Barriers to Adoption and Implementation of PBEE Innovations.* Peter J. May. August 2002.

PEER 2002/19 *Economic-Engineered Integrated Models for Earthquakes: Socioeconomic Impacts.* Peter Gordon, James E. Moore II, and Harry W. Richardson. July 2002.

PEER 2002/18 *Assessment of Reinforced Concrete Building Exterior Joints with Substandard Details.* Chris P. Pantelides, Jon Hansen, Justin Nadauld, and Lawrence D. Reaveley. May 2002.

PEER 2002/17 *Structural Characterization and Seismic Response Analysis of a Highway Overcrossing Equipped with Elastomeric Bearings and Fluid Dampers: A Case Study.* Nicos Makris and Jian Zhang. November 2002.

PEER 2002/16 *Estimation of Uncertainty in Geotechnical Properties for Performance-Based Earthquake Engineering.* Allen L. Jones, Steven L. Kramer, and Pedro Arduino. December 2002.

PEER 2002/15 *Seismic Behavior of Bridge Columns Subjected to Various Loading Patterns.* Asadollah Esmaeily-Gh. and Yan Xiao. December 2002.

PEER 2002/14 *Inelastic Seismic Response of Extended Pile Shaft Supported Bridge Structures.* T.C. Hutchinson, R.W. Boulanger, Y.H. Chai, and I.M. Idriss. December 2002.

PEER 2002/13 *Probabilistic Models and Fragility Estimates for Bridge Components and Systems.* Paolo Gardoni, Armen Der Kiureghian, and Khalid M. Mosalam. June 2002.

PEER 2002/12 *Effects of Fault Dip and Slip Rake on Near-Source Ground Motions: Why Chi-Chi Was a Relatively Mild M7.6 Earthquake.* Brad T. Aagaard, John F. Hall, and Thomas H. Heaton. December 2002.

PEER 2002/11 *Analytical and Experimental Study of Fiber-Reinforced Strip Isolators.* James M. Kelly and Shakhzod M. Takhirov. September 2002.

PEER 2002/10 *Centrifuge Modeling of Settlement and Lateral Spreading with Comparisons to Numerical Analyses.* Sivapalan Gajan and Bruce L. Kutter. January 2003.

PEER 2002/09 *Documentation and Analysis of Field Case Histories of Seismic Compression during the 1994 Northridge, California, Earthquake.* Jonathan P. Stewart, Patrick M. Smith, Daniel H. Whang, and Jonathan D. Bray. October 2002.

PEER 2002/08 *Component Testing, Stability Analysis and Characterization of Buckling-Restrained Unbonded Braces™.* Cameron Black, Nicos Makris, and Ian Aiken. September 2002.

PEER 2002/07 *Seismic Performance of Pile-Wharf Connections.* Charles W. Roeder, Robert Graff, Jennifer Soderstrom, and Jun Han Yoo. December 2001.

PEER 2002/06 *The Use of Benefit-Cost Analysis for Evaluation of Performance-Based Earthquake Engineering Decisions.* Richard O. Zerbe and Anthony Falit-Baiamonte. September 2001.

PEER 2002/05 *Guidelines, Specifications, and Seismic Performance Characterization of Nonstructural Building Components and Equipment.* André Filiatrault, Constantin Christopoulos, and Christopher Stearns. September 2001.

PEER 2002/04 *Consortium of Organizations for Strong-Motion Observation Systems and the Pacific Earthquake Engineering Research Center Lifelines Program: Invited Workshop on Archiving and Web Dissemination of Geotechnical Data, 4–5 October 2001.* September 2002.

PEER 2002/03 *Investigation of Sensitivity of Building Loss Estimates to Major Uncertain Variables for the Van Nuys Testbed.* Keith A. Porter, James L. Beck, and Rustem V. Shaikhutdinov. August 2002.

PEER 2002/02 *The Third U.S.-Japan Workshop on Performance-Based Earthquake Engineering Methodology for Reinforced Concrete Building Structures.* July 2002.

PEER 2002/01 *Nonstructural Loss Estimation: The UC Berkeley Case Study.* Mary C. Comerio and John C. Stallmeyer. December 2001.

PEER 2001/16 *Statistics of SDF-System Estimate of Roof Displacement for Pushover Analysis of Buildings.* Anil K. Chopra, Rakesh K. Goel, and Chatpan Chintanapakdee. December 2001.

PEER 2001/15 *Damage to Bridges during the 2001 Nisqually Earthquake.* R. Tyler Ranf, Marc O. Eberhard, and Michael P. Berry. November 2001.

PEER 2001/14 *Rocking Response of Equipment Anchored to a Base Foundation.* Nicos Makris and Cameron J. Black. September 2001.

PEER 2001/13 *Modeling Soil Liquefaction Hazards for Performance-Based Earthquake Engineering.* Steven L. Kramer and Ahmed-W. Elgamal. February 2001.

PEER 2001/12 *Development of Geotechnical Capabilities in OpenSees.* Boris Jeremić. September 2001.

PEER 2001/11 *Analytical and Experimental Study of Fiber-Reinforced Elastomeric Isolators.* James M. Kelly and Shakhzod M. Takhirov. September 2001.

PEER 2001/10 *Amplification Factors for Spectral Acceleration in Active Regions.* Jonathan P. Stewart, Andrew H. Liu, Yoojoong Choi, and Mehmet B. Baturay. December 2001.

PEER 2001/09 *Ground Motion Evaluation Procedures for Performance-Based Design.* Jonathan P. Stewart, Shyh-Jeng Chiou, Jonathan D. Bray, Robert W. Graves, Paul G. Somerville, and Norman A. Abrahamson. September 2001.

PEER 2001/08 *Experimental and Computational Evaluation of Reinforced Concrete Bridge Beam-Column Connections for Seismic Performance.* Clay J. Naito, Jack P. Moehle, and Khalid M. Mosalam. November 2001.

PEER 2001/07 *The Rocking Spectrum and the Shortcomings of Design Guidelines.* Nicos Makris and Dimitrios Konstantinidis. August 2001.

PEER 2001/06 *Development of an Electrical Substation Equipment Performance Database for Evaluation of Equipment Fragilities*. Thalia Agnanos. April 1999.

PEER 2001/05 *Stiffness Analysis of Fiber-Reinforced Elastomeric Isolators.* Hsiang-Chuan Tsai and James M. Kelly. May 2001.

PEER 2001/04 *Organizational and Societal Considerations for Performance-Based Earthquake Engineering.* Peter J. May. April 2001.

PEER 2001/03 *A Modal Pushover Analysis Procedure to Estimate Seismic Demands for Buildings: Theory and Preliminary Evaluation.* Anil K. Chopra and Rakesh K. Goel. January 2001.

PEER 2001/02 *Seismic Response Analysis of Highway Overcrossings Including Soil-Structure Interaction.* Jian Zhang and Nicos Makris. March 2001.

PEER 2001/01 *Experimental Study of Large Seismic Steel Beam-to-Column Connections*. Egor P. Popov and Shakhzod M. Takhirov. November 2000.

PEER 2000/10 *The Second U.S.-Japan Workshop on Performance-Based Earthquake Engineering Methodology for Reinforced Concrete Building Structures.* March 2000.

PEER 2000/09 *Structural Engineering Reconnaissance of the August 17, 1999 Earthquake: Kocaeli (Izmit), Turkey*. Halil Sezen, Kenneth J. Elwood, Andrew S. Whittaker, Khalid Mosalam, John J. Wallace, and John F. Stanton. December 2000.

PEER 2000/08 *Behavior of Reinforced Concrete Bridge Columns Having Varying Aspect Ratios and Varying Lengths of Confinement*. Anthony J. Calderone, Dawn E. Lehman, and Jack P. Moehle. January 2001.

PEER 2000/07 *Cover-Plate and Flange-Plate Reinforced Steel Moment-Resisting Connections.* Taejin Kim, Andrew S. Whittaker, Amir S. Gilani, Vitelmo V. Bertero, and Shakhzod M. Takhirov. September 2000.

PEER 2000/06 *Seismic Evaluation and Analysis of 230-kV Disconnect Switches.* Amir S. J. Gilani, Andrew S. Whittaker, Gregory L. Fenves, Chun-Hao Chen, Henry Ho, and Eric Fujisaki. July 2000.

PEER 2000/05 *Performance-Based Evaluation of Exterior Reinforced Concrete Building Joints for Seismic Excitation.* Chandra Clyde, Chris P. Pantelides, and Lawrence D. Reaveley. July 2000.

PEER 2000/04 *An Evaluation of Seismic Energy Demand: An Attenuation Approach.* Chung-Che Chou and Chia-Ming Uang. July 1999.

PEER 2000/03 *Framing Earthquake Retrofitting Decisions: The Case of Hillside Homes in Los Angeles.* Detlof von Winterfeldt, Nels Roselund, and Alicia Kitsuse. March 2000.

PEER 2000/02 *U.S.-Japan Workshop on the Effects of Near-Field Earthquake Shaking.* Andrew Whittaker, ed. July 2000.

PEER 2000/01 *Further Studies on Seismic Interaction in Interconnected Electrical Substation Equipment.* Armen Der Kiureghian, Kee-Jeung Hong, and Jerome L. Sackman. November 1999.

PEER 1999/14 *Seismic Evaluation and Retrofit of 230-kV Porcelain Transformer Bushings*. Amir S. Gilani, Andrew S. Whittaker, Gregory L. Fenves, and Eric Fujisaki. December 1999.

PEER 1999/13 *Building Vulnerability Studies: Modeling and Evaluation of Tilt-up and Steel Reinforced Concrete Buildings.* John W. Wallace, Jonathan P. Stewart, and Andrew S. Whittaker, editors. December 1999.

PEER 1999/12 *Rehabilitation of Nonductile RC Frame Building Using Encasement Plates and Energy-Dissipating Devices.* Mehrdad Sasani, Vitelmo V. Bertero, James C. Anderson. December 1999.

PEER 1999/11 *Performance Evaluation Database for Concrete Bridge Components and Systems under Simulated Seismic Loads.* Yael D. Hose and Frieder Seible. November 1999.

PEER 1999/10 *U.S.-Japan Workshop on Performance-Based Earthquake Engineering Methodology for Reinforced Concrete Building Structures.* December 1999.

PEER 1999/09 *Performance Improvement of Long Period Building Structures Subjected to Severe Pulse-Type Ground Motions*. James C. Anderson, Vitelmo V. Bertero, and Raul Bertero. October 1999.

PEER 1999/08 *Envelopes for Seismic Response Vectors.* Charles Menun and Armen Der Kiureghian. July 1999.

PEER 1999/07 *Documentation of Strengths and Weaknesses of Current Computer Analysis Methods for Seismic Performance of Reinforced Concrete Members.* William F. Cofer. November 1999.

PEER 1999/06 *Rocking Response and Overturning of Anchored Equipment under Seismic Excitations.* Nicos Makris and Jian Zhang. November 1999.

PEER 1999/05 *Seismic Evaluation of 550 kV Porcelain Transformer Bushings.* Amir S. Gilani, Andrew S. Whittaker, Gregory L. Fenves, and Eric Fujisaki. October 1999.

PEER 1999/04 *Adoption and Enforcement of Earthquake Risk-Reduction Measures.* Peter J. May, Raymond J. Burby, T. Jens Feeley, and Robert Wood.

PEER 1999/03 *Task 3 Characterization of Site Response General Site Categories.* Adrian Rodriguez-Marek, Jonathan D. Bray, and Norman Abrahamson. February 1999.

PEER 1999/02 *Capacity-Demand-Diagram Methods for Estimating Seismic Deformation of Inelastic Structures: SDF Systems*. Anil K. Chopra and Rakesh Goel. April 1999.

PEER 1999/01 *Interaction in Interconnected Electrical Substation Equipment Subjected to Earthquake Ground Motions.* Armen Der Kiureghian, Jerome L. Sackman, and Kee-Jeung Hong. February 1999.

PEER 1998/08 *Behavior and Failure Analysis of a Multiple-Frame Highway Bridge in the 1994 Northridge Earthquake.* Gregory L. Fenves and Michael Ellery. December 1998.

PEER 1998/07 *Empirical Evaluation of Inertial Soil-Structure Interaction Effects.* Jonathan P. Stewart, Raymond B. Seed, and Gregory L. Fenves. November 1998.

PEER 1998/06 *Effect of Damping Mechanisms on the Response of Seismic Isolated Structures.* Nicos Makris and Shih-Po Chang. November 1998.

PEER 1998/05 *Rocking Response and Overturning of Equipment under Horizontal Pulse-Type Motions.* Nicos Makris and Yiannis Roussos. October 1998.

PEER 1998/04 *Pacific Earthquake Engineering Research Invitational Workshop Proceedings, May 14–15, 1998: Defining the Links between Planning, Policy Analysis, Economics and Earthquake Engineering.* Mary Comerio and Peter Gordon. September 1998.

PEER 1998/03 *Repair/Upgrade Procedures for Welded Beam to Column Connections.* James C. Anderson and Xiaojing Duan. May 1998.

PEER 1998/02 *Seismic Evaluation of 196 kV Porcelain Transformer Bushings.* Amir S. Gilani, Juan W. Chavez, Gregory L. Fenves, and Andrew S. Whittaker. May 1998.

PEER 1998/01 *Seismic Performance of Well-Confined Concrete Bridge Columns.* Dawn E. Lehman and Jack P. Moehle. December 2000.

ONLINE REPORTS

The following PEER reports are available by Internet only at http://peer.berkeley.edu/publications/peer_reports.html

PEER 2011/106 *Self Compacting Hybrid Fiber Reinforced Concrete Composites for Bridge Columns.* Pardeep Kumar, Gabriel Jen, William Trono, Marios Panagiotou, and Claudia Ostertag. September 2011.

PEER 2011/105 *Stochastic Dynamic Analysis of Bridges Subjected to Spacially Varying Ground Motions.* Katerina Konakli and Armen Der Kiureghian. August 2011.

PEER 2011/104 *Design and Instrumentation of the 2010 E-Defense Four-Story Reinforced Concrete and Post-Tensioned Concrete Buildings.* Takuya Nagae, Kenichi Tahara, Taizo Matsumori, Hitoshi Shiohara, Toshimi Kabeyasawa, Susumu Kono, Minehiro Nishiyama (Japanese Research Team) and John Wallace, Wassim Ghannoum, Jack Moehle, Richard Sause, Wesley Keller, Zeynep Tuna (U.S. Research Team). June 2011.

PEER 2011/103 *In-Situ Monitoring of the Force Output of Fluid Dampers: Experimental Investigation.* Dimitrios Konstantinidis, James M. Kelly, and Nicos Makris. April 2011.

PEER 2011/102 *Ground-motion prediction equations 1964 - 2010.* John Douglas. April 2011.

PEER 2011/101 *Report of the Eighth Planning Meeting of NEES/E-Defense Collaborative Research on Earthquake Engineering.* Convened by the Hyogo Earthquake Engineering Research Center (NIED), NEES Consortium, Inc. February 2011.

PEER 2010/111 *Modeling and Acceptance Criteria for Seismic Design and Analysis of Tall Buildings.* Task 7 Report for the Tall Buildings Initiative - Published jointly by the Applied Technology Council. October 2010.

PEER 2010/110 *Seismic Performance Assessment and Probabilistic Repair Cost Analysis of Precast Concrete Cladding Systems for Multistory Buildlings.* Jeffrey P. Hunt and Božidar Stojadinovic. November 2010.

PEER 2010/109 *Report of the Seventh Joint Planning Meeting of NEES/E-Defense Collaboration on Earthquake Engineering. Held at the E-Defense, Miki, and Shin-Kobe, Japan, September 18–19, 2009.* August 2010.

PEER 2010/108 *Probabilistic Tsunami Hazard in California.* Hong Kie Thio, Paul Somerville, and Jascha Polet, preparers. October 2010.

PEER 2010/107 *Performance and Reliability of Exposed Column Base Plate Connections for Steel Moment-Resisting Frames.* Ady Aviram, Božidar Stojadinovic, and Armen Der Kiureghian. August 2010.

PEER 2010/106 *Verification of Probabilistic Seismic Hazard Analysis Computer Programs.* Patricia Thomas, Ivan Wong, and Norman Abrahamson. May 2010.

PEER 2010/105 *Structural Engineering Reconnaissance of the April 6, 2009, Abruzzo, Italy, Earthquake, and Lessons Learned.* M. Selim Günay and Khalid M. Mosalam. April 2010.

PEER 2010/104 *Simulating the Inelastic Seismic Behavior of Steel Braced Frames, Including the Effects of Low-Cycle Fatigue.* Yuli Huang and Stephen A. Mahin. April 2010.

PEER 2010/103 *Post-Earthquake Traffic Capacity of Modern Bridges in California.* Vesna Terzic and Božidar Stojadinović. March 2010.

PEER 2010/102 *Analysis of Cumulative Absolute Velocity (CAV) and JMA Instrumental Seismic Intensity (I_{JMA}) Using the PEER–NGA Strong Motion Database.* Kenneth W. Campbell and Yousef Bozorgnia. February 2010.

PEER 2010/101 *Rocking Response of Bridges on Shallow Foundations.* Jose A. Ugalde, Bruce L. Kutter, and Boris Jeremic. April 2010.

PEER 2009/109 *Simulation and Performance-Based Earthquake Engineering Assessment of Self-Centering Post-Tensioned Concrete Bridge Systems.* Won K. Lee and Sarah L. Billington. December 2009.

PEER 2009/108 *PEER Lifelines Geotechnical Virtual Data Center.* J. Carl Stepp, Daniel J. Ponti, Loren L. Turner, Jennifer N. Swift, Sean Devlin, Yang Zhu, Jean Benoit, and John Bobbitt. September 2009.

PEER 2009/107 *Experimental and Computational Evaluation of Current and Innovative In-Span Hinge Details in Reinforced Concrete Box-Girder Bridges: Part 2: Post-Test Analysis and Design Recommendations.* Matias A. Hube and Khalid M. Mosalam. December 2009.

PEER 2009/106 *Shear Strength Models of Exterior Beam-Column Joints without Transverse Reinforcement.* Sangjoon Park and Khalid M. Mosalam. November 2009.

PEER 2009/105 *Reduced Uncertainty of Ground Motion Prediction Equations through Bayesian Variance Analysis.* Robb Eric S. Moss. November 2009.

PEER 2009/104 *Advanced Implementation of Hybrid Simulation.* Andreas H. Schellenberg, Stephen A. Mahin, Gregory L. Fenves. November 2009.

PEER 2009/103 *Performance Evaluation of Innovative Steel Braced Frames.* T. Y. Yang, Jack P. Moehle, and Božidar Stojadinovic. August 2009.

PEER 2009/102 *Reinvestigation of Liquefaction and Nonliquefaction Case Histories from the 1976 Tangshan Earthquake.* Robb Eric Moss, Robert E. Kayen, Liyuan Tong, Songyu Liu, Guojun Cai, and Jiaer Wu. August 2009.

PEER 2009/101 *Report of the First Joint Planning Meeting for the Second Phase of NEES/E-Defense Collaborative Research on Earthquake Engineering.* Stephen A. Mahin et al. July 2009.

PEER 2008/104 *Experimental and Analytical Study of the Seismic Performance of Retaining Structures.* Linda Al Atik and Nicholas Sitar. January 2009.

PEER 2008/103 *Experimental and Computational Evaluation of Current and Innovative In-Span Hinge Details in Reinforced Concrete Box-Girder Bridges. Part 1: Experimental Findings and Pre-Test Analysis.* Matias A. Hube and Khalid M. Mosalam. January 2009.

PEER 2008/102 *Modeling of Unreinforced Masonry Infill Walls Considering In-Plane and Out-of-Plane Interaction.* Stephen Kadysiewski and Khalid M. Mosalam. January 2009.

PEER 2008/101 *Seismic Performance Objectives for Tall Buildings.* William T. Holmes, Charles Kircher, William Petak, and Nabih Youssef. August 2008.

PEER 2007/101 *Generalized Hybrid Simulation Framework for Structural Systems Subjected to Seismic Loading.* Tarek Elkhoraibi and Khalid M. Mosalam. July 2007.

PEER 2007/100 *Seismic Evaluation of Reinforced Concrete Buildings Including Effects of Masonry Infill Walls.* Alidad Hashemi and Khalid M. Mosalam. July 2007.

The Pacific Earthquake Engineering Research Center (PEER) is a multi-institutional research and education center with headquarters at the University of California, Berkeley. Investigators from over 20 universities, several consulting companies, and researchers at various state and federal government agencies contribute to research programs focused on performance-based earthquake engineering.

These research programs aim to identify and reduce the risks from major earthquakes to life safety and to the economy by including research in a wide variety of disciplines including structural and geotechnical engineering, geology/seismology, lifelines, transportation, architecture, economics, risk management, and public policy.

PEER is supported by federal, state, local, and regional agencies, together with industry partners.

PEER reports can be ordered at http://peer.berkeley.edu/publications/peer_reports.html or by contacting

Pacific Earthquake Engineering Research Center
University of California, Berkeley
325 Davis Hall, mail code 1792
Berkeley, CA 94720-1792
Tel: 510-642-3437
Fax: 510-642-1655
Email: peer_editor@berkeley.edu

ISSN 1547-0587X